Aus der Radiologischen Universitätsklinik Tübingen

Abteilung Diagnostische und Interventionelle Neuroradiologie

Representation of brain tumours in two-dimensional diffusion kurtosis imaging (DKI) histograms

Inaugural-Dissertation
zur Erlangung des Doktorgrades
der Medizin

der Medizinischen Fakultät
der Eberhard Karls Universität
zu Tübingen

vorgelegt von

Heilker, Clara

2024

Dekan: Professor Dr. B. Pichler

1. Berichterstatter: Professor Dr. U. Klose
2. Berichterstatter: Privatdozent Dr. M. Himmelbach

Tag der Disputation: 11.10.2023

Meinen Eltern

Table of Contents

List of Tables

List of Figures

List of Abbreviations

ADC	apparent diffusion coefficient
ATRX	alpha-thalassemia/mental retardation syndrome X-linked
AUC	area under the curve
CNS	central nervous system
CT	computed tomography
DKI	diffusion kurtosis imaging
DTI	diffusion tensor imaging
DWI	diffusion-weighted imaging
EGFR	epidermal growth factor receptor
ER	oestrogen receptor
FA	flip angle
FLAIR	fluid-attenuated inversion recovery
FOV	field of view
HER2	human epidermal growth factor receptor 2
HGG	high-grade gliomas
IDH	isocitrate dehydrogenase
LCNEC	large cell neuroendocrine carcinoma
LGG	low-grade gliomas
MD	mean diffusivity
MK	mean kurtosis
MR(I)	magnetic resonance (imaging)
NSCLC	non-small-cell lung cancer
PR	progesterone receptor
SCLC	small-cell lung cancer
TE	echo time
TR	repetition time
WHO	World Health Organization

1 Introduction

1.1 Motivation

Malignant brain tumours belong to the group of very severe cancer types because of their generally unfavourable prognosis. Due to their location, they are known to cause neurological deficits early on and therefore impose a significantly negative impact on the quality of life. Common serious symptoms include hemiparesis, imbalance, incontinence and personality changes (Omuro & DeAngelis, 2013). Moreover, surgical resection of the tumour can be difficult as it sometimes causes even more deficits when healthy tissue is also partially removed.

The most common primary malignant brain tumours are gliomas. In this group, glioblastomas are the most aggressive subtype: Even when implementing the standard procedure of administering temozolomide and radiotherapy, the two-year survival rate is extremely low with only 27% and the median survival is merely 15 months (Stupp et al., 2005). Metastases are another important class of malignant brain tumours which generally indicate an advanced stage of the primary cancer. The treatment of brain metastases is often challenging: The different environment in the brain can lead to changes of the tumorous tissue on the molecular level (Boire et al., 2020). Therefore, the metastases might not respond to the therapy intended for the primary tumour. Generally, the prognosis is very poor, when brain metastases are observed at the time of the primary malignancy diagnosis: The median survival is twelve months or less, dependent on the primary tumour type (Cagney et al., 2017). Due to the severity of malignant brain tumours, it is essential to diagnose the tumour entity correctly so that the right treatment can be chosen as quickly as possible. In this context, the discrimination from benign lesions like meningiomas is also necessary.

When diagnosing the histological type and malignancy grade of a brain tumour, the standard procedure is a biopsy. However, this is an invasive method, which can lead to neurological deficits or even death. These events are especially common in posterior fossa biopsies, which include the sample taking of the

cerebellum or brainstem (Tobin et al., 2015). In addition, some patients may not want an invasive procedure, have tumours in vital regions of the brain or it has been decided that a watchful waiting approach is the best choice. Especially in these cases, it is essential to have a non-invasive, reliable option for identifying the tumour type. Another drawback of a biopsy is that it only provides information about a small part of the tumour. Especially in glioblastomas, a pronounced intratumoral heterogeneity is very common (Patel et al., 2014). Because the tissue characteristics are crucial regarding the decision for the right therapy, it is important to get an overview of the whole tumour, which is better attainable with imaging than with a single biopsy (Hu et al., 2020). This shows that diffusion-weighted imaging (DWI) and diffusion kurtosis imaging (DKI) have potential in improving the diagnostic process in patients with brain tumours. However, it is necessary to further investigate how DWI and DKI can optimally be evaluated together in order to attain as much information as possible about the tumour.

1.2 Different groups of examined brain tumours

1.2.1 Gliomas

Gliomas are the most frequently diagnosed malign primary intracranial tumours (Ostrom et al., 2014). They can be located anywhere in the central nervous system (CNS) and originate from glial cells as the name reveals (Wesseling & Capper, 2018). Gliomas are usually malignant and can be divided into different groups. These categories are defined by the World Health Organization (WHO) classification of CNS tumours, whose fifth edition was published in 2021 (Louis et al., 2021). In general, one can distinguish between diffuse and circumscribed gliomas. Furthermore, a differentiation of adult and paediatric-type tumours is possible. The adult-type diffuse gliomas, which were investigated in this study, can be classified into three main groups called astrocytomas, glioblastomas and oligodendrogliomas.

According to the WHO, gliomas can be grouped depending on their histological appearance and certain molecular markers. Previously, these tumours were classified based only on their histology while the molecular findings were merely

seen as additional information. However, the molecular profile of a glioma can have diagnostic, predictive and prognostic significance (Louis et al., 2014). The most important molecular markers used to group gliomas, according to the WHO 2021 classification system, are the isocitrate dehydrogenase (IDH) mutation and the 1p/19q codeletion. While astrocytomas and oligodendrogliomas are typically IDH-mutated, glioblastomas usually possess the IDH-wildtype gene. The 1p/19q codeletion is useful for detecting oligodendrogliomas. When grouping gliomas according to the WHO 2021 classification, the genetic profile of a tumour can even be superordinate to the histological appearance.

In addition to the classification by histological and molecular information, the gliomas are also categorized by a malignancy grade, which is specified by the term WHO grade 1, 2, 3 or 4. This score is determined by investigating histological parameters like the degree of potential necrosis and the extent of microvascular proliferation, as well as molecular parameters. The WHO grade 1 and 2 tumours are also referred to as low-grade gliomas (LGG) while the group of high-grade gliomas (HGG) is formed by WHO grade 3 and 4 tumours (Erira et al., 2021).

1.2.2 Meningiomas

Meningiomas are the most prevalent primary intracranial tumours (Ogasawara et al., 2021). They are often detected incidentally on computed tomography (CT) or magnetic resonance (MR) images, which were acquired due to another indication. Even though meningiomas are mostly benign, they can cause severe neurological symptoms like general or partial seizures, headaches due to the elevated intracranial pressure and focal neurological deficits (Buerki et al., 2018). The expression and severity of these symptoms are influenced by the tumour's location and size.

Depending on histological criteria like mitotic rate and possible brain invasion, meningiomas are classified as WHO grade 1, 2 or 3. While grade 1 is most common with 80 to 85% and is classified as a benign tumour, the grade 2 subgroup makes up 15 to 20% and is also referred to as atypical meningioma.

The smallest fraction only makes up 1 to 2 percent and represents the malignant grade 3 anaplastic meningioma (Ostrom et al., 2016).

1.2.3 Brain Metastases

Another important group of brain tumours are metastases. The most common associated primary tumours are lung cancer, breast cancer and melanoma (Soffietti et al., 2006). The incidence of brain metastases is expected to increase further due to improved cancer therapy and superior MR imaging (Sacks & Rahman, 2020). Possible therapeutic options for metastases include systemic chemotherapy, biologicals, stereotactic radiosurgery and whole-brain radiation therapy (Soffietti et al., 2020).

1.3 Use of diffusion in magnetic resonance imaging (MRI)

1.3.1 Basic principles of diffusion and kurtosis

The term diffusion describes the random Brownian motion of molecules in gas or liquids, which is fuelled by thermal energy. If there is unrestricted diffusion, the molecules can move freely in every direction and spread out evenly in the medium. The arbitrary movements of diffusion can be described by a displacement distribution which ideally resembles a Gaussian curve (Hagmann et al., 2006).

In human tissue, diffusion of water molecules is often restricted. Barriers like cell membranes and other molecular hindrances limit the movement of particles. In consequence, diffusion is unequally restricted in different directions. For example, molecules in an axon can move more freely parallel to the axis of the axon than perpendicular to it because the diameter of the axon is smaller than its length. This uneven diffusion behaviour is called anisotropic. Opposed to that, isotropic diffusion describes a distribution pattern which is identical for all directions (Beaulieu, 2002).

In the case of restricted diffusion, the previously described Gaussian distribution transforms into a curve displaying a reduced width and increased height. The dimensionless metric “kurtosis” captures the sharpness of the distribution graph’s

tip. When the graph does not show deviation from the Gaussian curve, the kurtosis value equals 0. The kurtosis value increases when the ratio of peak height versus curve width goes up. Vice versa, the kurtosis value becomes negative when the ratio of peak height versus curve width is lower than that of a normal distribution (Marrale et al., 2016).

1.3.2 Diffusion-weighted imaging (DWI)

Diffusion of water molecules in tissues is the basis of DWI, a further development of magnetic resonance imaging (MRI). When employing MRI and DWI, one uses the spins of protons, which belong to hydrogen atoms. These spins can be influenced by a magnetic field, that is generated by the MRI scanner. When employing DWI sequences, the motion of molecules leads to a signal decay, which is represented by a lower signal intensity in DWI images. Opposed to that stand the regions of the brain where diffusion is more restricted. The resulting limited particle movement leads to the detection of a stronger signal in relation to that of other regions, which is represented by a higher signal intensity in the DWI images (Bammer, 2003).

The strength of the magnetic field gradients and their duration determines to which extent the MR signal is influenced by particle movement and therefore how strongly the resulting image is diffusion-weighted. This sensitivity for diffusion can also be described by the b-value, which is calculated by using the amplitude of the gradient pulses (G), their duration (δ) and the time between the pulses (Δ) (Maier et al., 2010):

$$b = (\gamma \times G \times \delta)^2 \times \left(\Delta - \frac{\delta}{3}\right)$$

Here, γ represents the gyromagnetic ratio of hydrogen. For DWI, the employed b-values are normally smaller than 2000 s/mm^2 (Mulkern et al., 1999).

As previously described, diffusion is not equally restricted in every direction due to cell membranes and other obstacles. When using DWI, it is therefore important to measure the motion of the particles in several directions. This is done by applying the magnetic field gradients in multiple orientations. Afterwards, one

calculates the average of all these measurements (Huisman, 2003). The central metric of DWI is the apparent diffusion coefficient (ADC). It is important to note that one never measures the real diffusion coefficient but rather estimates the ADC, which describes the diffusion of water in presence of movement restrictions within biological tissues.

This acquisition of the ADC value requires the performance of at least two MRI measurements with different b-values. The ADC value can then be calculated for each specific voxel. In case of only one b-value b in addition to a measurement without diffusion field gradients (b == 0), one can deduce the following equation for calculating this diffusion characteristic (Rosenkrantz et al., 2015):

$$ADC = \frac{\ln\left(\frac{S_b}{S_0}\right)}{-b}$$

b represents the previously described b-value while S_b depicts the signal intensity of a diffusion-weighted image, which is acquired with this specific b-value in one particular magnetic field gradient direction. The higher the b-value, the lower is the signal. S_0 displays the signal intensity of an MR image without diffusion weighting. The dimension of ADC is mm^2/s. If more MRI measurements are conducted with various b-values, the obtained signal intensities are displayed in dependence of b-values. The ADC value can then be determined by a fitting procedure assuming a monoexponential function of signal intensities (Koh & Collins, 2007).

Another common diffusion metric is the mean diffusivity (MD). This value originates from diffusion tensor imaging (DTI), which is a further development of DWI, and is calculated by averaging the three eigenvalues of the diffusion tensor. These eigenvalues represent the average diffusion in the three main directions that are used to calculate the diffusion tensor (Alexander et al., 2007).

The most common clinical use of DWI is the detection of strokes. Ischemia leads the affected brain cells to swell, which results in a higher degree of diffusion restriction. Therefore, the ischemic area is depicted as hyperintense when compared to the surrounding brain tissue (Roberts & Rowley, 2003).

1.3.3 Diffusion kurtosis imaging (DKI)

DKI is a further development of DWI and was introduced in 2005 (Jensen et al., 2005). The kurtosis describes the deviation from a monoexponential decay in multi-b measurements. It originates in the complexity of the tissue's structure. With the help of DKI, one can therefore quantify the divergence of the diffusion distribution graph from a normal Gaussian curve. For examining the brain with DKI, one needs to use higher b-values than in DWI: The maximal value for b in conventional DKI is usually between 2000 and 2500 s/mm^2 (Lu et al., 2006).

Like the previously described approximation of the ADC value, the obtained value for the kurtosis is the result of a fitting procedure. It is called apparent diffusional kurtosis K_{app}. The following equation displays the relationship between the various diffusion characteristics (Jensen & Helpern, 2010):

$$\ln\left[S(b)\right] = \ln\left[S(0)\right] - b \times ADC + \frac{1}{6} b^2 \times ADC^2 \times K_{app}$$

When conducting several measurements in different gradient directions, one can average the K_{app} values to obtain the mean kurtosis (MK).

1.4 Objective of this project

The clinical importance of DWI has significantly increased in recent years, e.g. for the detection of ischemic strokes in brain tissue. However, DWI also harbours a lot of potential in other areas like the differentiation between normal regions of the brain and tumorous tissue. Furthermore, current research also investigates how DKI, as a further development of DWI, can provide even more additional details about the tumour. These advanced imaging techniques are especially important when a biopsy is not possible. Thus, the DKI-based information regarding the malignancy grade and the tumour type can be crucial when selecting the right treatment.

While previous research has proven that DWI and DKI can separately differentiate between various tumour categories, the main goal of this project is to investigate a method by which the diffusion and kurtosis values are analysed

together. To achieve this, different types of brain tumours were investigated with DKI. Various sets of b-values were employed to identify the ones, which are most suitable for characterising the tumours. Based upon these measurements, two-dimensional histograms were created with the calculated diffusion and kurtosis values for each scanned subject.

The examined patients were categorized into four different groups, those (I) without a brain tumour, (II) with gliomas, (III) with meningiomas, and (IV) with metastases. The main purpose of this work was to investigate and systematically describe any differences between the histograms of the respective groups. Any observed dissimilarities could be useful to better differentiate between tumour and normal brain tissue or to distinguish between the various subcategories of tumours.

2 Materials and Methods

2.1 Characteristics of the study group

The final study group encompassed 39 patients and 10 healthy control subjects. Initially, MR imaging had been performed in 52 patients with brain tumours. However, 13 patients had to be excluded due to a small tumour volume, unclear biopsies, missing clinical data, flawed MR images or the diagnosis of pathologies which were not included in this study. Out of the remaining 39 patients, 20 had a glioblastoma, 4 an oligodendroglioma, 4 an astrocytoma, 5 a meningioma and 6 a brain metastasis. 28 out of the 39 patients had no prior tumour resection before the MR images were generated. 11 patients had previously had a resection before. For the latter group, recurrent or residual tumorous tissue was analysed. This research project was approved by the institutional review board (reference number 184/2021BO2).

2.2 MR image acquisition

MR imaging was carried out with three different 3-Tesla-MRI-scanners in the University Hospital Tübingen: MAGNETOM Vida, MAGNETOM Vida Fit and MAGNETOM Prisma Fit (all by Siemens Healthcare GmbH, Erlangen, Germany). The MRI scanners measured a 2D spin-echo echo-planar imaging DKI sequence of the brain in axial orientation with an acquisition time of approximately ten minutes. The b-values, which were used, equal 0, 500, 1000, 2000, 3000, 4000 for all subjects and 5000 s/mm^2 additionally for patients with a brain tumour. Moreover, the b-values were grouped into different sets: For example, the obtained data with a b-value of or lower than 2000 s/mm^2 was investigated together. This analysis was also conducted with the maximal b-values of 3000, 4000 and 5000 s/mm^2. Furthermore, b0 maps were calculated using the data which was obtained with the b-value 0. These images served as a base line when generating the two-dimensional diffusion-kurtosis histograms.

Diffusion measurements were performed in six directions. In order to establish the strong magnetic field gradients used in DKI, different MRI scanners take varying time intervals, depending on the capability of the device. Therefore, the sequence parameters slightly differ between the three scanners (Table 1).

Table 1. Sequence parameters for the three different MRI scanners.

Sequence parameters	MAGNETOM Prisma Fit	MAGNETOM Vida Fit	MAGNETOM Vida
echo time (TE)	66 or 68 ms	107 ms	90 ms
repetition time (TR)	3000 or 3200 ms	3500 ms	3300 ms
flip angle (FA)	90	90	90
field of view (FOV)	220 x 220 mm^2	223 x 223 mm^2	220 x 220 mm^2
Slice thickness	4 mm	4 mm	4 mm
Acquisition matrix	130 x 130	130 x 130	130 x 130
Slice number	30	30	30

With these MRI sequences, the MD and MK values were estimated for each individual voxel of the mapped brain by a fitting procedure. Furthermore, additional T2 fluid-attenuated inversion recovery (FLAIR) and contrast-enhanced T1 sequences were often acquired.

2.3 Generation of the histograms

In order to analyse the obtained MD and MK values, two-dimensional histograms were generated for each subject with MATLAB R2018b (MathWorks, Natick, Massachusetts, USA). These diffusion values were transformed into a matrix for two reasons: Firstly, it is required that the coordinates of the two-dimensional histogram must be integers. Secondly, if one directly used the diffusivity and kurtosis characteristics to create the histogram, the majority of the points would lie very closely together because the MD and MK values demonstrate relatively

little variance when comparing the different voxels. When the data is transformed into a matrix, it spreads the numbers more apart in the histogram. Here, a 200 x 200 matrix was used which means that all the transformed MD and MK values had to lie in this range between 0 and 200. Therefore, the following two equations were used for the transformation of the MD and MK values into a matrix:

$$x1 = MD \times 30 \qquad y1 = 200 - 150 \times MK$$

For each voxel, the transformed MD value was applied on the x-axis while the y-axis represented the transformed MK value.

In two-dimensional histograms, each pixel is defined by a specific x- and y-coordinate and can also be called a bin. This characterization of the pixels by their particular coordinates represents the first and second dimension of the histogram. If several voxels of the three-dimensional patient data set share the same coordinates x1 and y1, each voxel increases the event count of the respective bin. After the analysis of the whole data set, the event counts are visualized by signal intensities. The resulting event count map represents the third dimension of the histogram. By looking at the diagram, one can therefore see the quantitative distribution of the MK and MD values.

When generating these histograms, one can adjust the brightness of the bins. If the obtained event counts are restricted to a small upper value, it is easier to also see points whose coordinates exist rather seldom. Opposed to that, visualisation with a restriction to a higher upper value allows one to see a sharper form of the histogram and it is easier to distinguish the different spikes of the diagram. Since the varying degrees of brightness therefore all have their advantages, two diagram versions with different levels of upper value restriction were always displayed next to each other (Fig. 1).

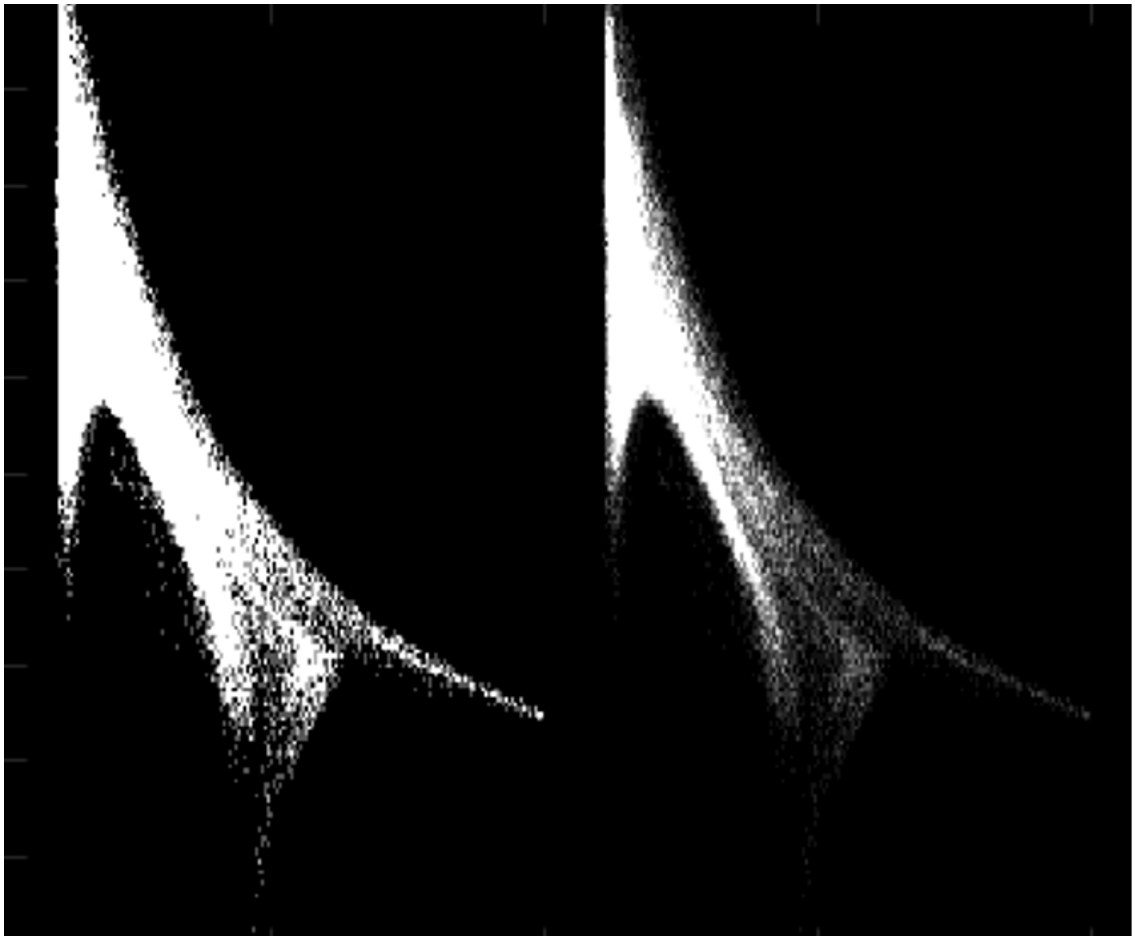

Fig. 1. Two different histogram versions of a subject without a brain tumour. The MD value is represented on the x-axis while the MK value is displayed on the y-axis. The chosen upper value for the event count is lower in the left histogram.

Another way to influence the appearance of the histogram was to adjust the noise level. Voxels with signal intensities lower than the noise level within the b0 maps were not considered for the estimation of the two-dimensional histogram. Especially in subjects without a tumour, the artefacts of the bone around the brain were often distracting when analysing the histograms. Therefore, the noise level was often increased in these cases.

Four histograms were generated for one patient: One for each of the maximal b-values 2000, 3000, 4000 and 5000 s/mm^2. For example, the histogram for the maximal b-value of 2000 s/mm^2 was generated with MD and MK values of measurements with the b-values 0, 500, 1000 and 2000 s/mm^2. Opposed to that, the analysis for the maximal b-value of 5000 s/mm^2 included the b-values 0, 500, 1000, 2000, 3000, 4000 and 5000 s/mm^2. Afterwards, the resulting diagrams

were compared in order to determine the most suitable maximal b-value for analysing the histogram's shape.

2.4 General analysis of the histograms

Two different approaches were used to examine the previously generated histograms of the subjects. Firstly, different coordinates, representing the MK and MD values, were selected in the histogram. Afterwards, the corresponding voxels with the same diffusion values were highlighted in the DKI images (Fig. 2).

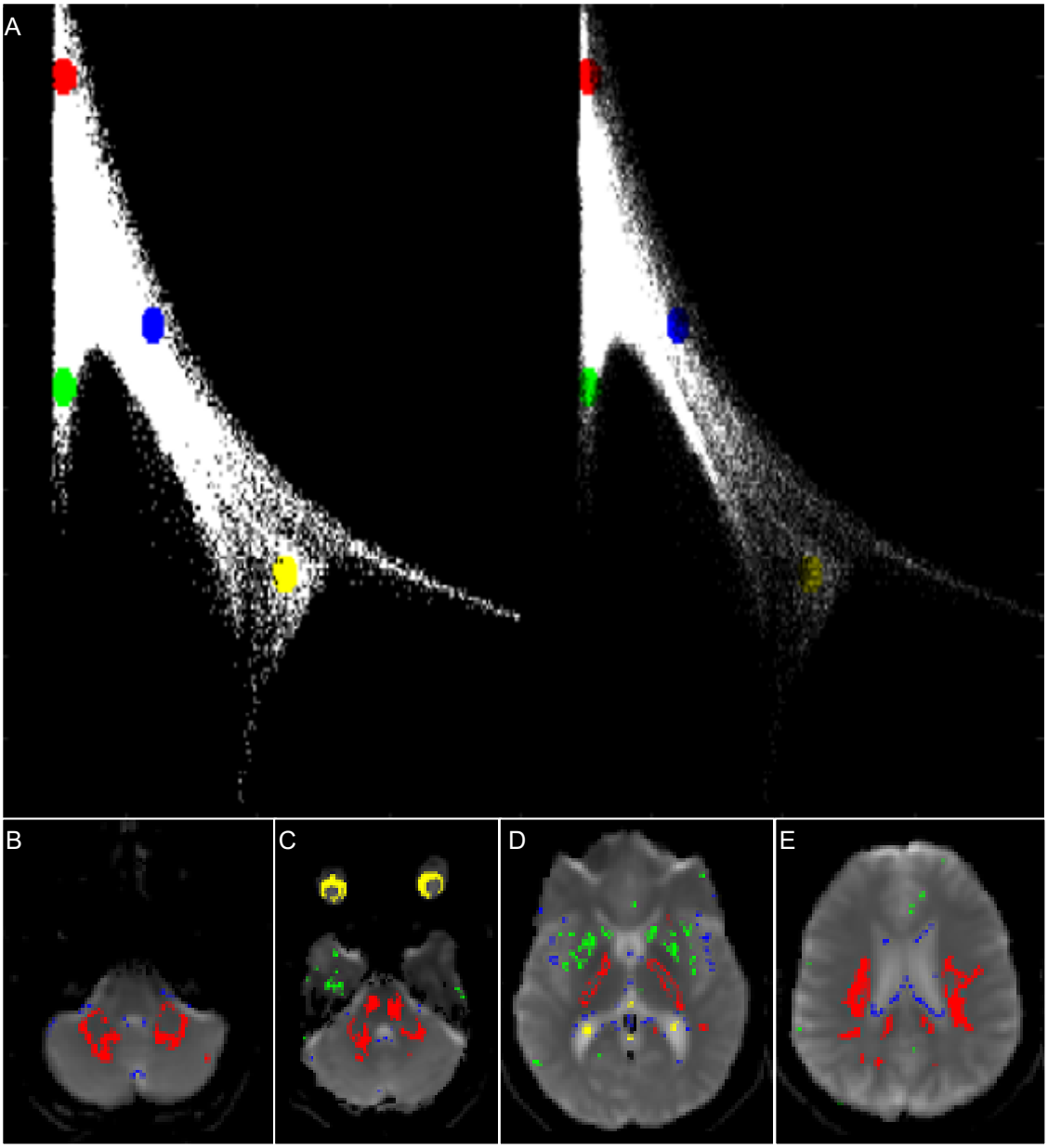

Fig. 2. Exemplary marked histogram regions and the related voxels. *A* displays the highlighted diagram fractions while *B-E* show the corresponding marked voxels in the DKI images of a subject without a brain tumour.

Secondly, parts of different anatomical regions were selected in the DKI images. Afterwards, the respective MK and MD values of these marked brain areas were highlighted in the histogram of the subject. In order to better distinguish the marked fractions of the diagram, a third version of the histogram was created. In this alternative diagram, only the highlighted coordinates were displayed, and the rest of the histogram was eliminated (Fig. 3).

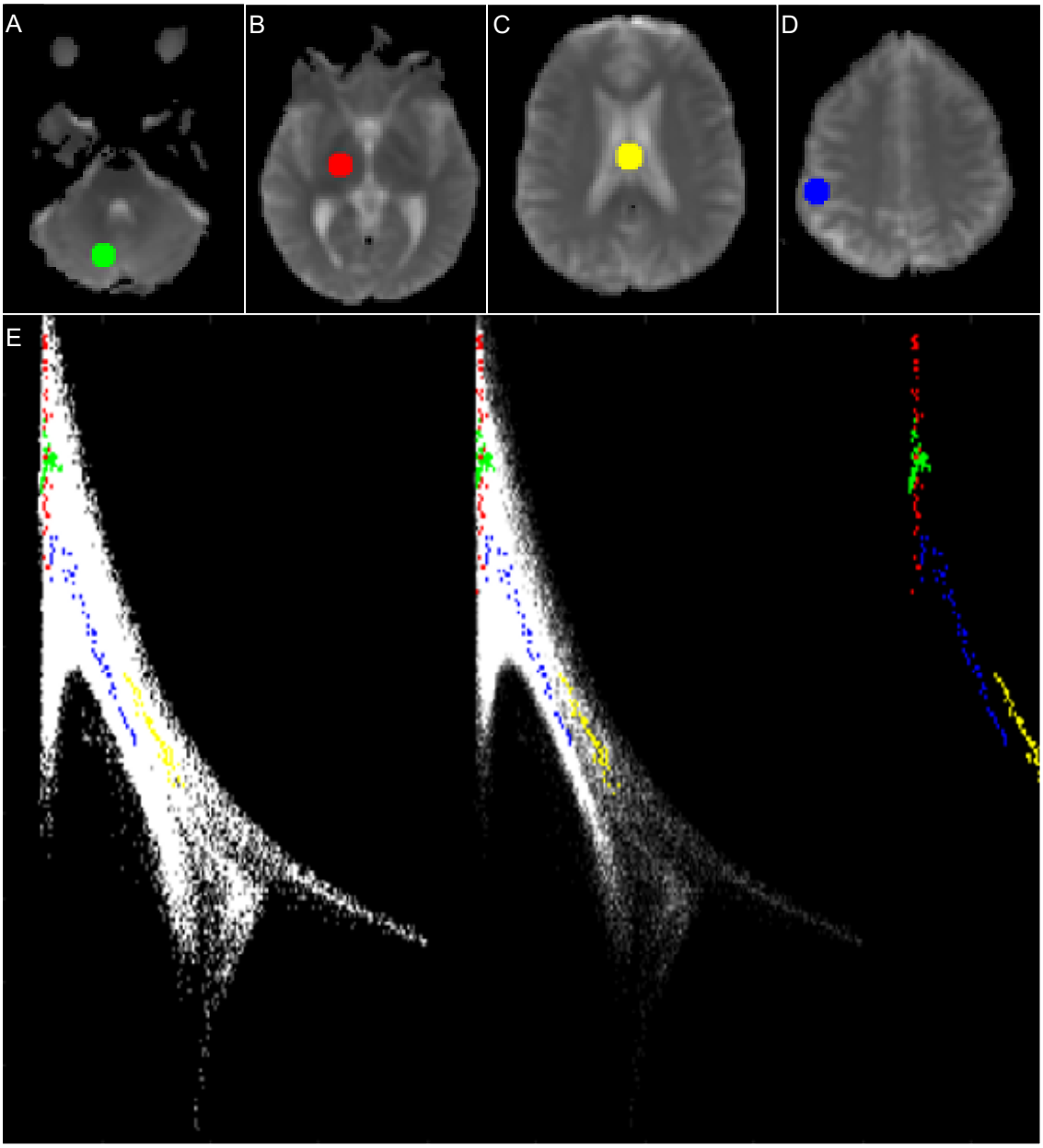

Fig. 3. Exemplary marked regions in the MR images of a subject without a brain tumour *(A-D)* and the corresponding highlighted areas in the histogram of the subject *(E)*. In the third version of the diagram on the right, only the highlighted coordinates are displayed.

With these two methods, the diagrams of the healthy subjects and patients with a brain tumour were analysed and compared. For example, the left border of the histogram was marked with various points, and the distribution pattern of the corresponding markings in the MR images was afterwards compared between different subjects. Moreover, various histogram extensions and their corresponding brain regions were analysed. Vice versa, some anatomical areas like the ventricles or the nose were marked in the MR images and the related fractions of the histogram were compared between the subjects.

2.5 Analysis of the tumour and oedema-specific histogram parts

Furthermore, the fractions of the histogram, which represent the tumorous tissue, were investigated. This was done separately for gliomas, meningiomas and metastases. Additionally, the same analysis was conducted for the peritumoral oedema. To examine the pathological tissue, some of the concerned voxels were marked in the DKI images and their corresponding regions in the histogram were determined like previously described. This process is displayed in Fig. 4, where the images show a diagram spike, which was only observed in tumour patients and that corresponds to the highlighted pathological tissue. In order to mark the tumour and oedema, it was often useful to also look at the T2 FLAIR or contrast-enhanced T1 images to get more information about the exact location of the pathological tissue.

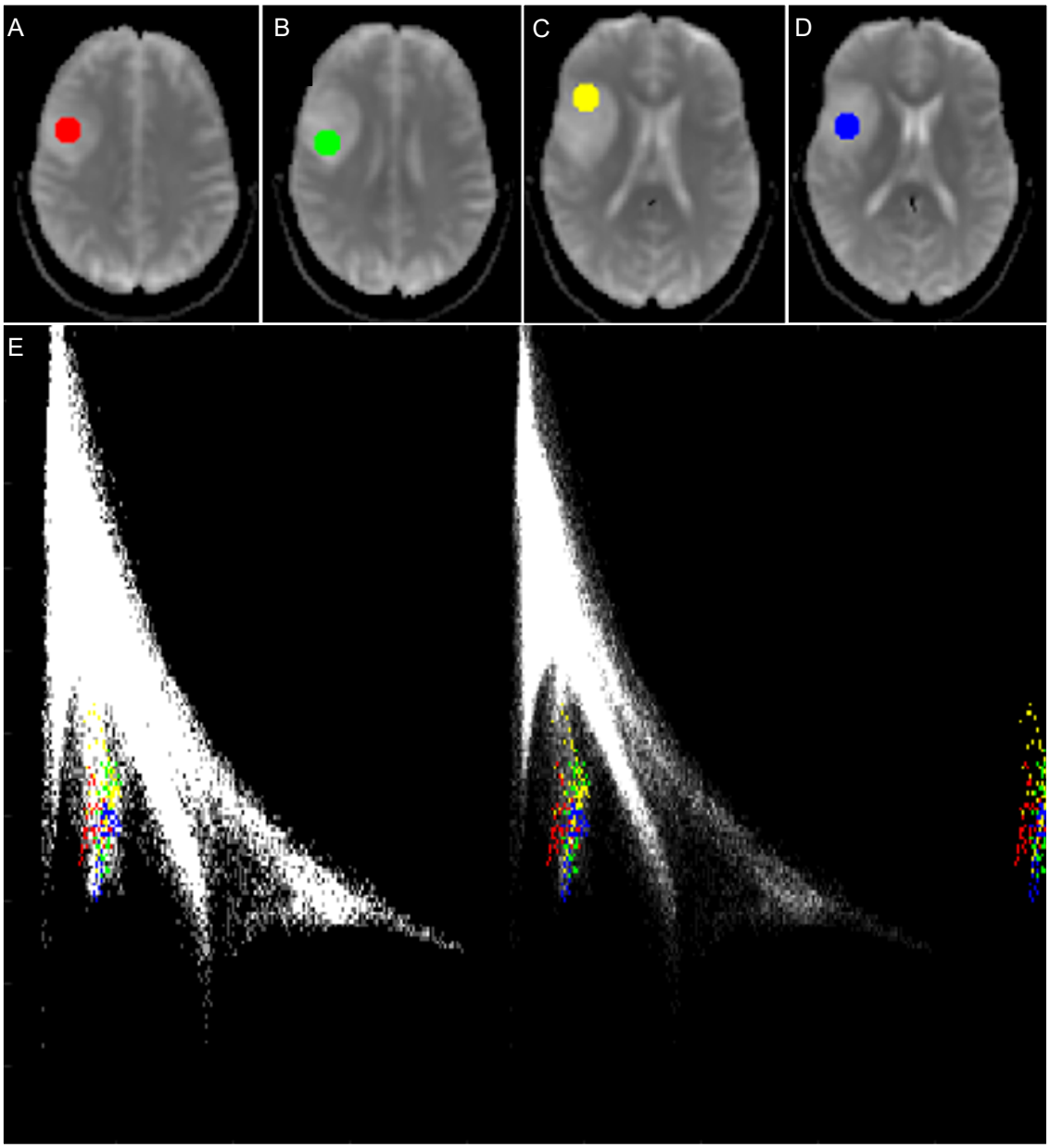

Fig. 4. Example of the representation of tumour tissue in the histogram. *A-D* display a marked oligodendroglioma in four different MR images while *E* shows the corresponding highlighted histogram region.

Vice versa, extensions of the diagram, which did not appear in subjects without a brain tumour, were highlighted and their related regions in the MR images analysed (Fig. 5).

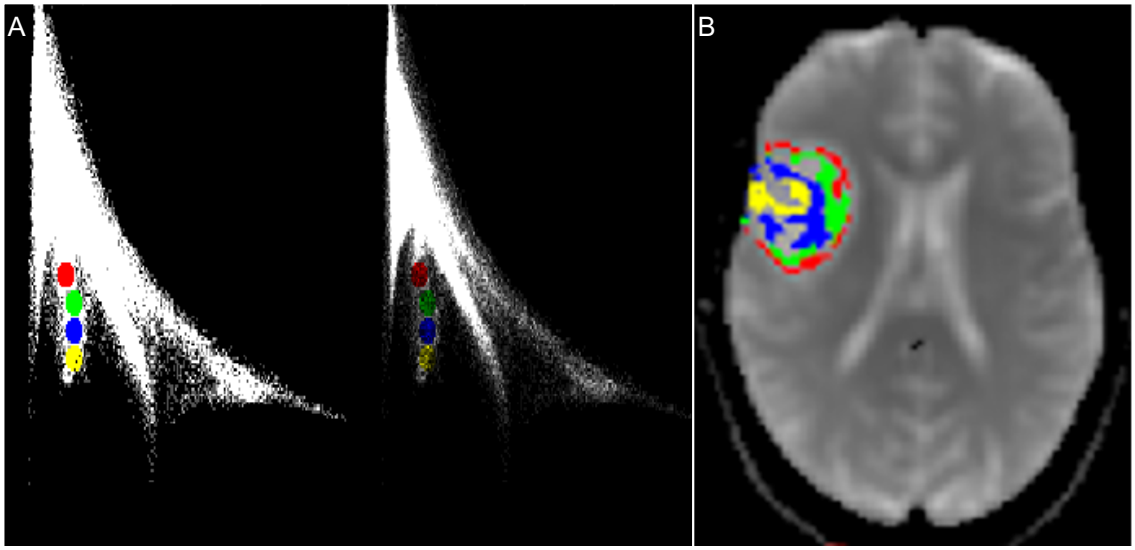

Fig. 5. Example of a highlighted histogram area and the corresponding marked tumour tissue. While *A* depicts the marked diagram area, *B* shows the respective highlighted brain tumour. The images belong to the patient with an oligodendroglioma that is also displayed in Fig. 4.

Moreover, it was also possible to use the results from the procedure shown in Fig. 4 in order to further examine the diagrams: When highlighting the tumour in the MR images, the corresponding histogram areas were marked. Vice versa, these diagram regions could be highlighted and the corresponding brain regions analysed. Thus, other brain areas were determined that also corresponded to that part of the diagram. This approach was especially helpful when tumours did not correspond to an abnormal extension of the histogram but rather lay in the physiological diagram fraction. Sometimes, the corresponding histogram spots of the tumour were scattered over a larger area of the diagram. In these cases, it was not possible to highlight one part of the histogram which related to most of the tumour tissue.

Furthermore, the representation of the entire pathological tissue in the histogram was analysed: The whole tumour and oedema were delineated in T2 FLAIR images. Then, the corresponding histogram areas of these brain regions were highlighted (Fig. 6). Thus, it was possible to investigate the representation of the

entire tumour and oedema in the histogram. The tumour and oedema were delineated together because it was often difficult to clearly separate these two entities, especially in the case of gliomas. This analysis was conducted in 25 out of the 39 tumour patients. In the other cases, the T2 or T1 sequences were not compatible with MATLAB and could therefore not be examined.

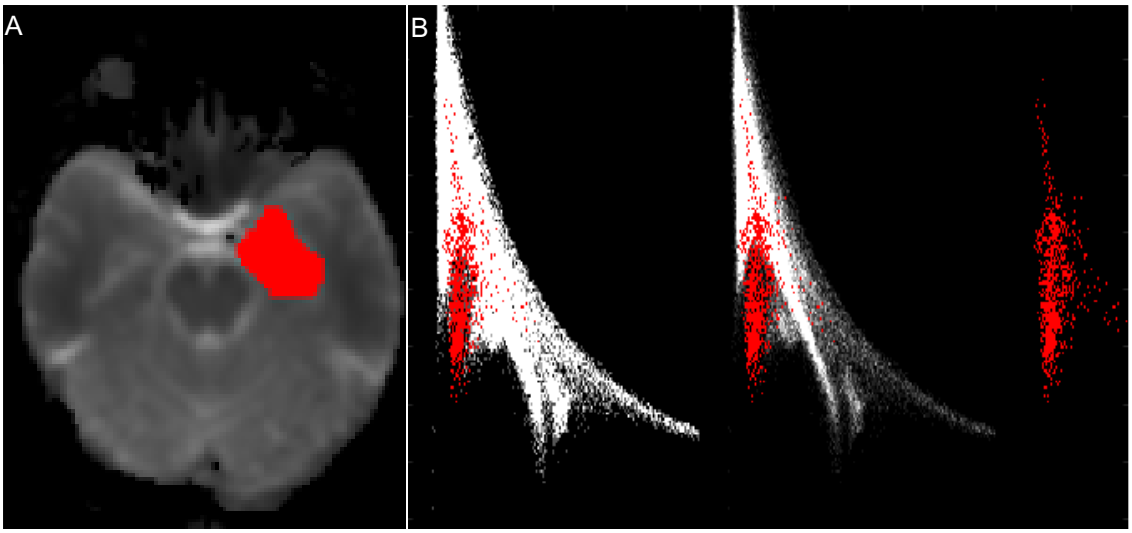

Fig. 6. Marked tumour and oedema with the corresponding histogram area. *A* displays the delineated tumour and oedema in a glioblastoma patient while *B* shows the respective highlighted histogram area.

As seen in Fig. 6, there is often one additional histogram extension in the lower area of the diagram in the case of gliomas when compared to subjects without a brain tumour. To further investigate that diagram region, a mask for the selection of pixels in this specific part of the histogram was constructed. Therefore, the event count maps of all subjects with and without a brain tumour were added pixelwise. The resulting map with a maximal event count of 7274 shows a clear pattern of an area with low event counts in the central lower part of the map (Fig. 7A). This region seems to be limited by straight lines. For the construction of a mask for this area, all event counts below 2500 were set to zero and two straight lines were designed to describe the left and right limits of the target region (Fig. 7B). After setting all pixels in the event count maps outside of the straight lines to 2500 (Fig. 7C), the mask was created by all pixels with an event count of zero. In Fig. 7D, the obtained mask is shown.

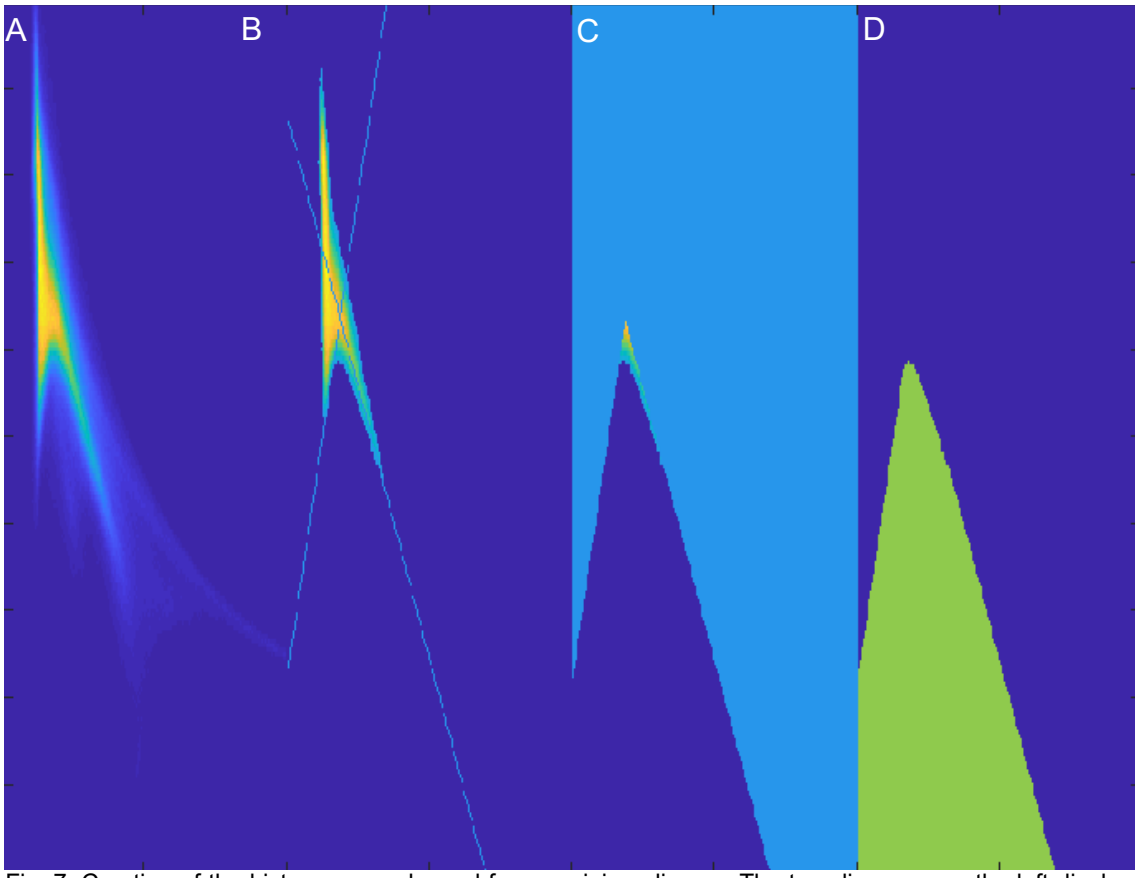

Fig. 7. Creation of the histogram mask used for examining gliomas. The two diagrams on the left display the sum histogram in decreasing intensity. The three diagrams on the right show the creation of the mask with the help of two straight lines.

When examining this histogram region in glioma patients, one can normally see the additional diagram spike (Fig. 8). Therefore, the mask was applied on all glioma patients.


Fig. 8. Marked histogram area, where the glioma-characteristic extension usually lies. On the left is the histogram of a glioblastoma patient. In the middle, the mask is displayed which normally encompasses the glioma-characteristic extension. On the right, the histogram area is shown that lies in the mask.

To further investigate this histogram mask, it was highlighted in different colours. Then, the corresponding voxels were marked in the DKI images with the respective colour. First, the colours were distributed over the mask in a way that was especially useful for separating the superior from the inferior mask fractions (Fig. 9).

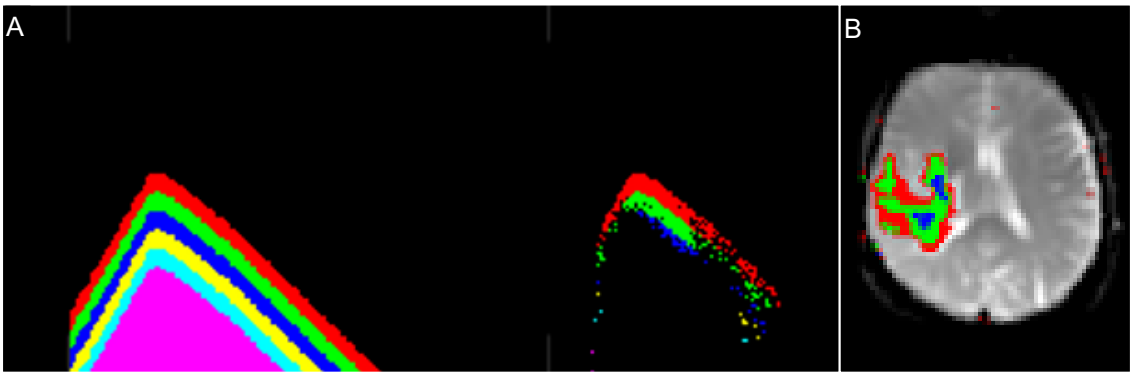

Fig. 9. First possibility for distributing the colours over the histogram mask. *A* shows the coloured mask on the left while it displays the applied mask on a glioblastoma patient on the right. *B* shows the corresponding highlighted voxels in an MR image of this patient.

Then, a second set of differently distributed colours was applied on the histogram mask that was practical for differentiating between the left and right fractions of the mask (Fig. 10).

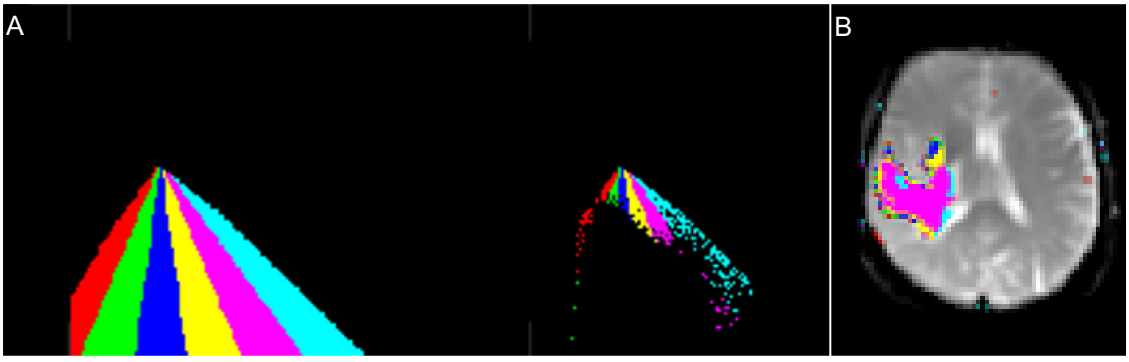

Fig. 10. Second possibility for distributing the colours over the histogram mask. *A* displays the coloured mask on the left and one can see the applied mask on the histogram of a glioblastoma patient on the right. *B* shows the highlighted corresponding voxels in an MR image of this patient.

Finally, a third way of colouring the histogram mask was investigated, which also separated the left and right fractions of the mask (Fig. 11).

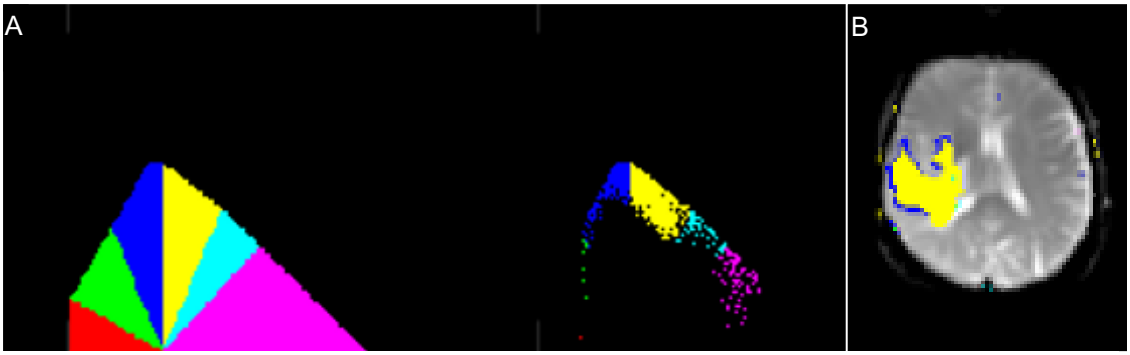

Fig. 11. Third possibility for distributing the colours over the histogram mask. *A* shows the coloured histogram mask on the left while the applied mask on the histogram of a glioblastoma patient is displayed on the right. *B* shows the corresponding voxels in a respective MR image.

3 Results

3.1 Histograms of different b-values

For each patient, various histograms were generated by using the MD and MK values, which were acquired with different b-values. The diagrams with the maximal b-value of 2000 s/mm^2 were most suitable for comparing the different tumours and analysing the general shape of the histogram. As shown in Fig. 12, the signal intensity continually declined when applying higher maximal b-values. This means, that some extension areas could not be seen on histograms of higher b-values, which made it more challenging to analyse the histogram shape and compare the diagrams of different tumours. Hence, only the diagrams with the maximal b-value of 2000 s/mm^2 were utilised.

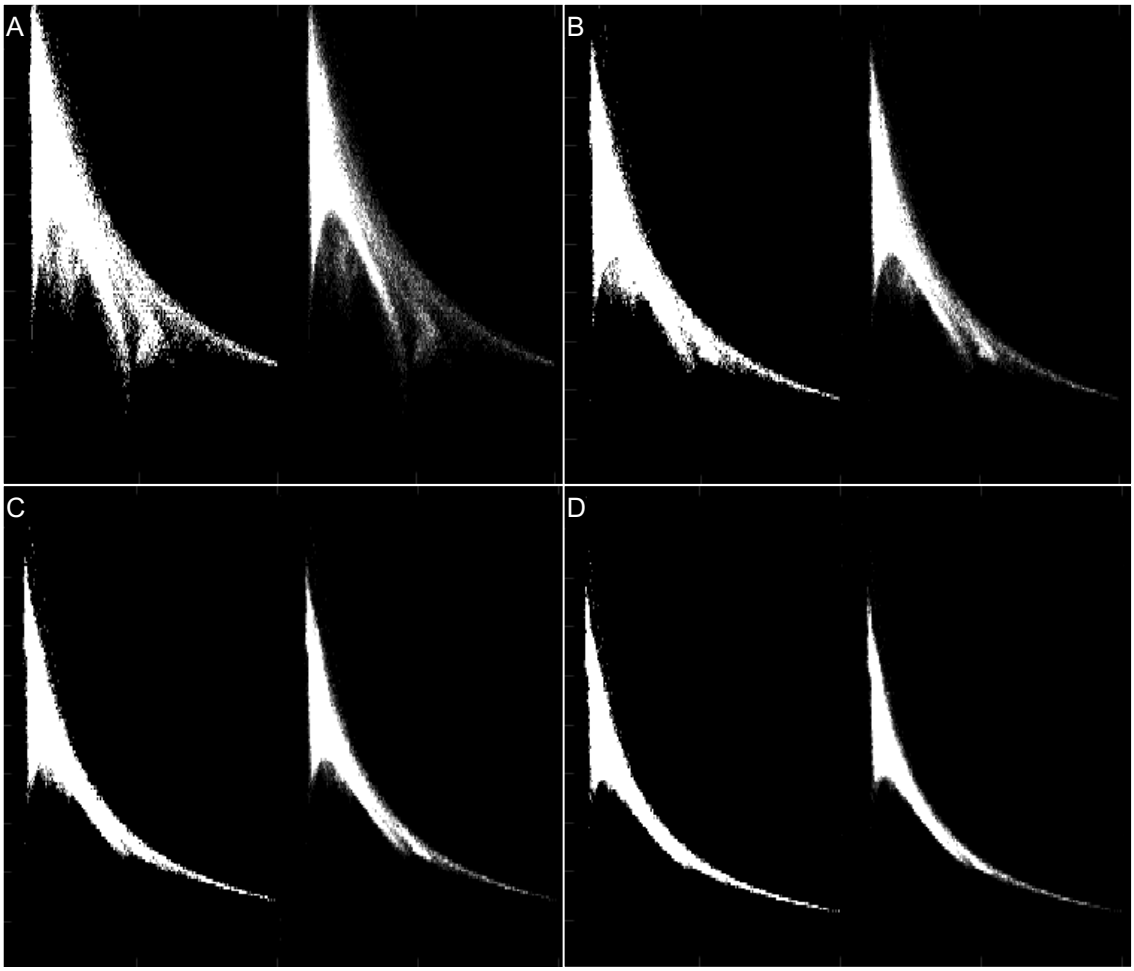

Fig. 12. Histograms acquired by using different maximal b-values on a glioblastoma patient. *A* represents the maximal b-value of 2000 s/mm^2, *B* the maximal b-value of 3000 s/mm^2, *C* the maximal b-value of 4000 s/mm^2 and *D* the maximal b-value of 5000 s/mm^2.

3.2 General histogram shape

The histograms had a characteristic overall shape, which was similar in subjects with or without a brain tumour. When highlighting certain parts of the histogram as previously described, specific diagram areas often corresponded to similar anatomical regions in the MR images when comparing different subjects. The same correlations between histogram areas and brain regions could usually be observed in healthy subjects and in brain tumour patients. Overall, four different diagram regions with the names A, B, C and D as defined below were investigated.

For example, a row of points was highlighted on the left border of the histogram, which represented diagram area A. The corresponding brain regions were then analysed. By marking the left histogram border, the voxels were highlighted which possess a rather low MD value. The resulting markings resembled layers in the MR images (Fig. 13). Regarding the superior part of the brain, the voxels that possessed higher MK values were mainly located in the inner regions, while the spots with low MK values predominantly lay in the outer brain areas. Another region with primarily low MK values was the inferior part of the temporal lobe. Layer-like markings could also be observed in the cerebellum, where the voxels with the highest MK values mostly could be found in the inner regions. Opposed to that, the spots with medium-high MK values mainly lay in the outer regions of the cerebellum. Other brain regions which primarily possessed higher MK values included the pons and the mesencephalon. The cortex was primarily highlighted in the occipital and temporal region.

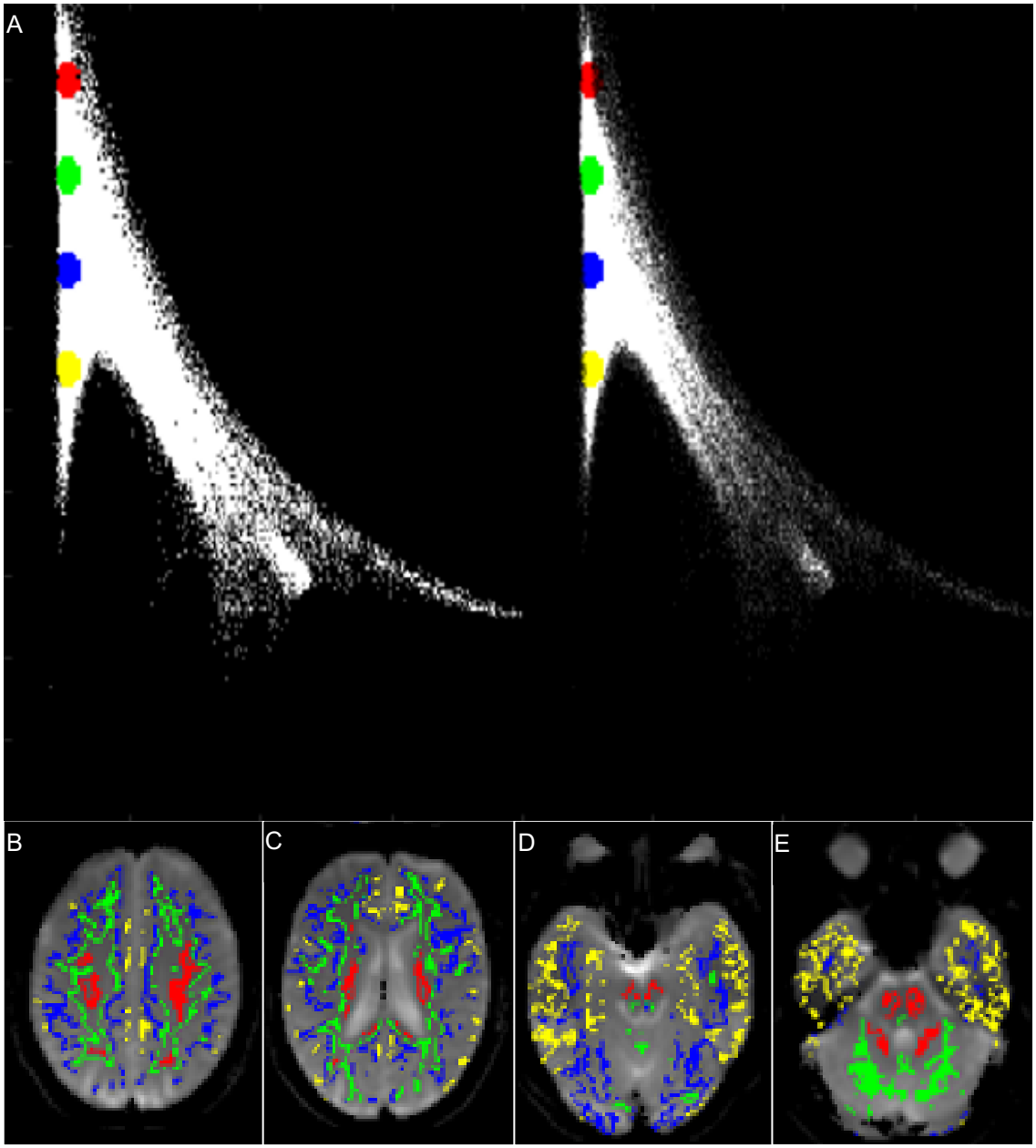

Fig. 13. Corresponding regions in the MR images concerning the left border of the histogram. *A* shows the four highlighted parts of the histogram. *B-E* show the related areas of the brain in one subject without a brain tumour.

When highlighting the lowest point of the left histogram border, it often corresponded to the inferior part of the temporal lobe where the cortex was also sometimes partially marked (Fig. 14).

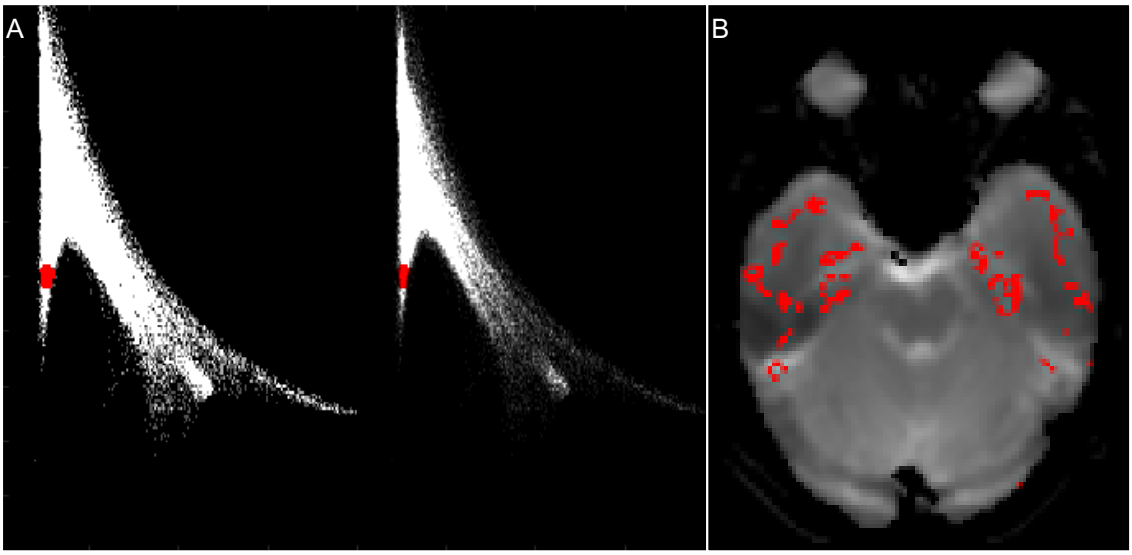

Fig. 14. Corresponding brain regions regarding the lowest point of the left histogram border. *A* shows the highlighted histogram area while *B* displays the corresponding voxels in the inferior part of the temporal lobe in a subject without a brain tumour.

In brain tumour patients, the pathologic tissue was usually not marked when highlighting the left histogram border. However, the rest of the brain, which was not pathologically changed, displayed the same layer-like markings that were also seen in subjects without a brain tumour (Fig. 15). Therefore, the tumour tissue and oedema were found to behave very differently when compared to physiological brain tissue. The layer-like markings resulting from the highlighting of the left histogram border could be observed in 85% of the patients and in all subjects without a brain tumour.

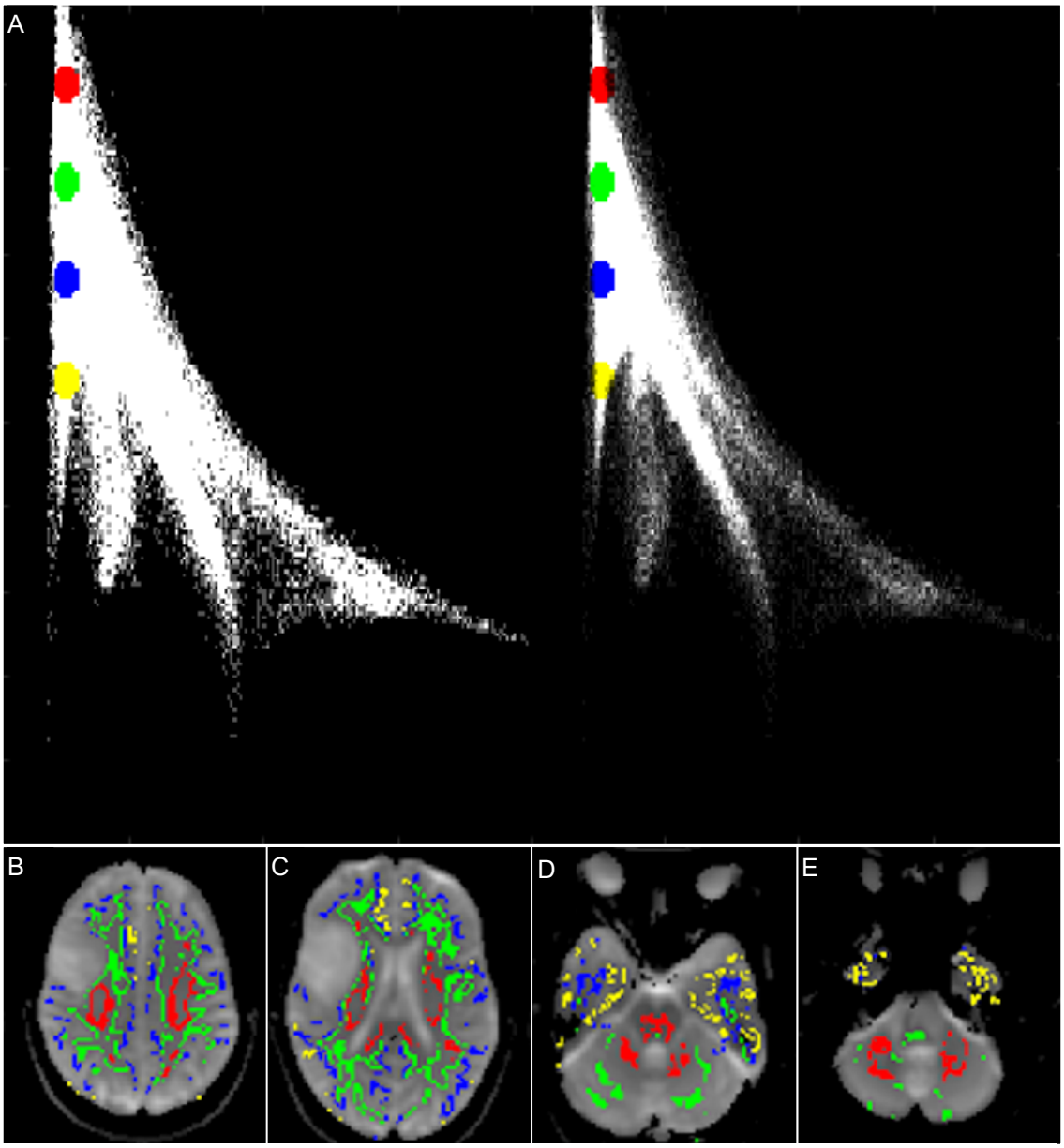

Fig. 15. Representation of the left histogram border in an oligodendroglioma patient. *A* displays the highlighted diagram area. *B-E* show the corresponding layer-like markings which do not include the tumour but otherwise look very similar when compared to a subject without a brain tumour.

As a second area, the large extension of the histogram was analysed which was located in the inferior middle portion of the diagram and can be referred to as diagram region B (Fig. 16). This spike could be found both in subjects with and without a brain tumour. When marking this large histogram extension, the highlighted areas were primarily located around the margin of the brain and along the longitudinal fissure. Furthermore, the markings seemed to follow the pattern of the sulci on the surface of the brain. Therefore, one can say that this large histogram extension corresponded to different parts of the subarachnoid space (Fig. 17). This connection between the histogram spike and the subarachnoid space could be observed in 90% of the brain tumour patients and in 90% of the healthy subjects.

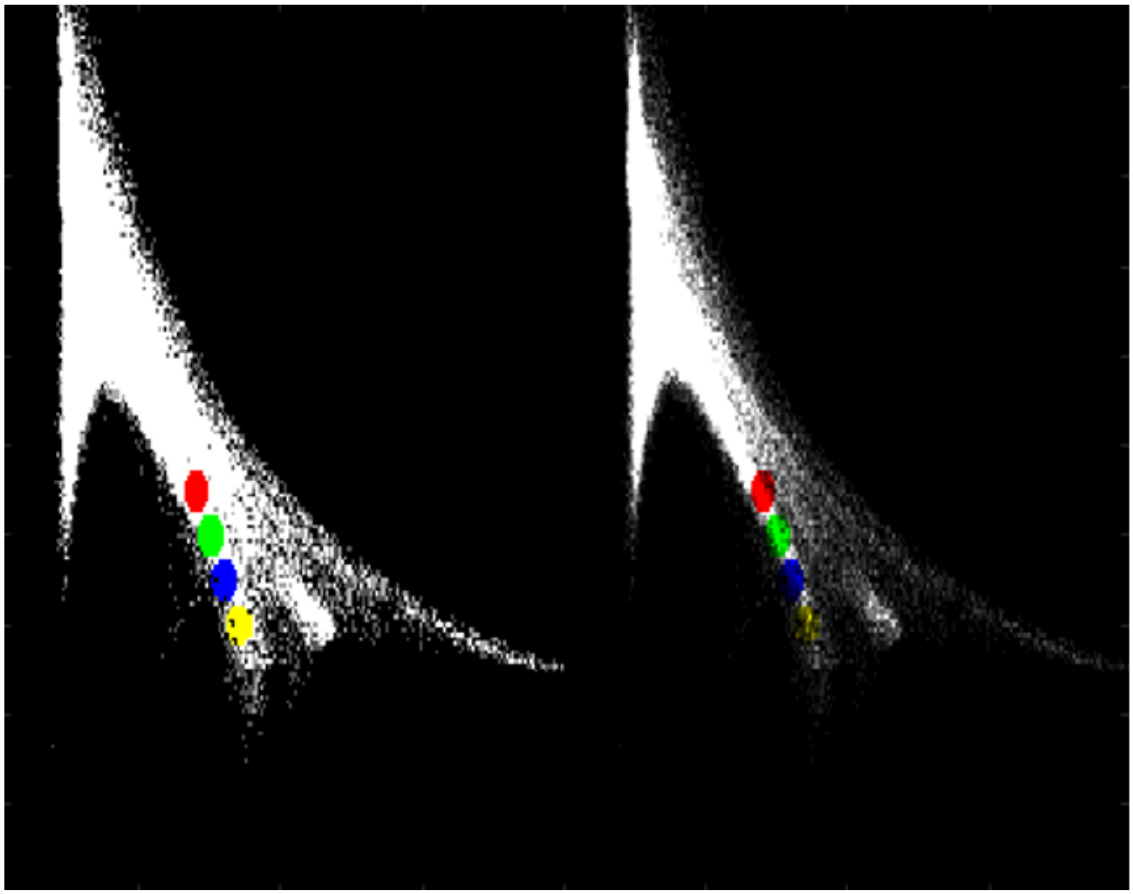

Fig. 16. Highlighted area of the histogram that generally corresponds to parts of the subarachnoid space. The diagram belongs to a subject without a brain tumour.

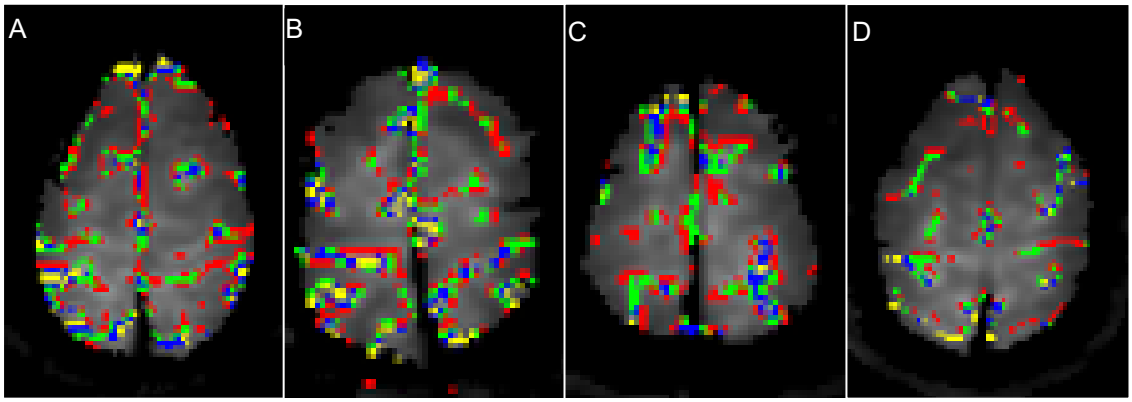

Fig. 17. Highlighted subarachnoid space corresponding to the histogram area, which is displayed in Fig. 16. *A-D* represent four different subjects without a brain tumour.

A third histogram area C was investigated which lay directly next to this large diagram spike (Fig. 18). When marking this area in the histogram, the corresponding voxels were primarily located in parts of the ventricular system (Fig. 19). Moreover, a few fractions of the subarachnoid space like the quadrigeminal cistern were also included in the highlighted brain regions. As both the ventricular system and the subarachnoid space contain cerebrospinal fluid, it is logical that they are represented very close to each other in the diffusion histogram. The relationship of this highlighted histogram area and the ventricular system could be observed in all subjects with or without a brain tumour.

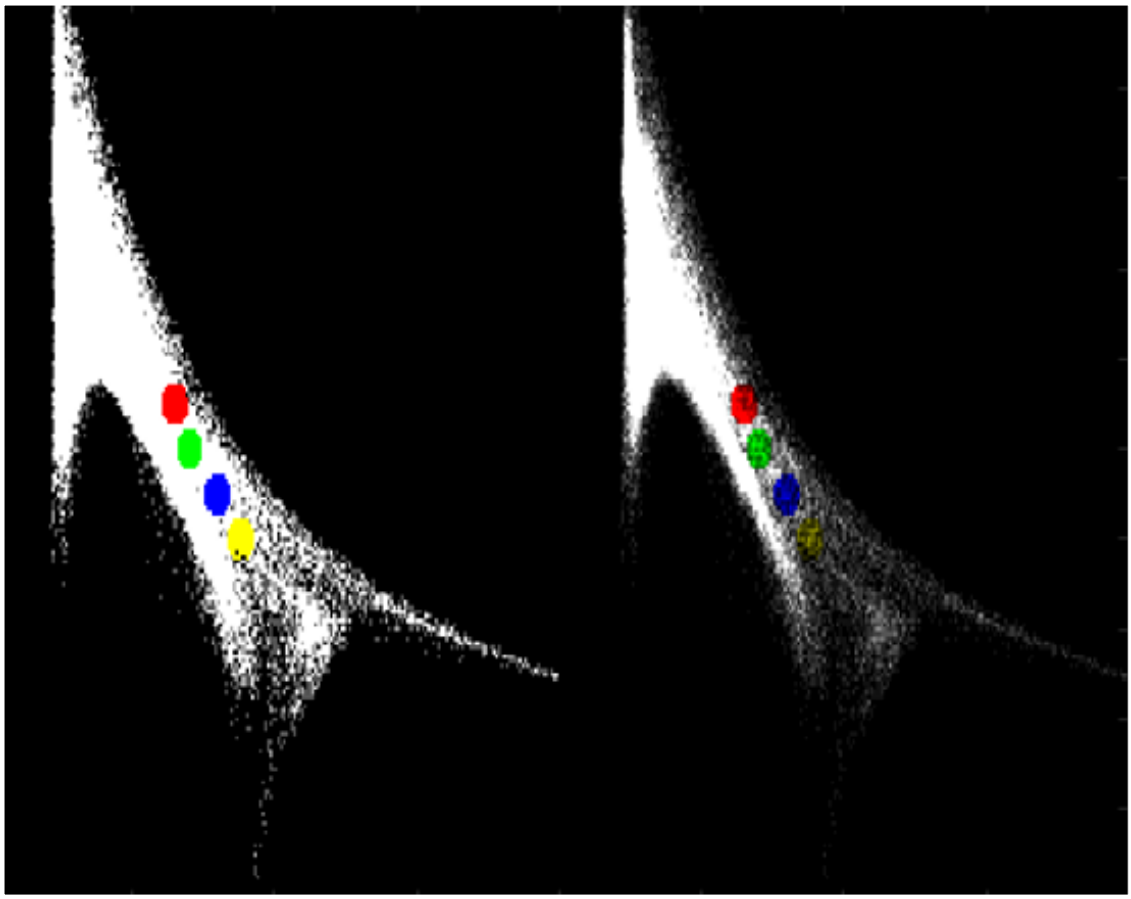

Fig. 18. Highlighted histogram area that usually relates to the ventricular system. The diagram was acquired from a subject without a brain tumour.

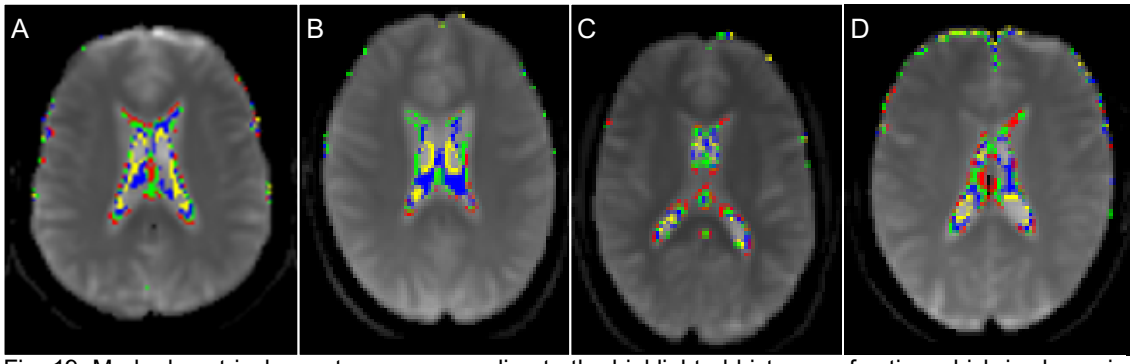

Fig. 19. Marked ventricular system corresponding to the highlighted histogram fraction which is shown in Fig. 18. *A-D* display the MR images of four different subjects without a brain tumour.

As the fourth area D, the diagram part was analysed which lies on the upper left margin of the previously described subarachnoid space histogram spike (Fig. 20). This diagram fraction principally corresponded to the nasal area in the MR images (Fig. 21). The connection between this histogram area and the nose could be observed in 87% of the brain tumour patients and in all healthy subjects.

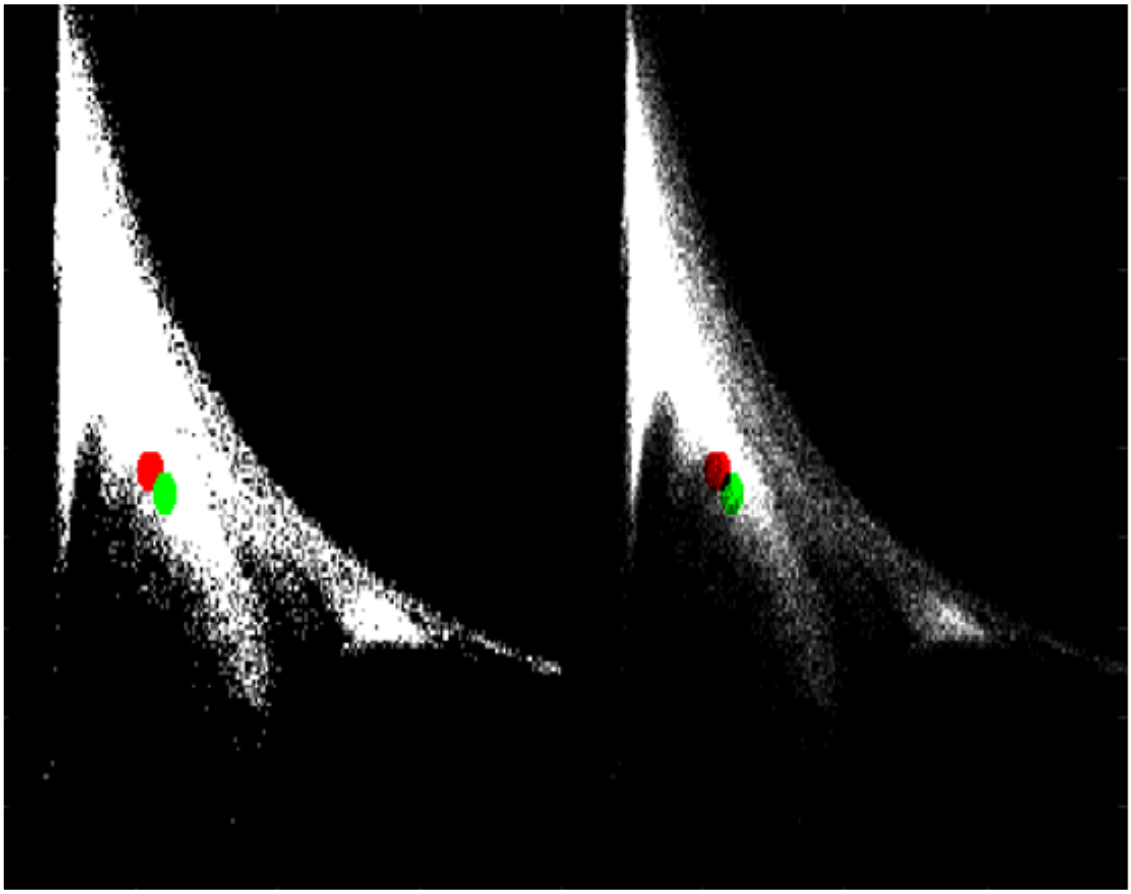

Fig. 20. Marked histogram area which generally relates to the nose. The diagram was created with the diffusion characteristics from a subject without a brain tumour.

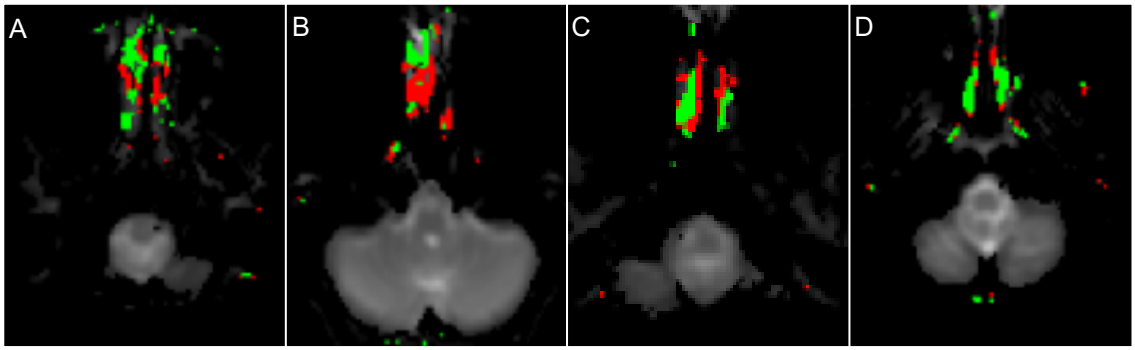

Fig. 21. Highlighted nose which relates to the histogram fraction that is shown in Fig. 20. *A-D* depict four different subjects without a brain tumour.

As shown in Fig. 20, the histogram region which often relates to the nose is located between the left border of the histogram and the subarachnoid space diagram spike. When excluding the MR image slices which depict the nose and increasing the noise level, this histogram area is generally blank in subjects without a brain tumour as seen in Fig. 22.

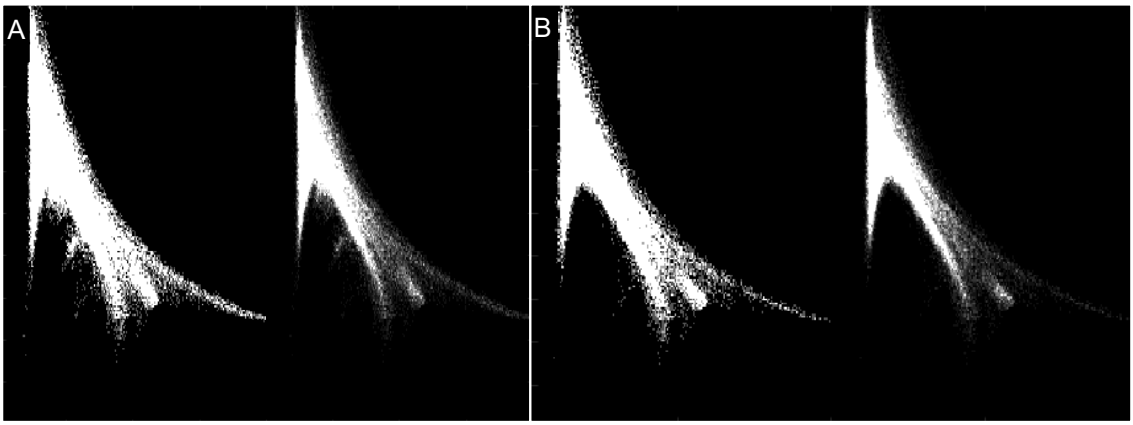

Fig. 22. Transformation of the histogram shape in a subject without a brain tumour when excluding the nose and increasing the noise level. *A* depicts the original diagram while *B* shows the changed histogram in which case there is a mostly blank area between the left histogram border and the subarachnoid space extension.

In conclusion, areas in the histogram could be defined, which separately correlated to the ventricles, parts of the subarachnoid space or the nose. These mentioned regions mainly lay in extensions, that were located inferior to the main section of the histogram. Moreover, highlighting the left histogram border regularly led to marked layer-like structures in the MR images. The same correlations between diagram areas and brain regions could be observed in healthy subjects and brain tumour patients.

3.3 Tumour and oedema regions in the histogram

3.3.1 Gliomas

As previously described, the overall histogram shape was similar when comparing healthy subjects and brain tumour patients. However, a significant difference could be observed: In patients with gliomas, there was one additional histogram spike. It was located between two diagram extensions, which could also be found in people without a glioma. Thus, a diagram without this glioma-specific extension can be referred to as possessing a physiological histogram

shape. The glioma spike was located below this physiological diagram region. In Fig. 23, a histogram from a subject without a brain tumour was compared to a diagram that belongs to a patient with a glioma. In both cases, the MR slices which depict the nose were excluded and the noise level was increased.

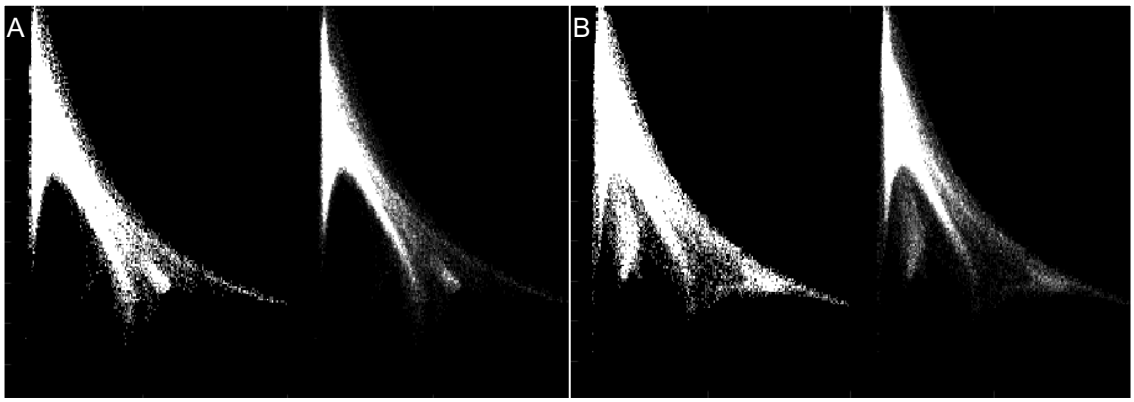

Fig. 23. Comparison of histograms belonging to one subject without and one subject with a brain tumour. *A* shows the diagram of a subject without a brain tumour whereas *B* depicts the histogram of an oligodendroglioma patient with the typical glioma spike.

To get a general overview where most of the pathological tissue is located, it was helpful to firstly delineate the tumour and oedema. Then, it was possible to examine the corresponding highlighted histogram areas. In the great majority of glioma patients, most of the pathological tissue was located in and above the characteristic histogram spike (Fig. 24).

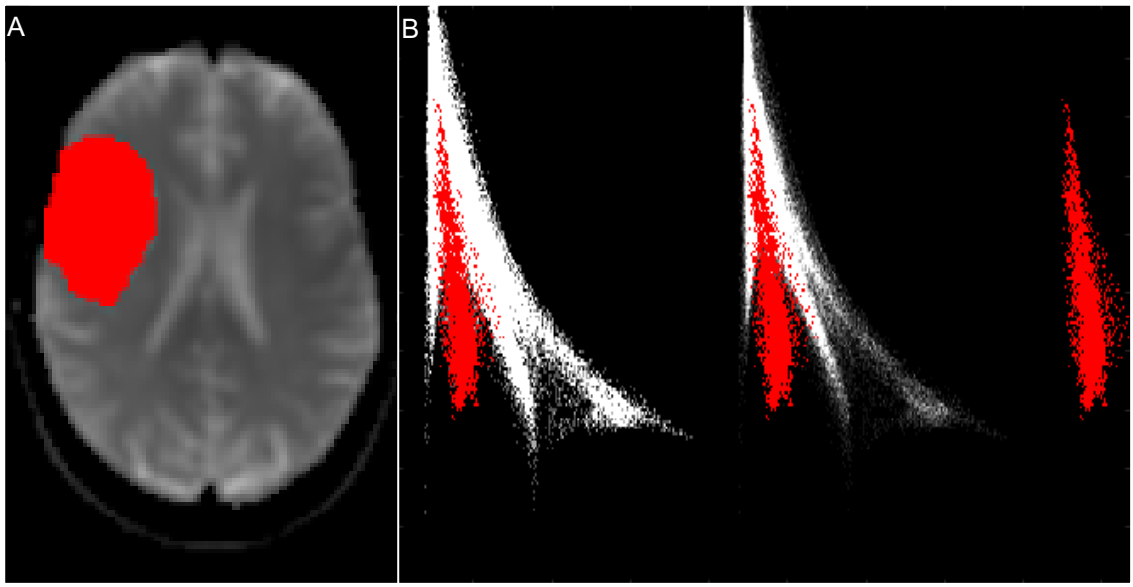

Fig. 24. Delineated oligodendroglioma/oedema and the corresponding histogram regions. *A* shows the marked pathological tissue while *B* displays the respective highlighted diagram region which is mainly located in and above the glioma-characteristic histogram spike.

In some cases, histogram areas which were located to the immediate right of the glioma-characteristic diagram spike were also highlighted (Fig. 25). This was especially the case regarding glioblastoma patients with intratumoral necrosis.

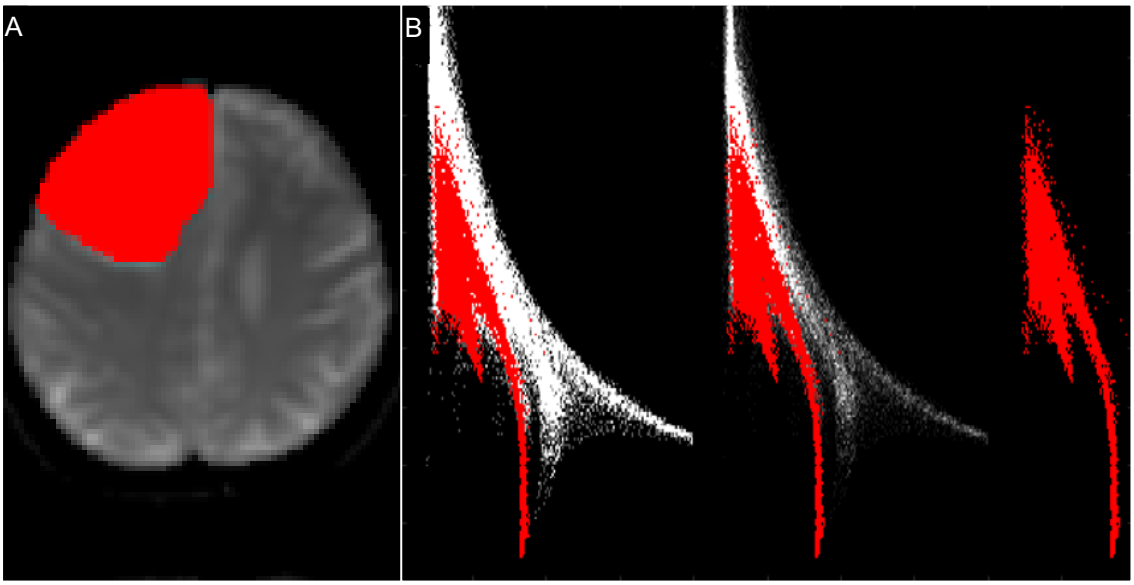

Fig. 25. Marked pathological tissue in a glioblastoma patient with intratumoral necrosis and the corresponding histogram areas. The delineated tumour and oedema are displayed in *A* while *B* shows the correlated highlighted diagram region, which is partially located on the immediate right of the glioma-characteristic spike.

In glioma patients, the part of the histogram was then highlighted which generally depicted the glioma region in the diagrams. However, it was not possible to compare the exact same MK and MD values across the whole patient population, because the tumour-equivalent parts of the histogram were slightly different for each patient. In some cases, the tumour spike was nearly vertical and thereby represented very similar MD values for the tumour tissue. However, the tumour spike could also lean to the right and thus demonstrate a greater heterogeneity of MD values regarding the tumour.

When comparing the different glioma subtypes, certain patterns regarding their representation in the histogram were observed. The tumour spike of oligodendrogliomas and astrocytomas tended to go straight down. Thus, this resulting diagram form can be referred to as the oligo/astro histogram shape.

Opposed to that, the characteristic histogram extension of glioblastomas often leaned more to the right. Hence, this specific diagram form can be referred to as the glioblastoma shape. Because of the varying diagram shape, two different sets of histogram markings were used in order to optimally define the tumour spike. The first set was used for highlighting the tumour extension in oligodendrogliomas and astrocytomas (Fig. 26 and 27).

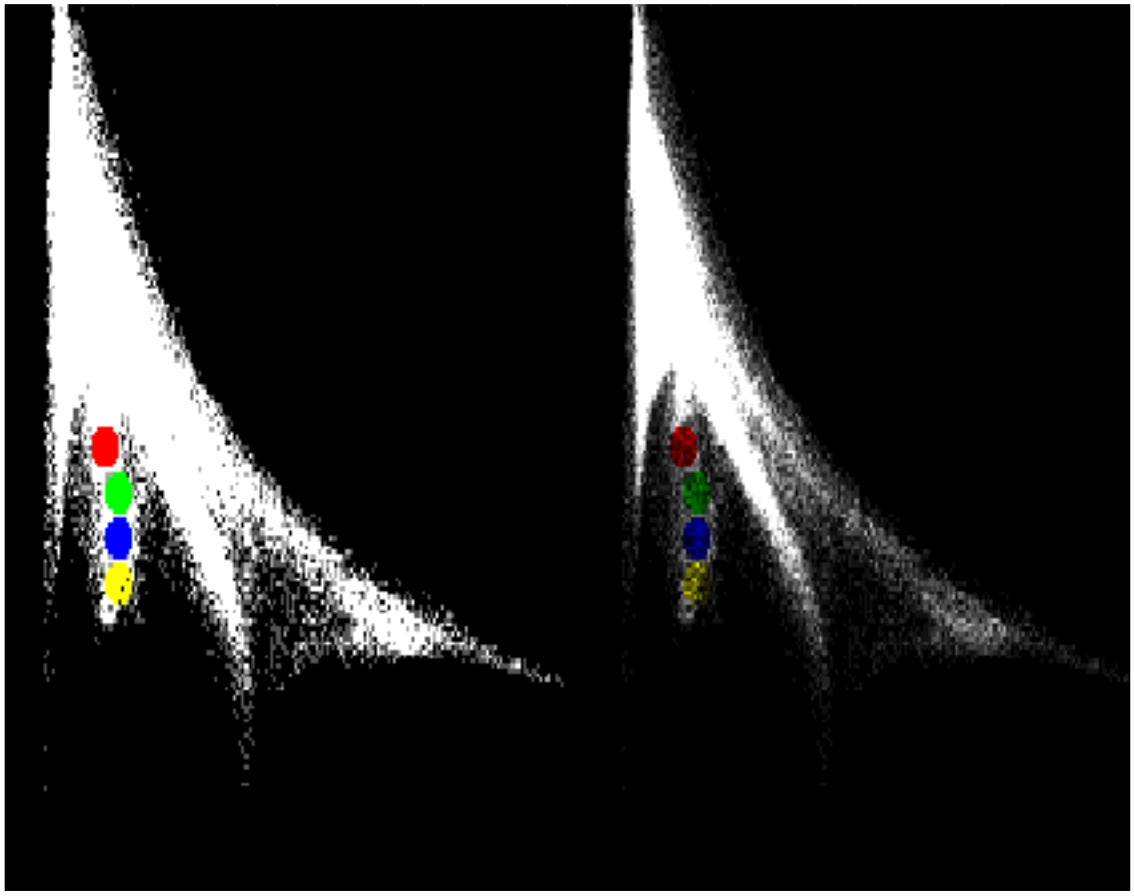

Fig. 26. Highlighted histogram area that usually corresponds to tumorous tissue and peritumoral oedema in patients with astrocytomas or oligodendrogliomas. The tumour spike is vertical and thus represents the typical oligo/astro histogram shape. This diagram belongs to a patient with an oligodendroglioma.

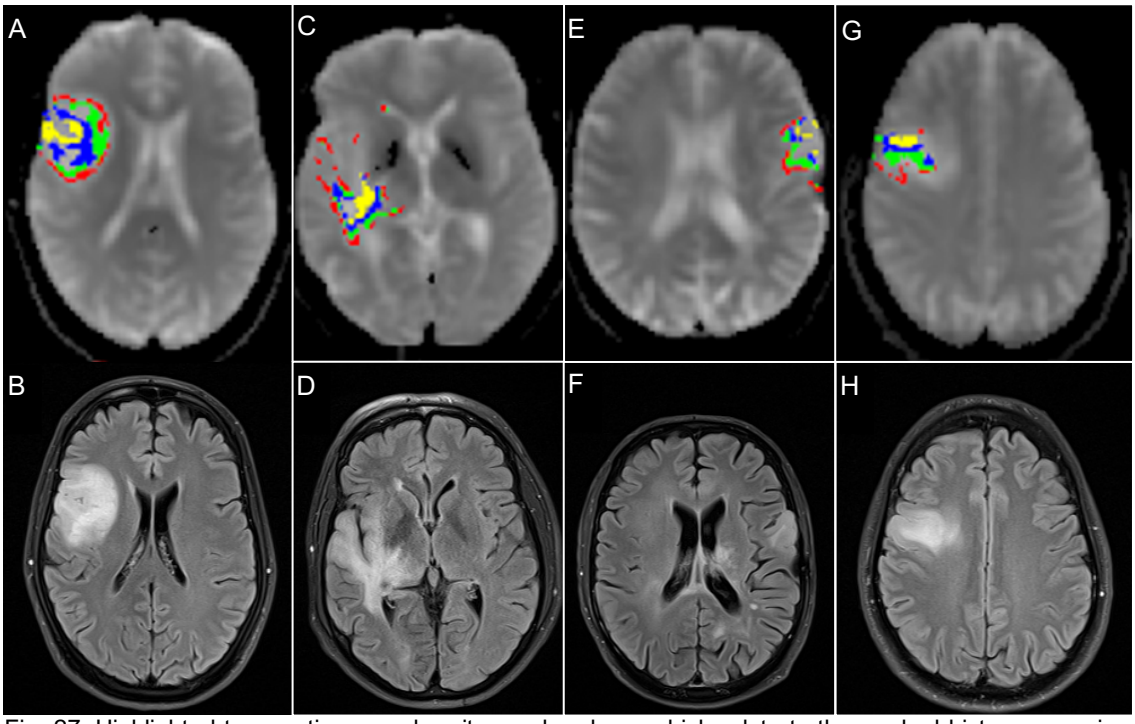

Fig. 27. Highlighted tumour tissue and peritumoral oedema which relate to the marked histogram region shown in Fig. 26. The first row of images displays the marked pathological tissue in DKI images while the second row shows the respective T2 FLAIR images. *A-D* represent two oligodendroglioma patients whereas *E-H* represent two astrocytoma patients.

The second set of histogram markings for the glioma spike was applied on glioblastoma patients (Fig. 28 and 29).

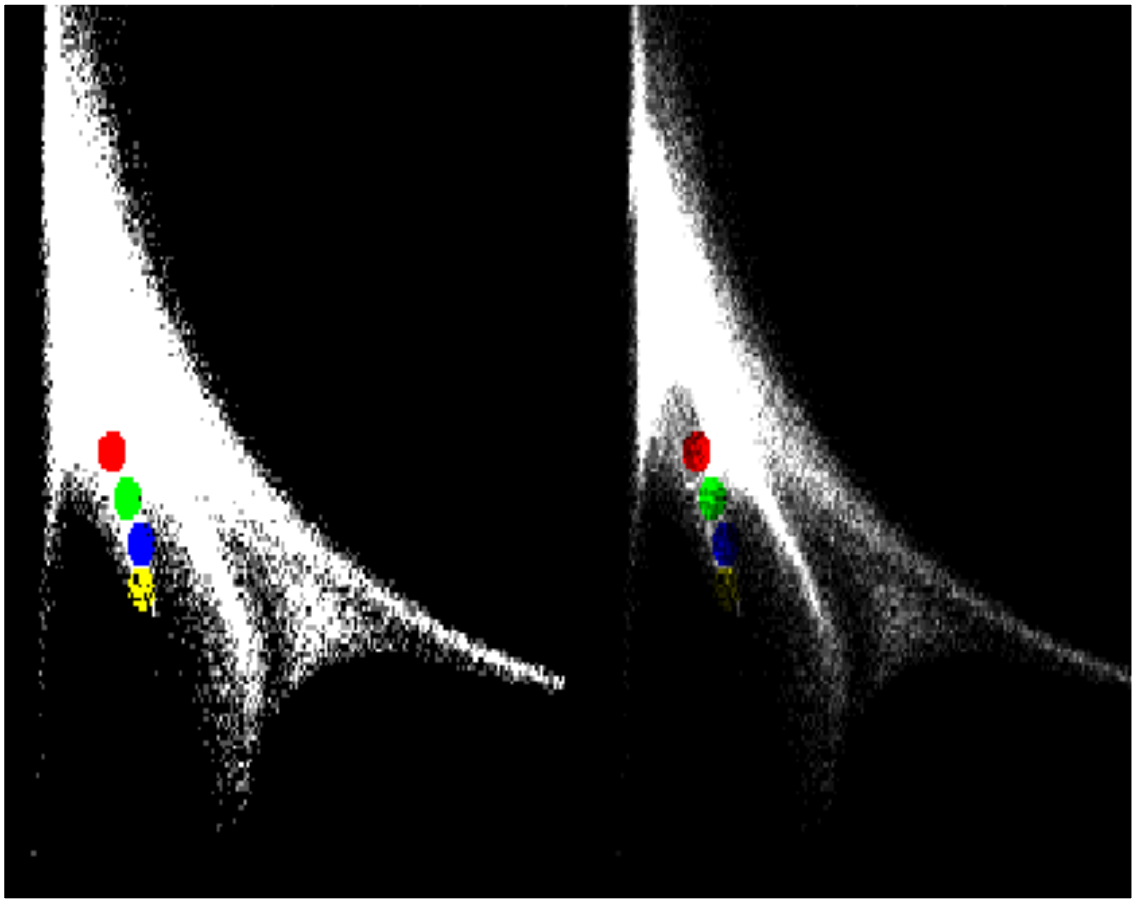

Fig. 28. Highlighted histogram region that generally relates to tumorous tissue and peritumoral oedema in patients with larger glioblastomas. This diagram was generated with diffusion characteristics from a glioblastoma patient and thus represents the typical glioblastoma histogram shape.

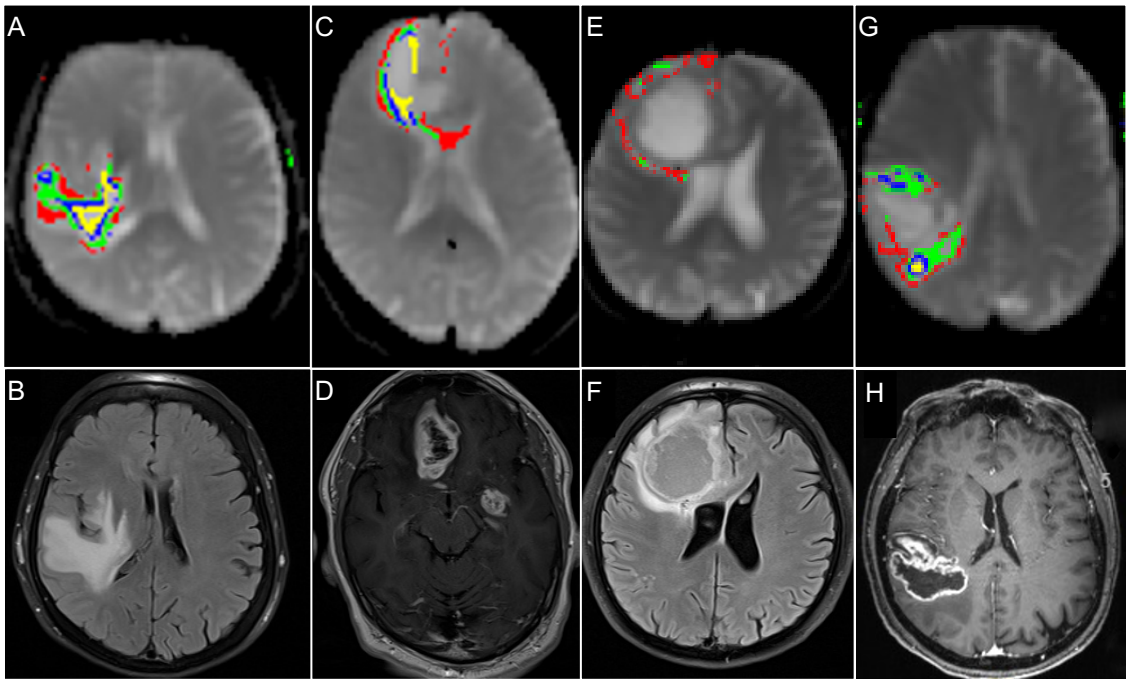

Fig. 29. Marked tumorous tissue and peritumoral oedema which relate to the highlighted histogram fraction displayed in Fig. 28. The images display four subjects with a glioblastoma: The first row represents the marked vital tumour and oedema in DKI images while the second row shows T2 (*B* and *F*) or contrast-enhanced T1 images (*D* and *H*) of the respective patients.

Exceptions to the trends of characteristic tumour spike shapes in different glioma subgroups were smaller glioblastomas. The diagrams of these tumours resembled the oligo/astro histogram shape (Fig. 30). This stands in contrast to larger glioblastomas which usually possessed the typical glioblastoma histogram shape.

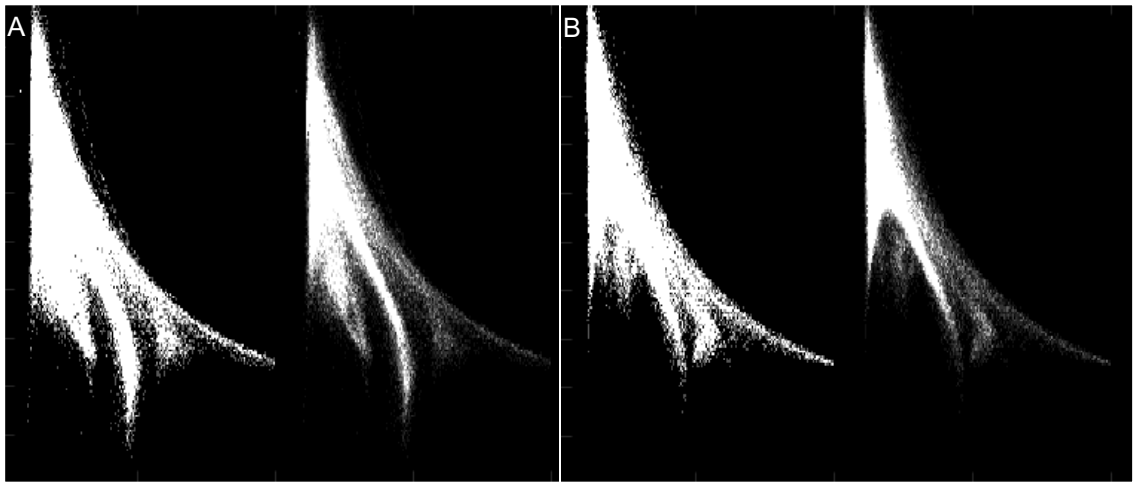

Fig. 30. Histograms of two different glioblastomas. *A* shows a larger tumour with a glioblastoma histogram shape while *B* displays a smaller glioblastoma with an oligo/astro histogram shape.

When highlighting the glioma histogram spike with the respective set of markings for the specific tumour type, most of the tumour tissue was often marked in the MR images. Moreover, the peritumoral oedema corresponded as well to the glioma histogram spike and was therefore also highlighted. Hence, this diagram extension can also be referred to as the glioma/oedema histogram spike. It was difficult to distinguish between solid tumorous lesions and the surrounding oedema merely by comparing their distribution of MK and MD values in the histogram. The area of the oedema was located in different parts of the glioma/oedema spike, depending on the patient. It was therefore not possible to derive an approximate position where the oedema was mainly located in this histogram spike. Because of their shared location in the diagram, oedema and vital tumorous tissue were analysed together in the case of gliomas. Another reason for this approach is the difficulty of clearly separating tumour and peritumoral oedema on the MR images.

When using the first set of histogram markings for the oligo/astro histogram shape in the four oligodendroglioma patients, a large fraction of the vital tumour and oedema area was marked in all subjects. Furthermore, this set of histogram markings corresponded to a great portion of the vital tumour and oedema region in two of the four astrocytomas. In the case of the other two astrocytomas, smaller parts of these pathologic areas were highlighted.

The second set of histogram markings was used for the glioblastoma histogram shape. When using these markings for the glioblastoma patients, a large fraction of the vital tumour and oedema region was highlighted in 13 of the 20 subjects (65%). Some of the other tumours, that were not highlighted as clearly, were often small and thus did not possess a big tumour spike, which could be marked properly with the standard histogram coordinates. In the case of very large tumours and oedemas, the histogram markings were sometimes too small to highlight the glioma/oedema spike well. This resulted in an incomplete marking of the pathological tissue in the MR images.

Additionally, it was already described previously that the smaller glioblastomas often had an oligo/astro histogram shape. Therefore, the first set of histogram markings was sometimes better suited in order to highlight the tumour spike in the case of smaller glioblastomas. Thus, the glioblastomas for which the majority of the tumour was not highlighted by the second set of histogram markings, were also analysed with the first set of diagram markings. In the respective seven patients, it was however not possible to highlight most of the vital tumour and oedema area, even with the first set of histogram markings. Nevertheless, in three of these seven patients, the first set of markings highlighted a larger tumour region than the second set. Furthermore, previous radiation therapy did not impact the histogram shape or the representation of the tumour in the diagram.

Glioblastomas frequently had a central necrotic core. This tissue often corresponded to the area on the immediate right of the tumour spike (Fig. 31 and 32). It was regularly a part of the large physiological histogram peak, which corresponded to parts of the subarachnoid space as previously described. The necrosis was often observed in the left fraction of this large histogram extension. However, there were also some irregularities: Sometimes, the necrosis was situated in the middle of the histogram's physiological part or in the tumour spike. Due to its different location in the diffusion diagram, the central necrotic areas were analysed separately from the vital tumour tissue and the peritumoral oedema.

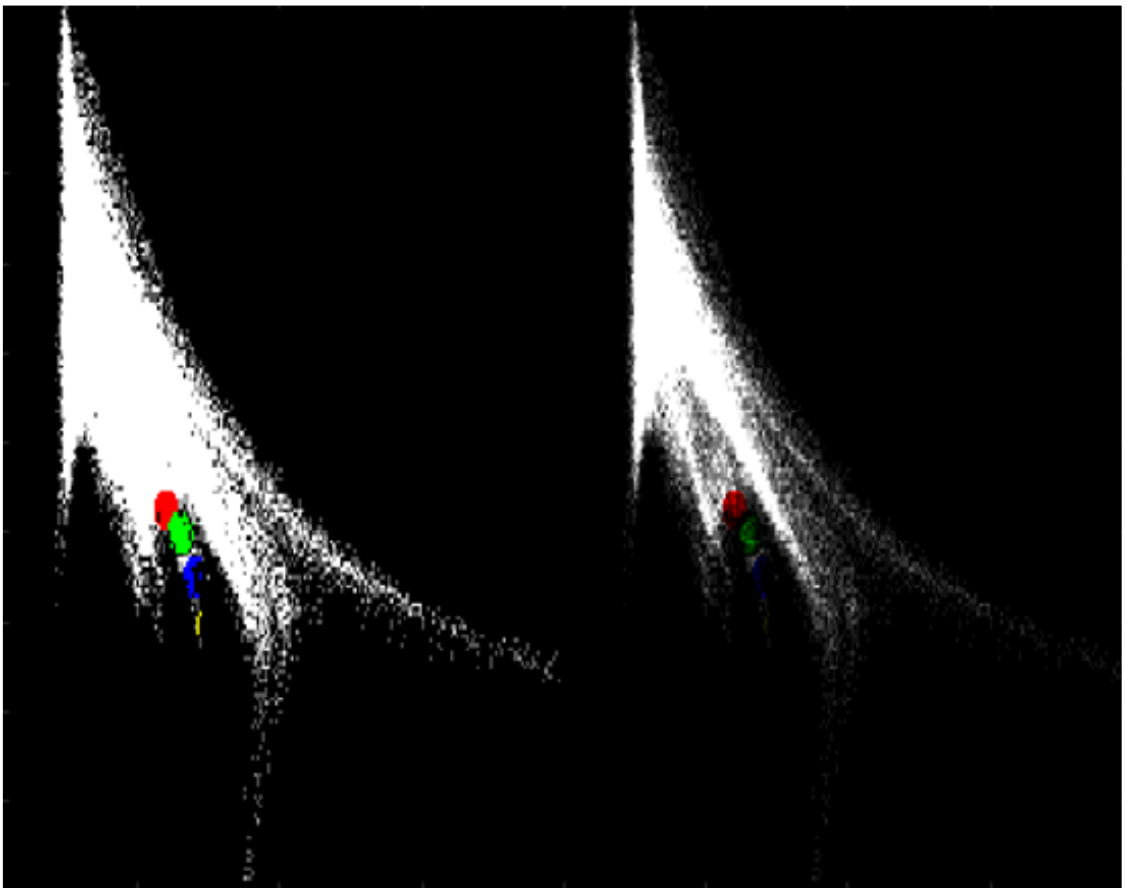

Fig. 31. Highlighted histogram area that often relates to intratumoral necrosis in glioblastomas.

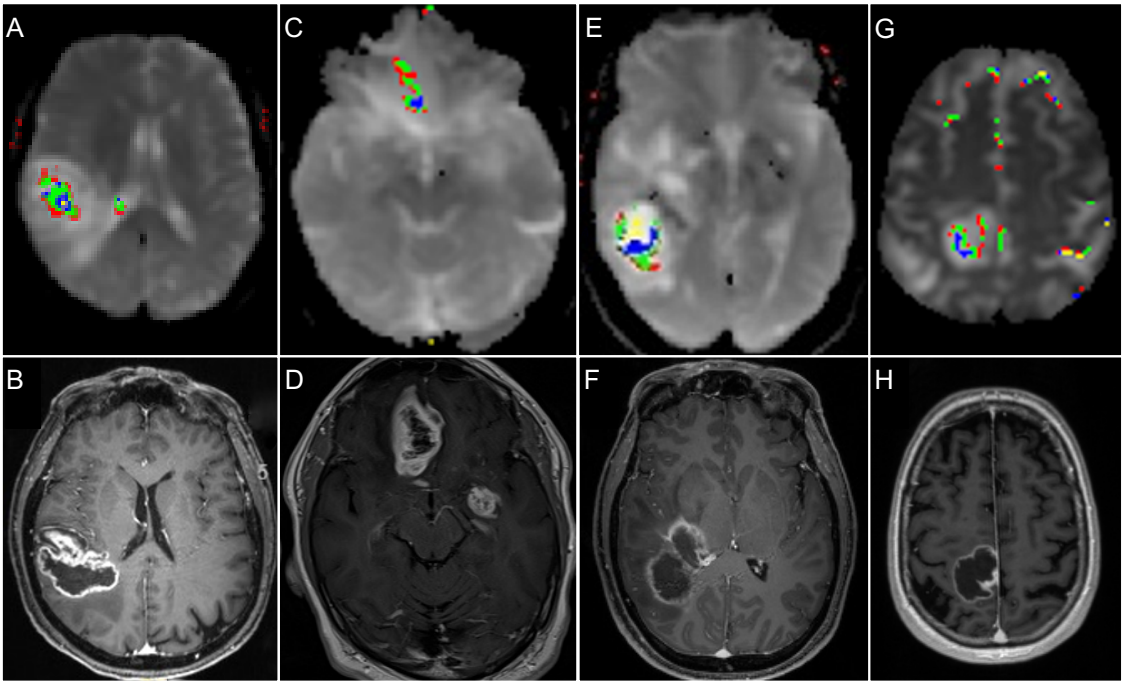

Fig. 32. Marked intratumoral necrosis which corresponds to the highlighted histogram region displayed in Fig. 31. The images display four patients with glioblastomas. The first row represents the highlighted intratumoral necrosis in DKI images, whereas the second row shows the respective contrast-enhanced T1 images.

As described previously, a histogram mask was generated, which usually encompassed the glioma diagram spike. By colouring the mask, it is possible to further investigate the heterogeneity of tumour tissue and oedema. The first way of distributing the colours over the histogram mask was especially helpful regarding the differentiation between the upper and lower fractions of the glioma/oedema spike. Generally, the points with lower MK values in the glioma extension regularly corresponded to central parts of the vital tumour tissue and the oedema (Fig. 33). Meanwhile, the spots with the higher MK values were often located near the margins of the pathological tissue. These spots in the tumour spike with the higher MK values lay closer to the normal physiological portion of the histogram. Due to this distribution of colours, the vital tumour tissue and oedema often demonstrated characteristic layer-like markings.

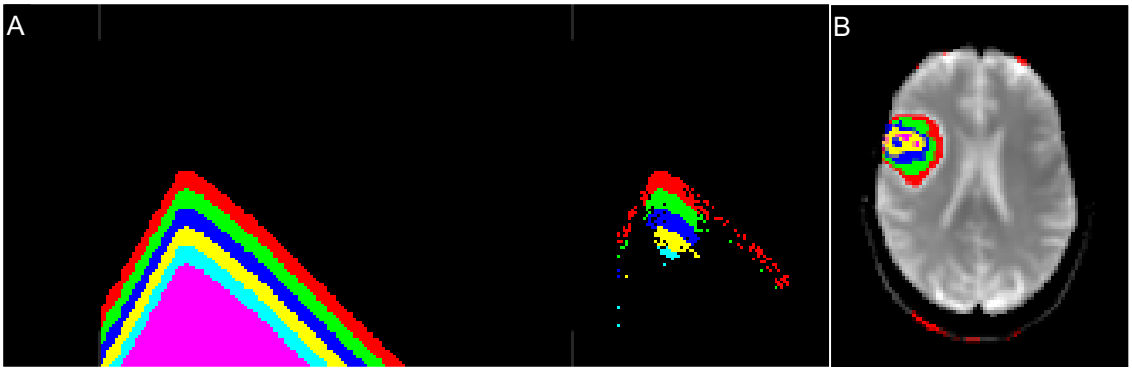

Fig. 33. Analysis of intratumoral heterogeneity by colouring the histogram mask. *A* displays the coloured histogram mask on the left and shows the applied mask on an oligodendroglioma patient on the right. *B* displays the corresponding marked voxels in a respective MR image, where one can see the characteristic layer-like markings.

As previously mentioned, the intratumoral necrosis was often represented on the right side of the glioma spike in the diagram. The histogram mask normally encompassed this region as well. When colouring the mask in a way that was useful for separating the left from the right mask fractions, it was often possible to distinguish the vital tumour tissue and oedema from intratumoral necrosis (Fig. 34). Overall, 13 glioblastomas with necrosis were investigated. In six cases, the necrosis was located in the right part of the histogram mask and a clear differentiation between vital tumour tissue/oedema and necrosis was possible. This evident discrimination was also observed in five other cases where the necrosis was not located inside the histogram mask. Here, the necrosis was not

highlighted in comparison to vital tumour tissue and oedema. The remaining two patients possessed only small intratumoral necrotic areas, which could not be clearly distinguished from vital tumour tissue and oedema. In conclusion, the differentiation between vital tumour/oedema and necrosis was possible in 85% of the patients.

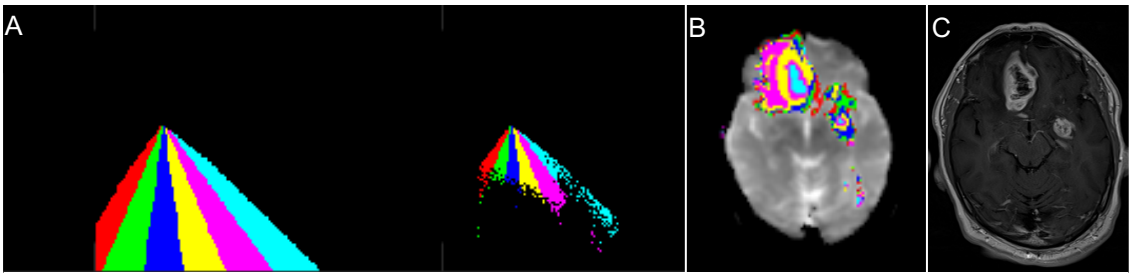

Fig. 34. Distinguishing the vital tumour tissue and oedema from necrosis by colouring the histogram mask. *A* shows the coloured mask on the left and the applied mask on a glioblastoma patient on the right. *B* displays the highlighted voxels in a DKI image of this patient while *C* shows a contrast-enhanced T1 MR image. The necrosis is predominantly marked blue, which is the colour furthest to the right in the mask.

Furthermore, the central parts of the vital tumour and oedema region were often represented in the right portion of the histogram mask while the outer border of the pathological region tended to correspond to the left histogram mask fraction (Fig. 35).

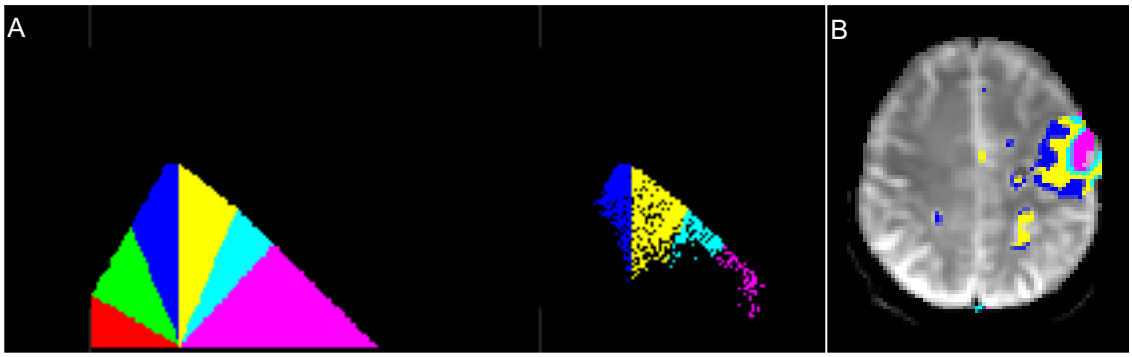

Fig. 35. Separation of the central parts and the outer border of the vital tumour and oedema. *A* shows the coloured histogram mask and its application on an astrocytoma patient. *B* shows the corresponding highlighted voxels in an MR image. The pink area represents a resection cavity from a previous operation.

As previously described, two different ways of colouring the histogram mask were both helpful in distinguishing between left and right mask fractions. The diagram mask that is shown in Fig. 35 is especially suitable for roughly separating the glioma/oedema histogram extension in a left and right part. Opposed to that, the

mask displayed in Fig. 36 separates the glioma/oedema spike in more fractions. Therefore, it is particularly convenient for demonstrating the intratumoral heterogeneity which is characteristic for gliomas: Most of the tumours are highlighted in various colours when applying this histogram mask.

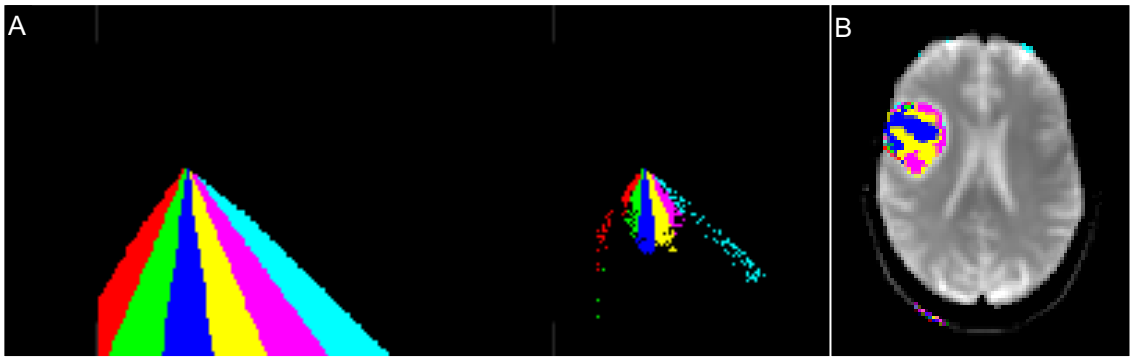

Fig. 36. Applied coloured histogram mask that demonstrates intratumoral heterogeneity in gliomas. *A* displays the mask and its application on the diagram of an oligodendroglioma patient. *B* shows the corresponding marked voxels in an MR image where the multiple colours demonstrate the intratumoral heterogeneity.

In conclusion, there was a spike of the diagram that corresponded to vital tumour tissue and peritumoral oedema of gliomas and can therefore be described as the glioma/oedema histogram spike. The form of this spike varied and was influenced by the tumour subtype: Oligodendrogliomas and astrocytomas often exhibited a different histogram form when compared to glioblastomas. Furthermore, the intratumoral necrosis of glioblastomas was normally not located in the glioma/oedema spike.

3.3.2 Meningiomas

The representation of meningioma tissue in the respective histograms was analysed. In Table 2, the six analysed meningiomas of five patients are displayed with their corresponding histogram areas.

Table 2. Overview of meningioma patients and the corresponding histogram regions, which relate to the tumours.

Patients	WHO grade	Recurrent	Previous operation	Radiation	Corres-ponding histogram area
Patient 1	Grade 2	no	no	no	Upper part of the histogram
Patient 2	Grade 2	yes	yes	no	Upper part of the histogram
Patient 3	Unclear	no	no	yes	Right border of the histogram
Patient 4 – Tumour 1	Grade 1 before the recurrence	yes	yes	yes	Near the subarachnoid spike
Patient 4 – Tumour 2	unclear	no	no	no	Upper part of the histogram
Patient 5	Grade 3	yes	yes	yes	Intratumoral necrosis in the upper part of the histogram

The meningiomas of patients 1 and 2 were both located in the upper part of the histogram (Fig. 37 and 38). They both were similar in the sense that they had been classified as WHO grade 2 tumours and had received no radiation or chemotherapy.

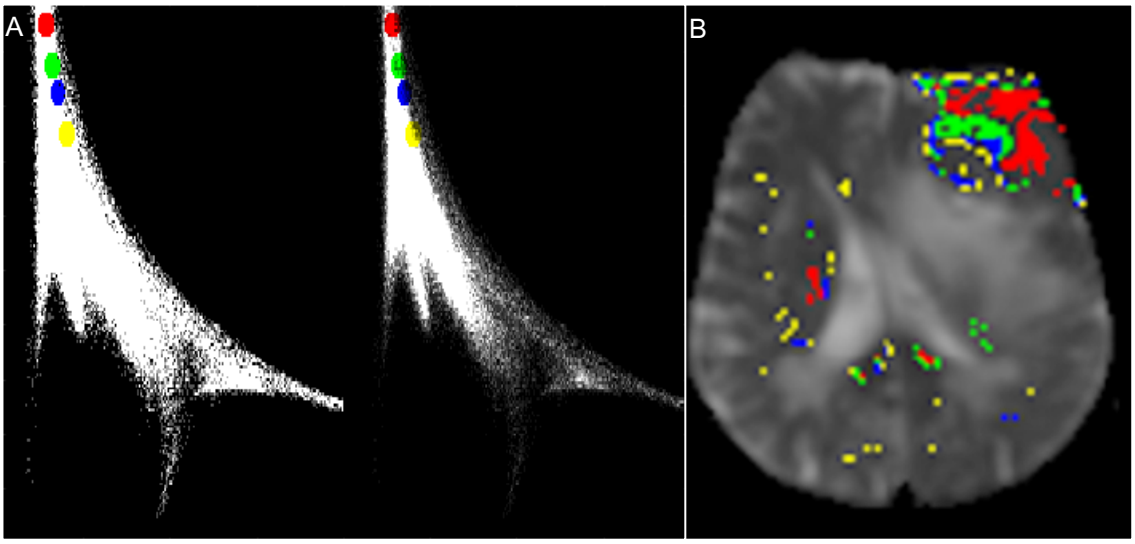

Fig. 37. Representative histogram region regarding the grade 2 meningioma of patient 1. *A* depicts the marked histogram area whereas *B* displays the related highlighted voxels in an MR image.

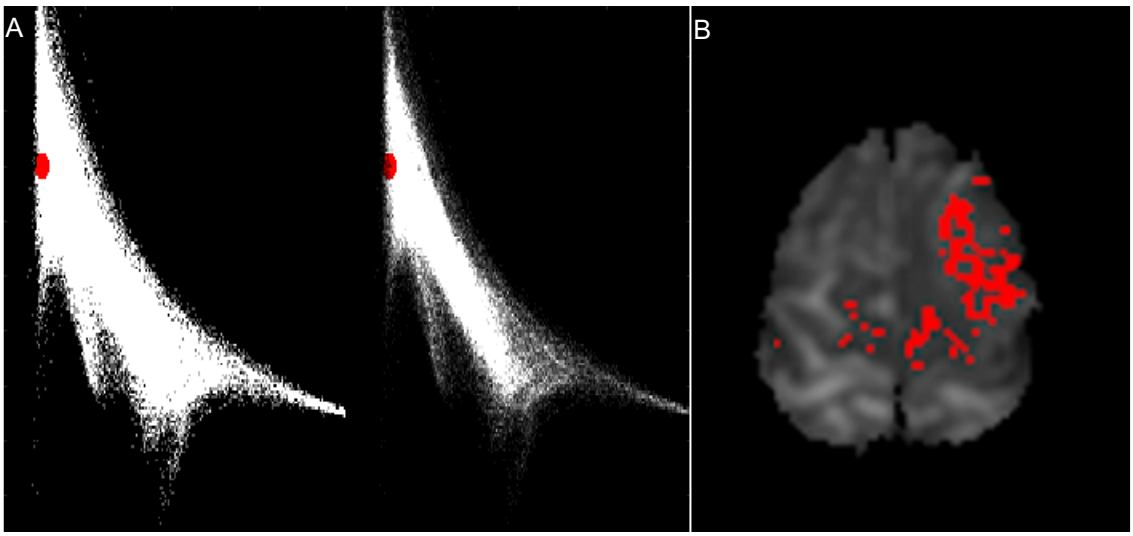

Fig. 38. Highlighted histogram area which relates to the grade 2 meningioma of patient 2. *A* shows the highlighted histogram area while *B* displays the corresponding marked voxels in the respective MR image.

In contrast to these first two cases, the meningioma of patient 3 corresponded to a histogram area that stretched itself along the right border of the diagram (Fig. 39).

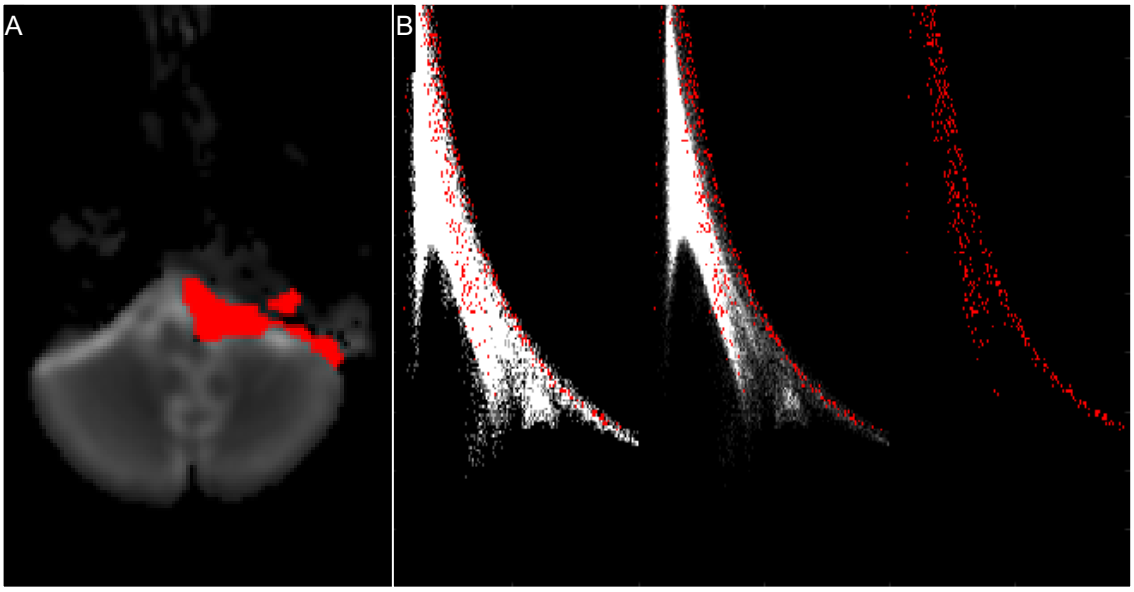

Fig. 39. Corresponding histogram region concerning the meningioma of patient 3. *A* shows the delineated marked tumour while *B* displays the highlighted correlated histogram area.

In contrast to the previous patients, the first meningioma of patient 4 was located in a lower histogram region, which usually corresponds to the subarachnoid space (Fig. 40).

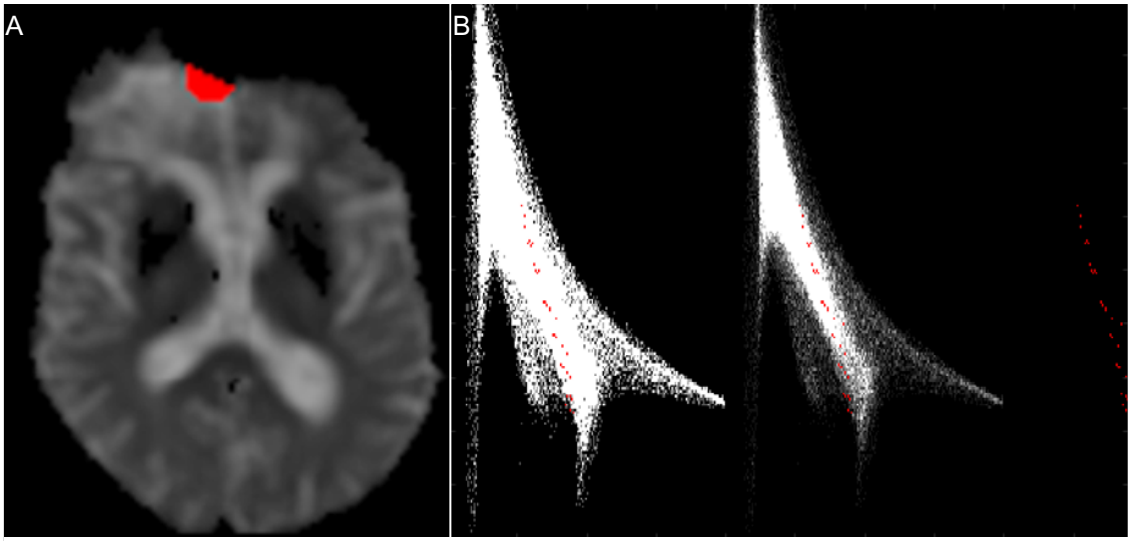

Fig. 40. Corresponding histogram area relating to the first meningioma of patient 4. *A* depicts the highlighted brain region while *B* shows the corresponding histogram area.

The second meningioma of patient 4 was located in the upper half of the diagram and was therefore found to behave differently than the first tumour of this patient (Fig. 41).

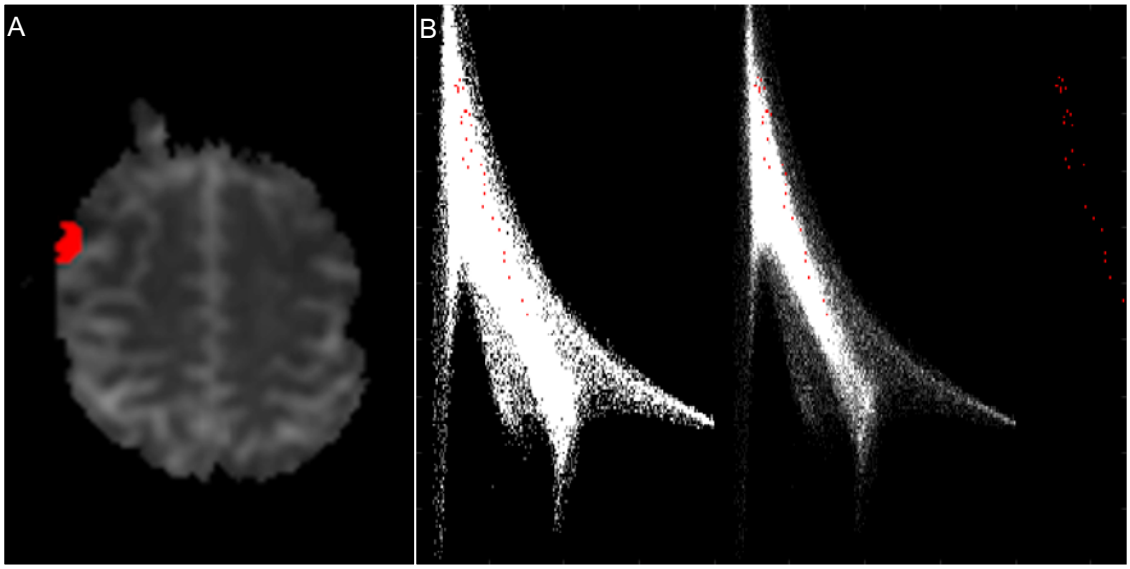

Fig. 41. Representative histogram region of the second meningioma of patient 4. *A* depicts the marked fraction of the tumour while *B* shows the corresponding highlighted histogram area.

Regarding patient 5, there was not enough vital meningioma tissue to analyse. However, there was a larger area of intratumoral necrosis, whose representation in the histogram was investigated: This necrotic area mainly corresponded to the upper half of the diagram (Fig. 42).

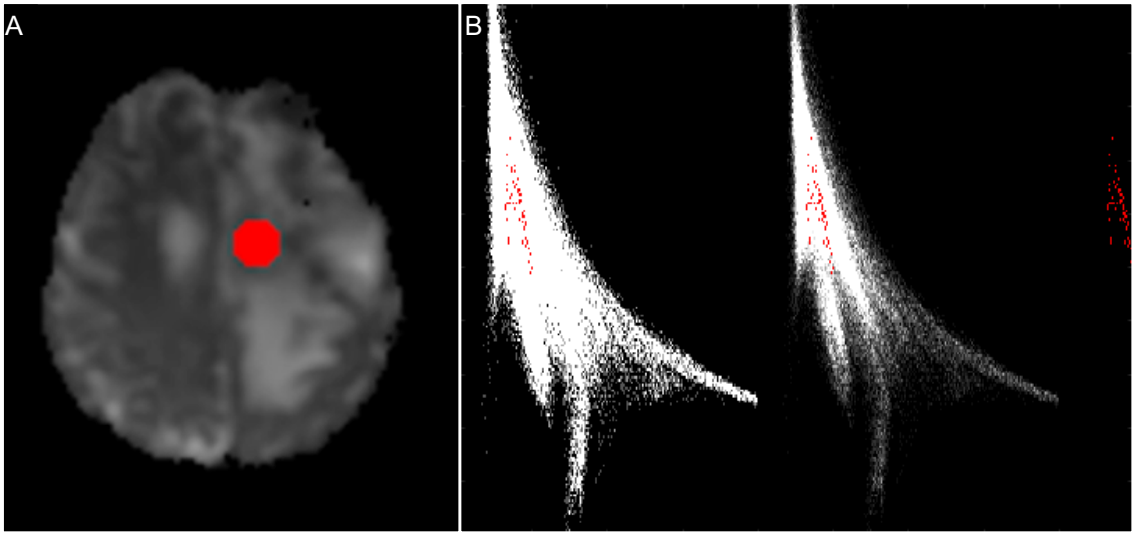

Fig. 42. Highlighted histogram region relating to intratumoral necrosis of the grade 3 meningioma which belongs to patient 5. *A* displays the marked necrosis while *B* shows the highlighted related histogram region.

In some cases, the corresponding histogram spots of the tumour were widely scattered in the main part of the diagram. Therefore, it was difficult to highlight one area of the histogram, which related to most of the tumorous tissue. If it was still attempted to mark one histogram area, where some of the corresponding tumour spots lay, larger areas of physiological brain tissue were often simultaneously highlighted. This was because the corresponding histogram spots of the tumour were mostly located in the physiological fraction of the diagram in the case of meningiomas.

In conclusion, the location of meningiomas in the histogram could not be generalised as easily when compared to gliomas. However, one could discriminate reliably between gliomas and meningiomas by analysing their respective histograms: While the data did not show any area in the diagram where all meningiomas were represented, none of them were located in the typical glioma region of the histogram.

3.3.3 Metastases

The representation of brain metastases in the diffusion histograms was investigated. The six analysed patients with metastases and their corresponding histogram areas are displayed in Table 3 along with more clinical information.

Table 3. Overview of patients with metastases that were analysed and the corresponding histogram areas of the tumours.

Patients	Primary tumour	Previous operation near the metastasis	Radiation	Corresponding histogram area
Patient 6	Breast cancer	no	yes	Both metastases near the subarachnoid space spike
Patient 7	Breast cancer	yes	yes	Both metastases near the subarachnoid space spike
Patient 8	Non-small-cell lung cancer (NSCLC)	no	yes	Near the subarachnoid space spike
Patient 9	Large cell neuroendocrine lung carcinoma (subtype of NSCLC)	no	no	Upper half of the histogram
Patient 10	Nodular malignant melanoma	no	yes	All three metastases in the upper half of the histogram
Patient 11	Nodular malignant melanoma	no	no	Upper half of the histogram

Both patients with breast cancer (patient 6 and 7) each had two brain metastases. Patient 6 was human epidermal growth factor receptor 2 (HER2) negative while the other one was HER2 positive. Both patients were oestrogen receptor (ER) and progesterone receptor (PR) positive. All four of the tumours were located in the inferior region of the diagram, that lay near the extension which usually corresponded to subarachnoid space (Fig. 43 and 44).

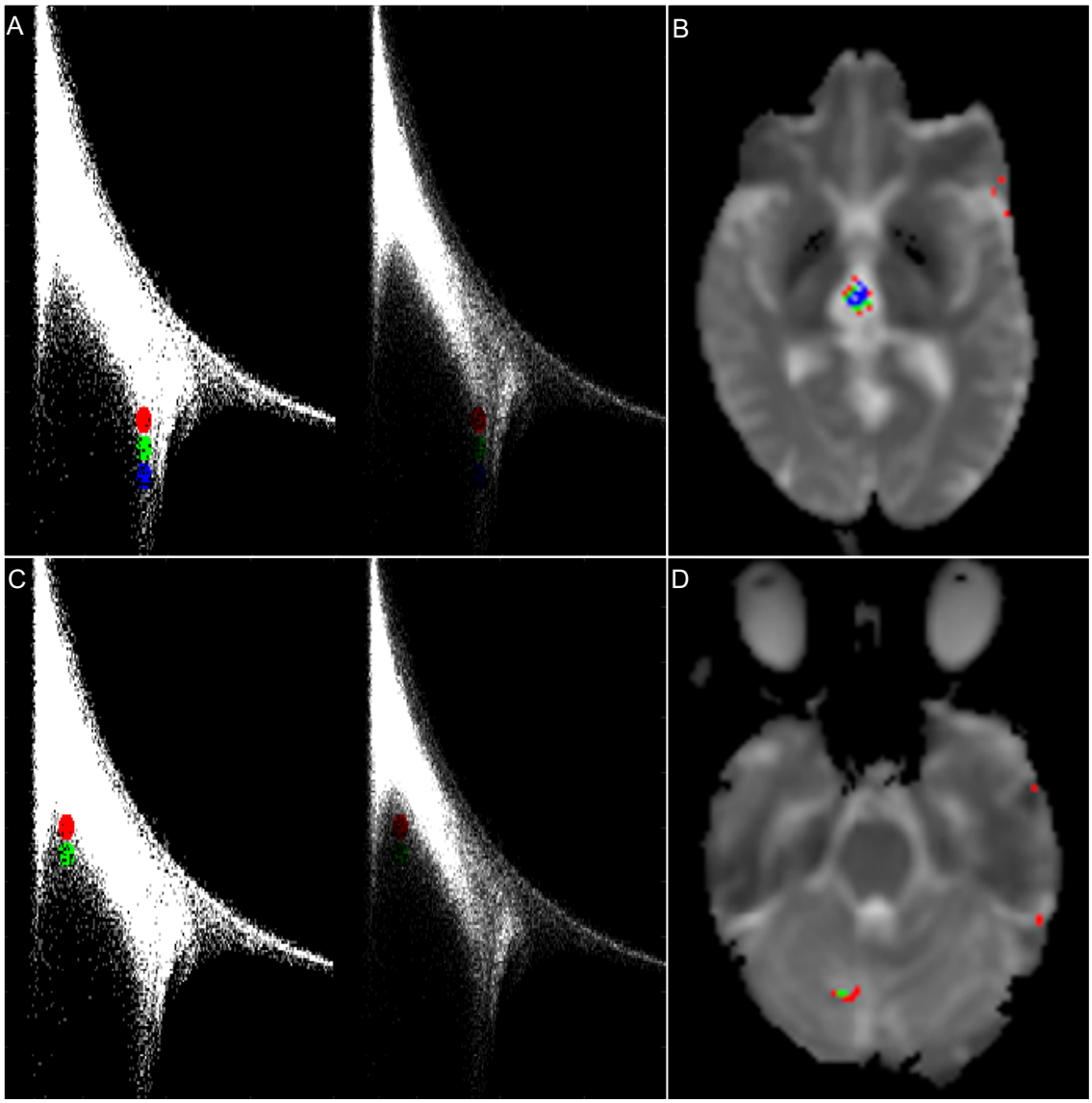

Fig. 43. Histogram areas corresponding to two metastases of a breast cancer patient (patient 6). *A* displays the highlighted area of the histogram, which corresponds to the first metastasis *(B)*, while *C* marks the diagram region for the second metastasis *(D)*.

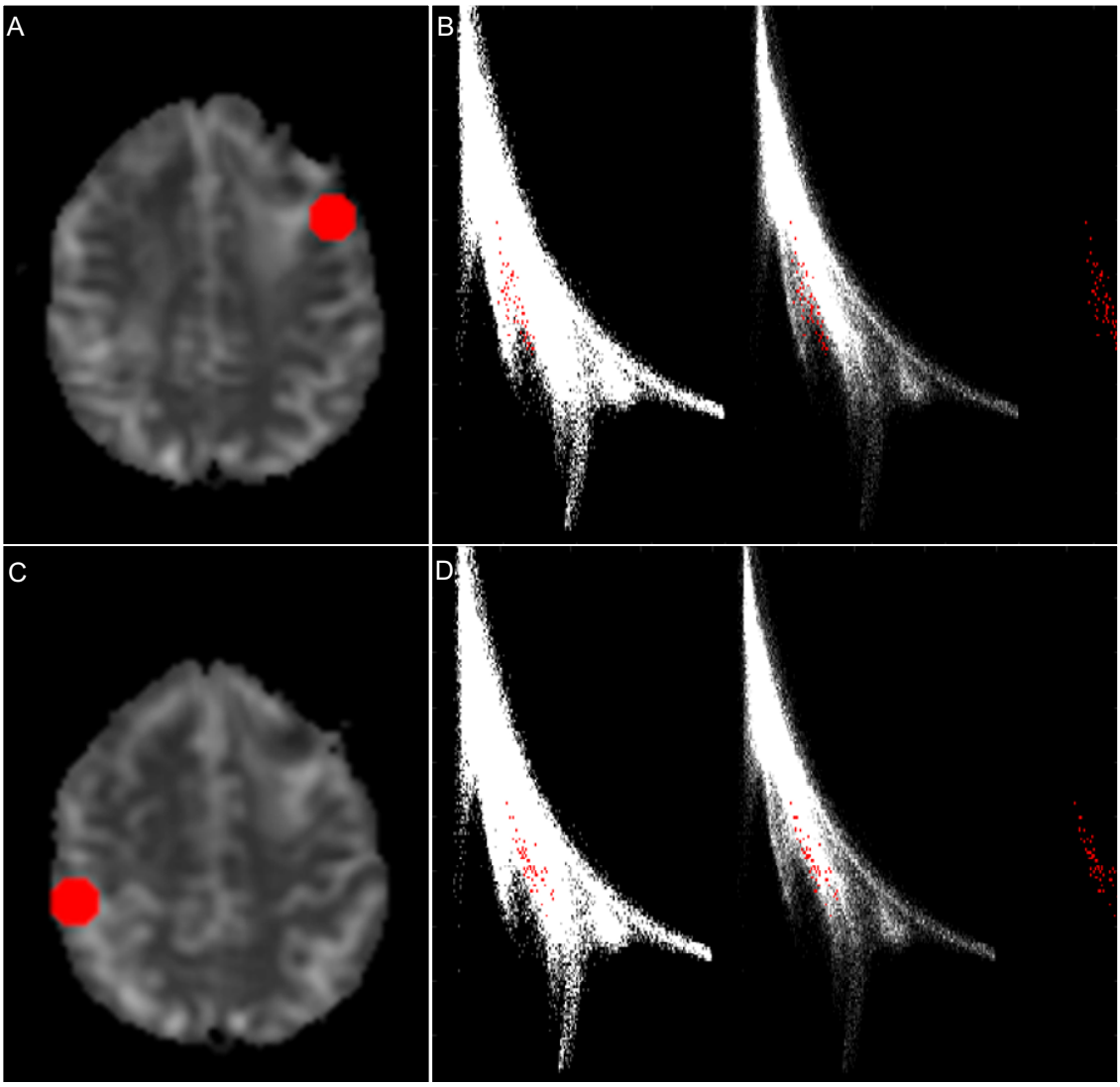

Fig. 44. Respective histogram regions regarding two metastases of another breast cancer patient (patient 7). *A* shows the marked first metastasis and *B* the corresponding highlighted diagram area while *C* displays the second metastasis and *D* the related histogram region.

Patients 8 and 9 both had been diagnosed with non-small cell lung cancer (NSCLC). However, the tumour of patient 8 belongs to the adenocarcinoma subtype while patient 9 possesses the subtype large cell neuroendocrine lung carcinoma (LCNEC). The brain metastasis of patient 8 was represented by an area near the subarachnoid space spike, similar to the breast cancer patients (Fig. 45). In contrast to this, the metastasis of patient 9 with LCNEC corresponded to the upper half of the histogram (Fig. 46).

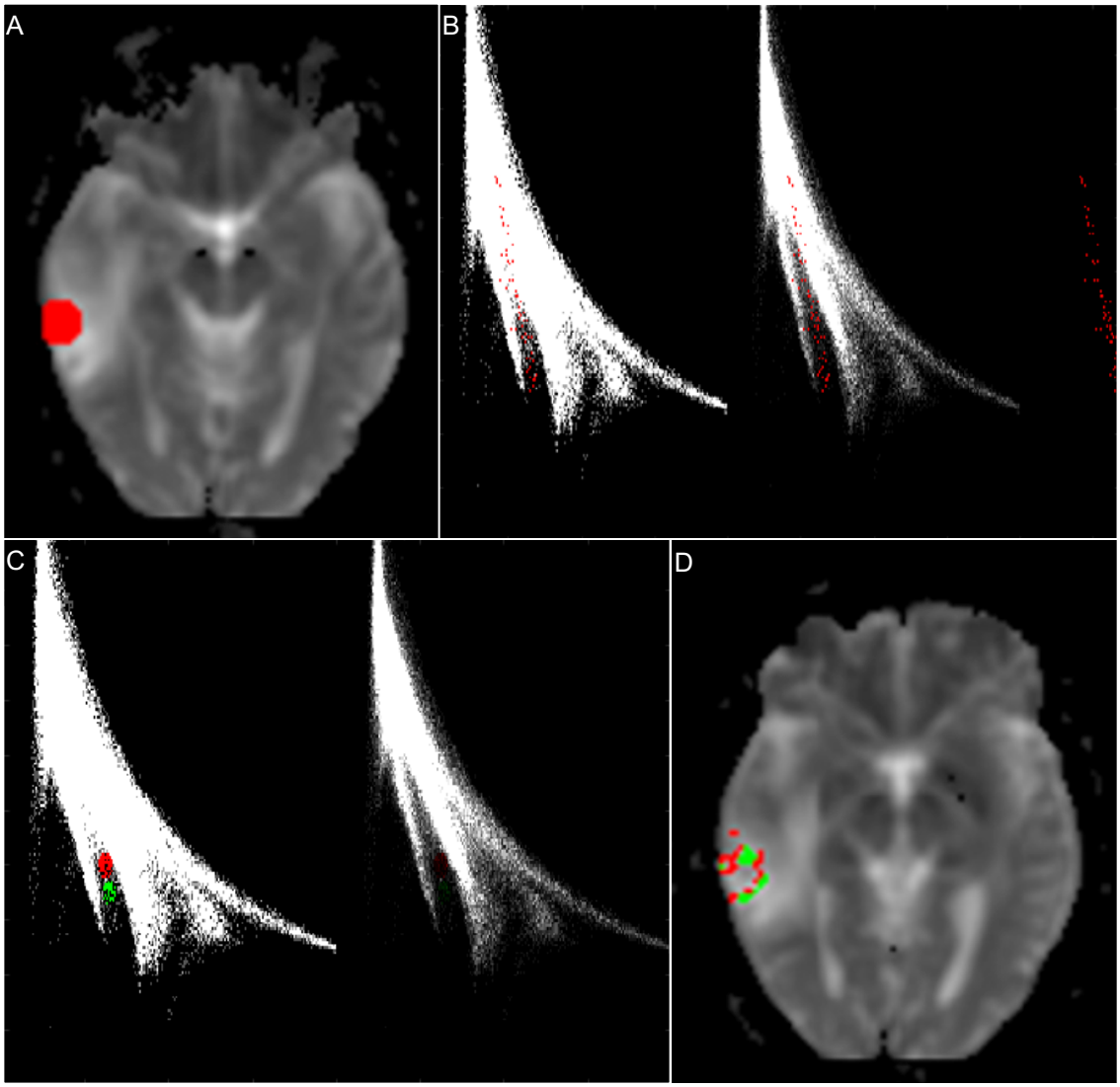

Fig. 45. Corresponding region of the histogram concerning the metastasis of patient 8 with NSCLC. *A* shows the marked tumour while *B* displays the associated histogram area. *C* shows the highlighted region of the histogram while *D* displays the corresponding tumour.

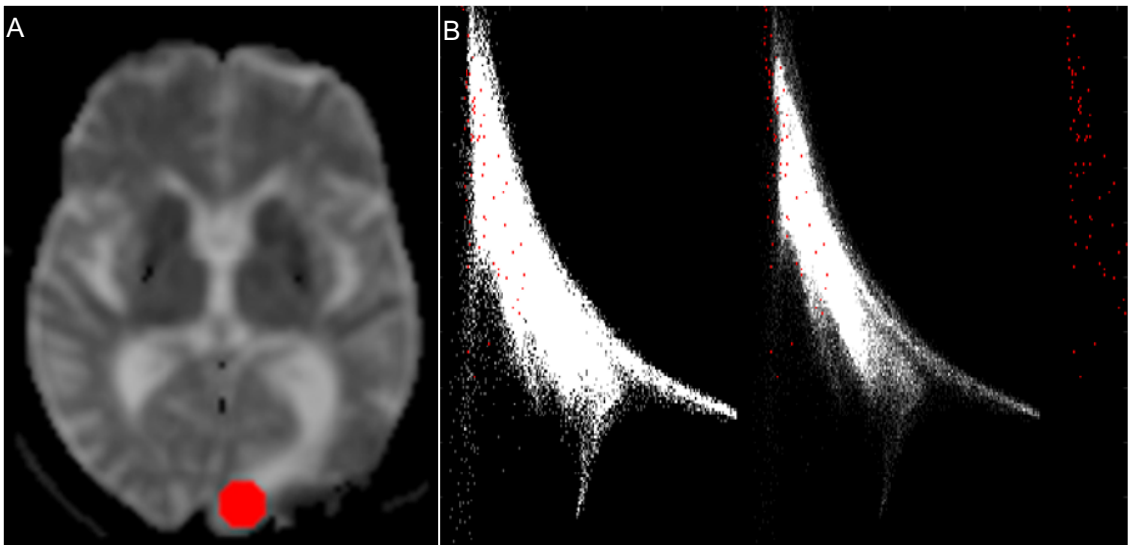

Fig. 46. Associated histogram area of an LCNEC metastasis (patient 9). *A* displays the highlighted tumour tissue while *B* shows the corresponding marked histogram area.

The remaining two patients with brain metastases had a nodular malignant melanoma as the primary tumour (patients 10 and 11). All four metastases from these two patients lay in the upper half of the histogram (Fig. 47 and 48).

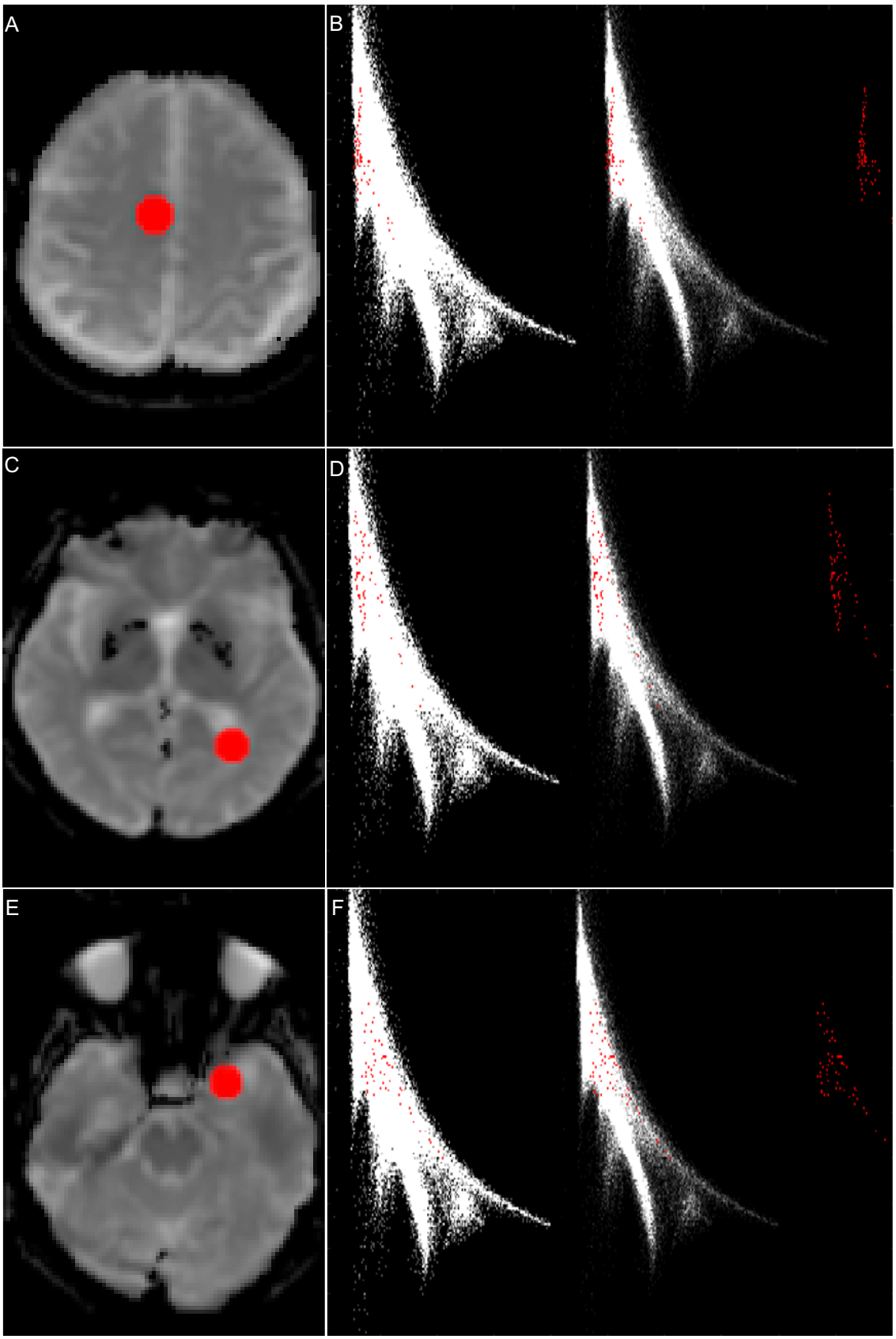

Fig. 47. Areas of the histogram relating to three different metastases of patient 10 with malignant melanoma. *A*, *C* and *E* show the highlighted different metastases while *B*, *D* and *F* display the corresponding histogram regions.

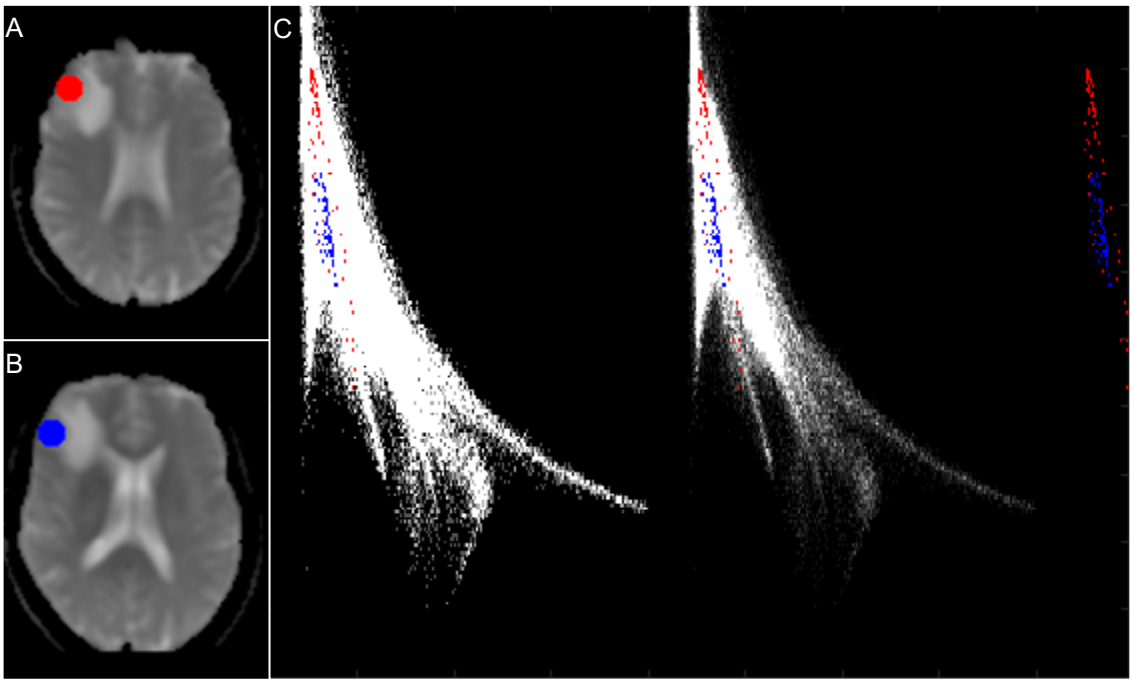

Fig. 48. Corresponding histogram area of the nodular melanoma metastasis of patient 11. *A* and *B* display the marked tumour while *C* shows the respective histogram region.

In conclusion, the subjects with the same kind of primary tumour often had metastases, which were displayed in similar areas of the histogram. Similar to meningiomas, there was not one specific region in the diagram, where all tumours lay. The corresponding spots of metastases in the histogram were often widely spread in the physiological diagram fraction, which was also previously observed in meningiomas. Thus, many parts of the physiological brain tissue were marked as well, when highlighting the corresponding histogram regions of metastases.

When compared with gliomas, metastases did not usually lie in the glioma-specific histogram spike. Therefore, it was often possible to differentiate between gliomas and metastases simply by investigating their respective histograms.

To summarise, brain metastases correlated to different parts of the histogram. Here, connections between the diagram location and the type of primary tumour could be observed. Similar to meningiomas, one can also often differentiate between gliomas and metastases by examining the corresponding areas in the histogram.

3.3.4 Peritumoral oedema

Furthermore, peritumoral oedema of meningiomas and metastases was analysed regarding its representation in the diffusion histograms. The oedema mostly corresponded to the previously described glioma/oedema extension of the diagram. Therefore, the same set of markings was chosen for highlighting the oedema, which also had been used for the tumour spike of larger glioblastomas.

Fig. 49 and 50 depict the histogram with the marked glioma/oedema spike and the corresponding MR images of various meningioma patients. The highlighted oedema often seemed to be separated into layers by the various colours. This phenomenon was also observed in oedema and vital tumour tissue of gliomas. As one can see in Fig. 50, the diagram areas with the higher MK values in the colours red and green were usually represented in the outer region of the oedema. Opposed to that, the histogram fractions with the lower MK values, coloured in blue and yellow, tended to correspond to the inner parts of the oedema.

Substantial peritumoral oedema was visible in four of the five meningioma patients. In all four cases, the oedema was highlighted when applying the histogram coordinates shown in Fig. 49.

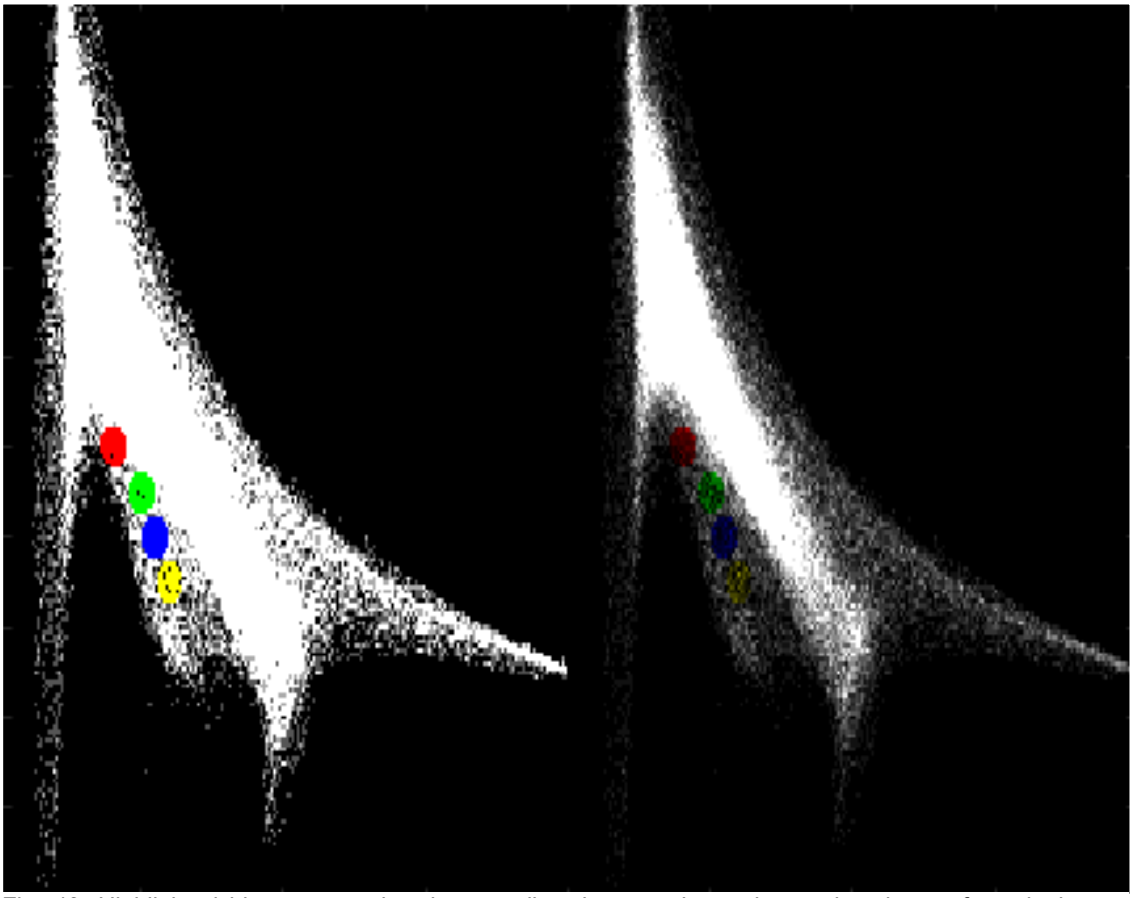

Fig. 49. Highlighted histogram region that usually relates to the peritumoral oedema of meningiomas, metastases and gliomas as well as the vital tumour tissue of gliomas. The displayed diagram was generated from the diffusion characteristics of a meningioma patient.

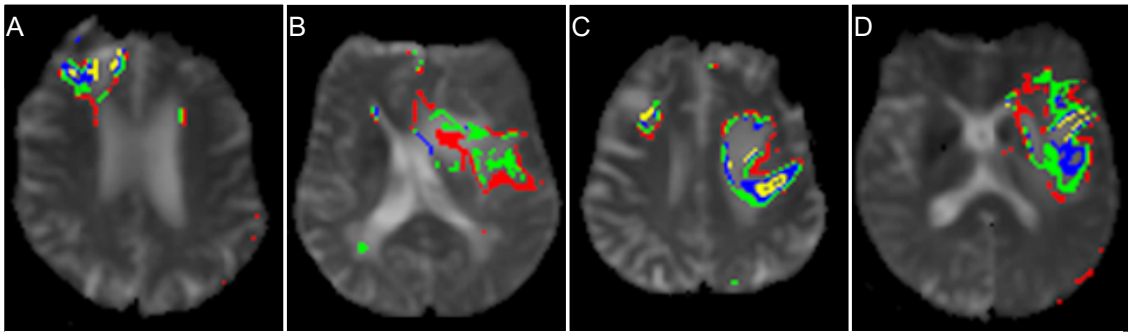

Fig. 50. Highlighted peritumoral oedema which corresponds to the marked histogram area shown in Fig. 49. *A-D* depict the marked oedema in the MR images of four different meningioma patients.

Fig. 51 and 52 show the histogram coordinates, that were used for highlighting the oedema of metastases, and the respective marked voxels in MR images of different patients with brain metastases. Similar to the oedema of meningiomas, the colours often formed layers, where the higher MK values were located in the outer region of the oedema while the lower MK values could usually be found mainly in the inner oedema areas.

In four out of the six patients with brain metastases, substantial peritumoral oedema could be found on the MR images. In all of these cases, the oedema was highlighted when marking the histogram area displayed in Fig. 51.

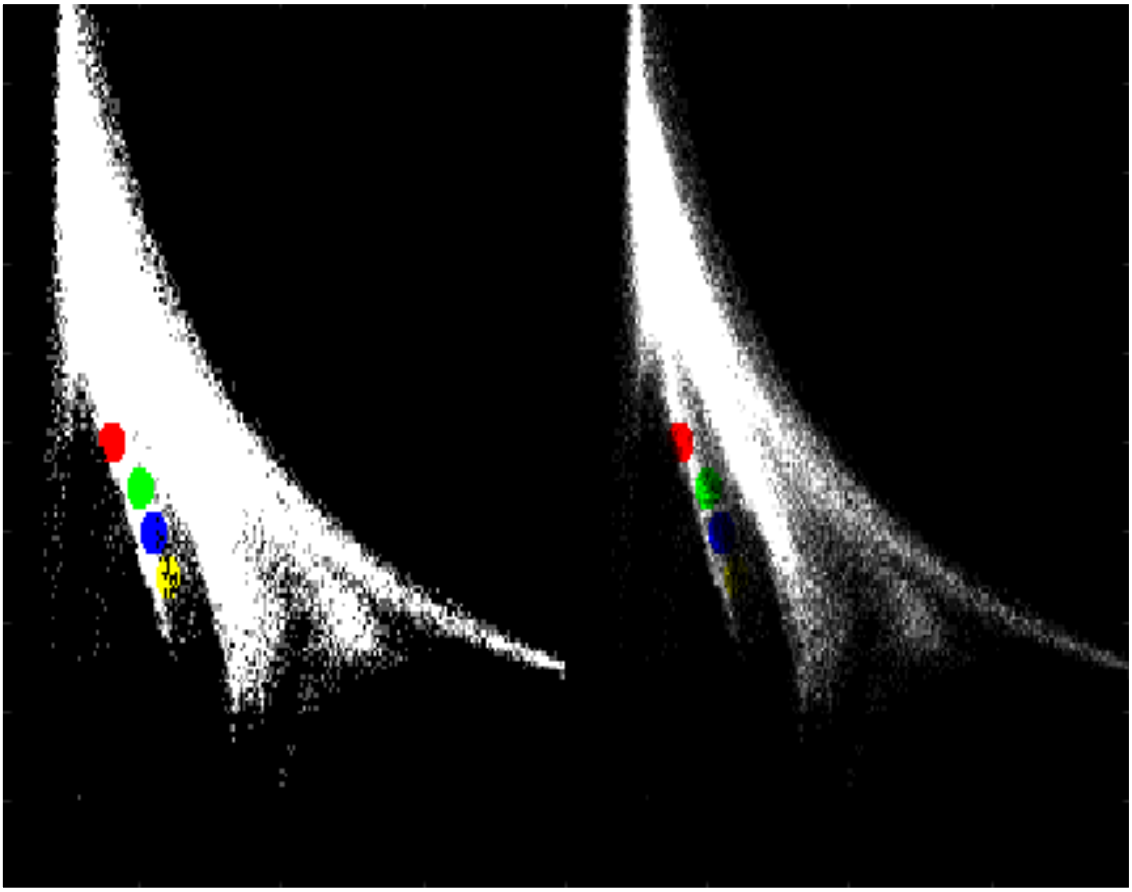

Fig. 51. Highlighted histogram region that normally corresponds to the peritumoral oedema of metastases, meningiomas and gliomas as well as the vital tumour tissue of gliomas. The displayed diagram belongs to a patient with a brain metastasis.

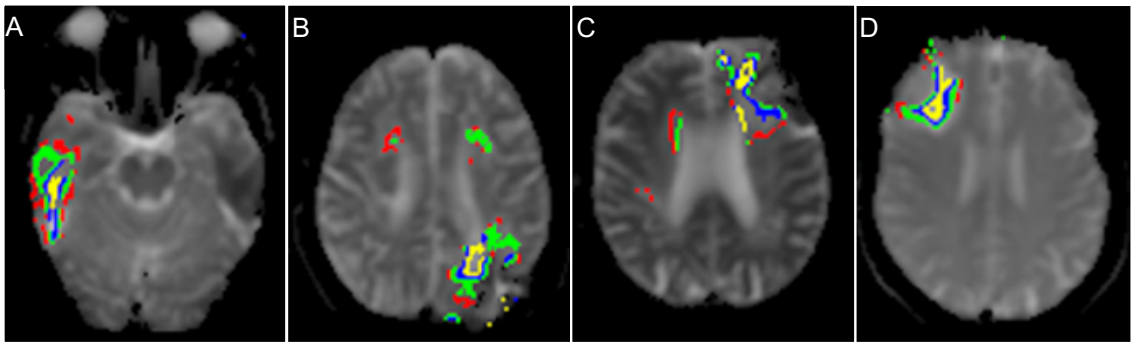

Fig. 52. Highlighted peritumoral oedema which corresponds to the marked histogram area displayed in Fig. 51. *A-D* depict the MR images of four different patients with metastases.

In summary, the oedema of meningiomas and metastases mainly corresponded to the previously described glioma/oedema histogram spike. In glioma patients, this diagram extension was shown to relate to the vital tumour tissue as well as the peritumoral oedema. Therefore, this histogram spike generally related to oedema, regardless of the primary tumour type.

Because gliomas and their peritumoral oedema both corresponded to this extension of the diagram, it was not possible to differentiate between gliomas and their peritumoral oedema. Opposed to that, most metastases and meningiomas were located in different histogram regions and not in this glioma/oedema spike. Therefore, it was often possible to discriminate tumour from oedema in these tumour subgroups.

In Table 4, statistics are displayed about how many subjects demonstrated a correlation between a certain histogram area and the respective brain region. As previously described, there was a set of standard coordinates determined for each of the mentioned brain regions in the table. This chart now displays the percentage of subjects, where this correlation of the standard histogram coordinates and the respective brain region could be confirmed. Therefore, this table should serve as an overview regarding the statistical findings previously described.

Table 4. Subjects where the described correlations between a specific histogram area and a brain region were observed.

Brain regions	Subjects without a brain tumour, where this correlation between histogram area and brain region was observed	Subjects with a brain tumour, where this correlation between histogram area and brain region was observed
Layer-like markings	100%	85%
Subarachnoid space	90%	90%
Ventricular System	100%	100%
Nose	100%	87%
Vital tumour tissue of glioblastoma and peritumoral oedema	-	65% of glioblastomas
Oligodendroglioma and peritumoral oedema	-	100% of oligodendrogliomas
Astrocytoma and peritumoral oedema	-	50% of astrocytomas
Peritumoral oedema of meningiomas	-	100% of meningiomas with visible oedema
Peritumoral oedema of metastases	-	100% of metastases with visible oedema

3.3.5 Comparison of the tumour types

Moreover, the representations of different tumour subgroups in the histograms were directly compared. As already mentioned, the majority of meningiomas and metastases were not represented by the glioma/oedema histogram spike. Only the peritumoral oedema of all the tumour types usually lay in this specific diagram extension.

In order to directly compare different tumour subcategories, the two different sets of histogram markings, which were previously used for highlighting vital glioma tissue, were applied on patients with meningiomas or metastases. Fig. 53 displays an example of a meningioma patient where the histogram coordinates for the glioma/oedema spike were applied. In this case, only the oedema correlates to this specific histogram extension whereas the meningioma itself is represented in the upper half of the diagram and is therefore not highlighted. When applying the histogram coordinates for the glioma/oedema spike on the other meningioma patients, none of the tumours was marked.

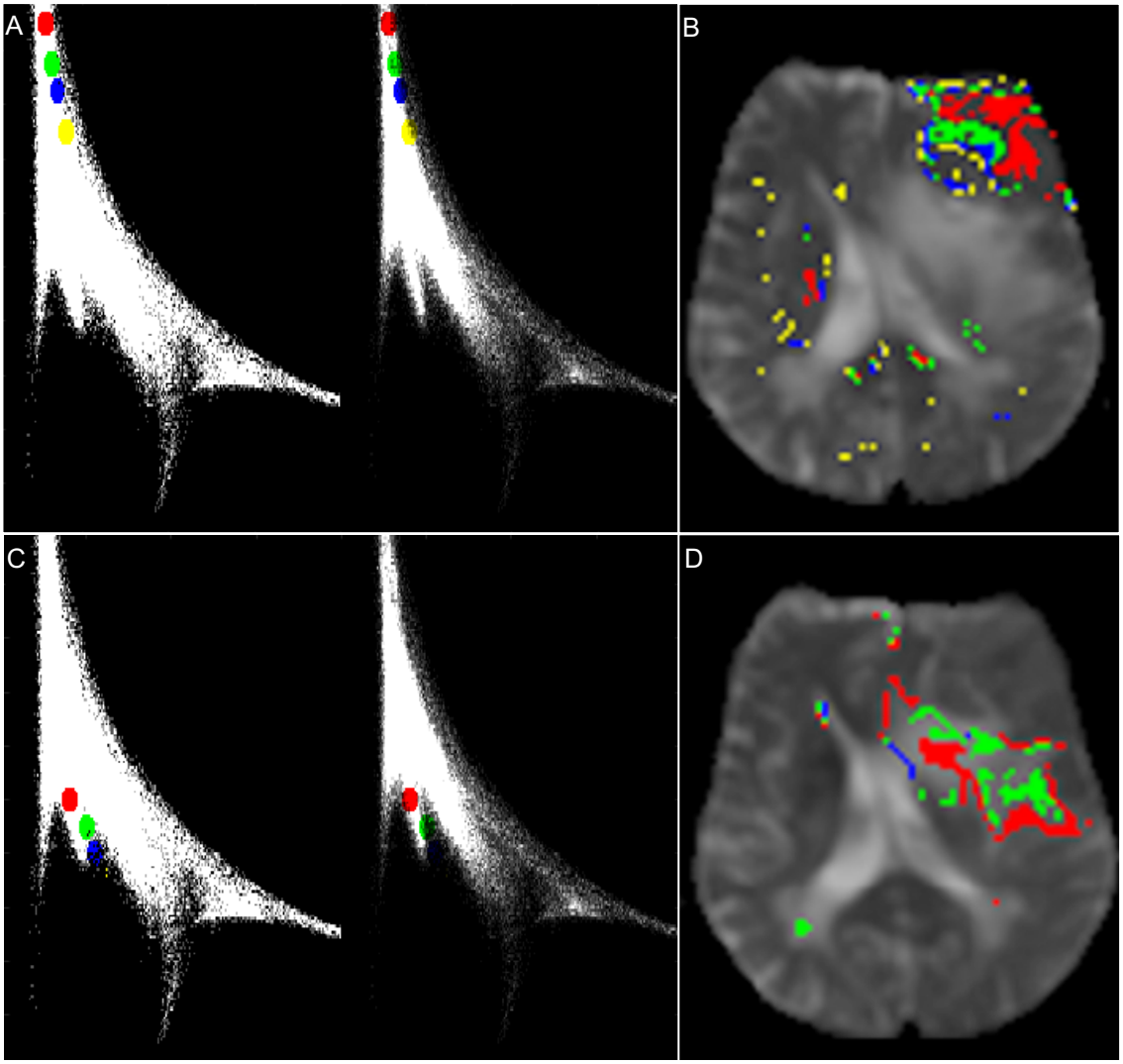

Fig. 53. Highlighted tumorous tissue and peritumoral oedema of a meningioma. *A* shows the marked histogram fraction corresponding to the tumour, which is marked in *B*. *C* depicts the highlighted glioma/oedema histogram spike, which only corresponds to the oedema and not to the tumour, as shown in *D*.

Fig. 54 displays the same concept in a patient with a brain metastasis. While the oedema corresponds to the typical histogram coordinates for the glioma/oedema spike, the metastasis is represented in a different part of the histogram. When investigating the other metastases, only one of the ten analysed tumours corresponded to the histogram coordinates for the glioma/oedema spike.

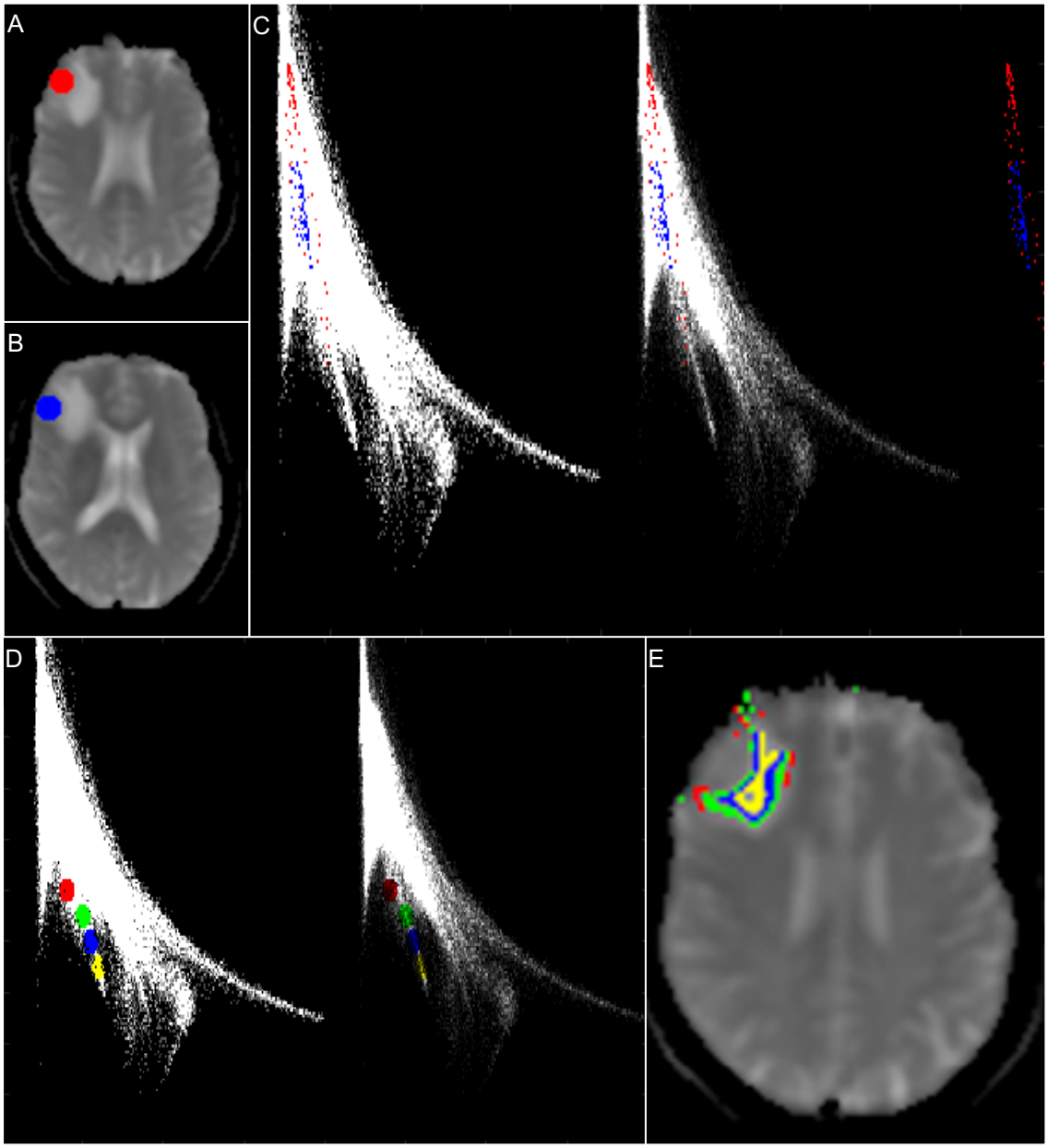

Fig. 54. Highlighted tumorous tissue and peritumoral oedema of a metastasis. *A* and *B* show the marked metastasis, while *C* shows the corresponding diagram spots, which mainly lie in the upper half of the histogram. *D* depicts the glioma/oedema histogram spike, that corresponds only to oedema and not to the tumour as shown in *E*.

In conclusion, the meningiomas and metastases were distributed over various diagram locations. However, nearly none of these tumours lay in the glioma/oedema histogram spike, unlike the vital tumour tissue of gliomas. Therefore, it is normally possible to distinguish meningiomas and metastases from gliomas by analysing the representation of vital tumour tissue in the histogram.

4 Discussion

4.1 Comparison of the findings and literature

4.1.1 Optimal b-value choice

An objective of this project was to find the optimal maximal b-value for the generation of two-dimensional diffusion histograms, which were used for investigating physiological brain tissue and brain tumours. B-values as high as 5000 s/mm^2 were employed. The most promising histograms were those, that utilised b-values up to 2000 s/mm^2. In these diagrams, the extensions were better visible and therefore easier to analyse.

A study comparing specific diffusion histograms of the brain with regard to different b-values has not been reported previously. However, there is emerging evidence, which indicates that higher b-values can be helpful in characterising tumour tissue in some cases. Two separate studies indicated that ADC values, which were acquired with b-values of 3000 s/mm^2, exhibited a better diagnostic performance in differentiating LGG and HGG, when compared to b-values of 1000 s/mm^2 (Kang et al., 2011; Seo et al., 2008). Another study utilised b-values between 500 and 2500 s/mm^2 to differentiate oligodendrogliomas, astrocytomas and glioblastomas, in which case the highest b-value demonstrated the best diagnostic performance (Nuessle et al., 2021). Another investigation showed that employing a high b-value like 4000 s/mm^2 helped to distinguish pseudo-response from true response of gliomas after bevacizumab treatment (Yamasaki et al., 2012).

Therefore, high b-values can be helpful in diagnosing brain tumours. However, in the here described case of the MD and MK histograms, the usage of higher b-values did not produce a benefit and rather led to inferior diagrams with less informative value.

4.1.2 General shape of the histogram

As part of this project, the question was addressed, which regions of the brain corresponded to certain histogram areas. When looking at previous research, the concept of MD and MK diagrams had previously been described (Chen et al., 2012; Jensen et al., 2005). In these studies, the diffusion characteristics were displayed as a scatter plot, which looked very similar to our two-dimensional histograms, regarding the general diagram shape. This confirmed the accuracy of the here described findings concerning the histogram form in subjects without a brain tumour.

In contrast to this project, none of these studies had investigated, which brain areas correspond to specific parts of the diagram. Thus, these correlations cannot be compared to former research. However, it is possible to partially explain the layer-like markings, which resulted from highlighting the left border of the histogram. A study found that MK values were significantly higher in white matter when compared to grey matter (Maiter et al., 2021). In the diffusion histograms of this project, the cortex, which belongs to the grey matter, was also represented in a diagram area with lower MK values, while a lot of the white matter corresponded to a histogram area with higher MK values.

4.1.3 Glioma-characteristic histogram region

As described previously, patients with gliomas possessed a spike in their diffusion histogram, which is normally not found in individuals without a brain tumour. This glioma spike had already been reported in one study (Hempel et al., 2021). Here, MD and MK values had been displayed in a scatter plot, which greatly resembled our two-dimensional histograms regarding the general diagram shape and the glioma spike. Moreover, the same study had also demonstrated, that the tumour area corresponds to the diagram spike by manually segmenting the pathological tissue and investigating the related diagram regions. Vice versa, a large portion of the tumour was highlighted when the glioma extension was marked in the diagram. Therefore, this study supports the here described findings regarding the glioma-characteristic histogram spike.

4.1.4 Differentiation of glioma subtypes

The different glioma subcategories were often represented in the histogram by characteristic shapes of the glioma-specific diagram spike. While this histogram extension of oligodendrogliomas and astrocytomas usually lay vertical, it often leaned to the right in glioblastomas. An exception to this tendency were smaller glioblastomas, that often possessed a vertical tumour spike like oligodendrogliomas and astrocytomas.

As previously mentioned, glioblastomas are usually WHO grade 4 tumours, while astrocytomas and oligodendrogliomas are often classified as grade 2 or 3. This means that the observed differences regarding the histogram shape of the glioma subgroups can also hint to the WHO tumour grade. Moreover, the molecular-histological subgroups of gliomas are partially defined by mutations of the tumour: For example, an IDH-mutation leads to the classification of an oligodendroglioma or astrocytoma whereas the IDH-wildtype is characteristic for glioblastomas. Thus, the differentiation between these subgroups of gliomas can also hint as to which mutations the tumour possesses. No other study could be found, which compared these specific diffusion histograms between the glioma subtypes. However, there had been a lot of research regarding the differentiation of gliomas with diffusion characteristics.

For example, DWI and DKI were used to distinguish between different WHO grades of gliomas. In general, MD values were often smaller in HGG because the cellularity is normally increased when compared to LGG: This leads to less extracellular space and therefore, less space for the molecules to move freely (Cha, 2006). Regarding DKI, MK values were normally higher in HGG, which also represents the restricted diffusion. Overall, DKI often exhibited a superior performance in differentiating between various tumour grades when compared to DWI. For example, in the group of astrocytomas, MK values could distinguish grade 2 from 3, which could not be found for ADC values (Raab et al., 2010). However, the same study stated, that both ADC and MK values were able to discriminate between astrocytoma grade 3 and glioblastoma. Other research also showed, that it was possible to differentiate between grade 2 and 4, as well as

between grade 3 and 4, with MD values, while MK values could additionally also distinguish grade 2 from 3 (Maximov et al., 2017).

While the general trend of research indicates the superior diagnostic performance of MK values, the results vary across studies when discriminating the various tumour grades. For example, in contrast to the previously mentioned research, another study showed that MD values could indeed discriminate between grade 2 and 3 (Hempel et al., 2017). In accordance with former research, the same could be proven for MK values in this study. However, it is only possible with MK values to distinguish grade 2 from 4 according to this work.

Furthermore, it had been shown, that even though ADC, MD and MK values could differentiate between LGG and HGG, the area under the curve (AUC) and therefore the diagnostic performance was optimal when using MK values (Bai et al., 2016; Qi et al., 2018; Tan et al., 2016). Moreover, a meta-analysis had evaluated 10 studies with a total of 430 patients and calculated an AUC value of 0.94 for discriminating between LGG and HGG with the help of MK values (Falk Delgado et al., 2018). Another meta-analysis had also confirmed these findings by calculating an AUC of 0.92 regarding the diagnostic performance of DKI (Abdalla et al., 2020).

Apart from being able to aid in assigning gliomas a WHO grade, DWI and DKI can furthermore be helpful in attaining histological and molecular information about the tumour. For example, one study demonstrated, that astrocytomas and glioblastomas could be differentiated by the utilisation of MD and MK values (Hempel et al., 2017). Furthermore, the same study indicated, that it is also possible to distinguish oligodendrogliomas from glioblastomas when using MK values. Moreover, another investigation demonstrated, that MK values are significantly lower in IDH-mutated astrocytomas than in oligodendrogliomas or IDH-wildtype glioblastomas (Hempel et al., 2018). Two other studies also showed that MD and MK values can distinguish IDH-mutated from IDH-wildtype gliomas, in which case MK values demonstrated a better diagnostic performance (Tan et al., 2019; Zhao et al., 2019).

These studies generally confirm the findings of this work, as they show that one can differentiate various glioma subgroups with diffusion characteristics: The distinguishment between the WHO tumour grades, the molecular-histological subcategories and the IDH-mutation status is often possible with the above-described histograms.

4.1.5 Meningiomas

When analysing the location of meningiomas in the histograms, it was difficult to deduce any regularities. One could observe that the two analysed grade 2 tumours were in the same diagram region. However, it was not possible to state any reliable rules regarding the distinguishment of the different WHO grades, which was also due to the fact that only six meningiomas were examined.

The literature about the characterisation of meningiomas with the help of diffusion characteristics is rather discordant. There is a meta-analysis, which stated that DWI could differentiate between low and high-grade meningiomas (Siempis et al., 2020). The low-grade subcategory consists of the grade 1 tumours while high-grade meningiomas represent grade 2 and 3. Two other studies also indicated that ADC values were significantly lower in high-grade than in low-grade meningiomas (Lin et al., 2019; Sacco et al., 2020). However, another meta-analysis concluded, that there was no reliable ADC cut-off value regarding the discrimination of low and high-grade meningiomas (Meyer et al., 2020). A study that was included in that meta-analysis even claimed, that there was no significant difference in ADC values when comparing low and high-grade meningiomas (Santelli et al., 2010).

Investigations have produced more explicit findings regarding the use of DKI in the grading of meningiomas: Three studies compared both MD and MK values and stated, that MK values demonstrated a better diagnostic performance in differentiating between low and high-grade meningiomas (Chen et al., 2020; Lin et al., 2018; Xing et al., 2017).

In summary, it is challenging to compare the findings of this work to the current state of research due to the limited patient number. However, literature suggests, that at least MK values hold the ability to aid in the grading of meningiomas.

4.1.6 Metastases

Regarding the representation of brain metastases in the diffusion histograms, it is not possible to determine one characteristic location, where most of these tumours are depicted. However, there is evidence that metastases, which originate from the same kind of primary tumour, tend to correlate to the same diagram region. There was no literature found, that also analysed the location of brain metastases in these diffusion histograms.

However, there has been some research conducted about the diagnostic value of DWI in differentiating various subcategories of metastases. For example, there were significant ADC value differences when comparing the metastases from the two lung cancer subgroups small-cell lung cancer (SCLC) and NSCLC (Meyer et al., 2015). This study also showed significant ADC value differences when comparing SCLC and NSCLC separately with breast cancer and melanoma. However, it was not possible to distinguish breast cancer from melanoma by simply analysing the respective ADC values of the brain metastases, according to this study.

Additional research also demonstrated the ability to discriminate between metastases from SCLC and NSCLC by analysing the ADC values. In one case, the AUC value was as high as 0.99 for the distinction between these two histological lung cancer subcategories when using the ADC ratio: It was calculated by dividing the ADC value of the solid tumour fraction by an ADC value of an equivalent, healthy region in the contralateral hemisphere (Müller et al., 2021). Another study generated one-dimensional ADC histograms, which displayed the distribution of ADC values for an individual tumour: For example, by analysing the 25^{th} percentile of the ADC value, it was also possible to differentiate NSCLC and SCLC with an AUC as high as 0.922 (Bozdağ et al., 2021). However, other research could not find a significant difference of the

minimum ADC value in different histological lung cancer subgroups (Jung et al., 2018). This study only stated that there was a significant ADC value difference of lung cancer metastases with epidermal growth factor receptor (EGFR) mutation and wildtype.

Moreover, research was conducted about categorising various subgroups of breast cancer metastases. One study found no significant differences between HER2 positive and negative tumours when analysing one-dimensional ADC histogram parameters (Ahn et al., 2018). However, this work stated that some of these ADC histogram parameters were significantly different when comparing ER/PR positive to ER/PR negative breast cancer metastases. A different study could also find no significant discrepancies of ADC values between HER2 positive and negative tumours (Meyer et al., 2015).

Furthermore, studies employed themselves with the distinguishment of brain metastases from gliomas by using DWI and DKI. For instance, a meta-analysis calculated a mean sensitivity of 0.81 and an average specificity of 0.84 in differentiating metastases and glioblastomas with the help of DWI parameters (Zhang & Liu, 2020). Another study also showed that it was possible to discriminate between glioblastomas and solitary brain metastases by analysing the parameters of one-dimensional histograms generated either by MD or MK values (Gao et al., 2022). However, other research stated that only MD values and not MK or ADC values were significantly different between high-grade gliomas and solitary brain metastases regarding the contrast-enhancing tumour fraction (Mao et al., 2020). Another work could also not find significant ADC value discrepancies of the contrast-enhancing tumour part when comparing glioblastomas and solitary brain metastases (Thammaroj et al., 2020).

Furthermore, a study investigated a different approach to examining DWI parameters: ADC maps were generated of glioblastomas and metastases, and afterwards, a texture analysis was performed based on these diffusion maps (Zhang et al., 2019). The resulting parameters represented the tissue's homogeneity and were significantly different when comparing the two tumour groups.

In summary, the diagnostic performance of DWI in differentiating various subtypes of metastases is controversial. This can also be said for the distinction of brain metastases and gliomas utilising DWI and DKI. However, some studies were successful in discovering significant differences when analysing the diffusion parameters. No research could be found on the value of DKI in discriminating between brain metastases, which originate from different primary tumours.

As previously mentioned for meningiomas, it is challenging to compare the findings of this work with literature due to the limited number of subjects. However, this work and other studies show that DWI and DKI may be useful in classifying brain metastases.

4.1.7 Peritumoral oedema

The great majority of the examined tumour patients had a peritumoral oedema, which was represented in the typical glioma/oedema histogram spike, regardless of the tumour subtype. A previously mentioned study also investigated diffusion parameter scatterplots, that are very similar to the here described two-dimensional histograms (Hempel et al., 2021). They examined glioma patients and stated, that the tumorous tissue, as well as the peritumoral oedema, both lay in the same diagram extension, which corroborates the findings of this work. No other research could be found, that had investigated the representation of peritumoral oedema in the diffusion histograms, which are described in this work.

However, there is some literature on the distinction of various tumours by analysing diffusion parameters of their oedema. The histological picture of these oedemas can vary, depending on the tumour subgroup. In the case of gliomas, there were often tumour cells in the oedema, which could be detected by analysing biopsies and T2-weighted images (Watanabe et al., 1992). In contrast to that, metastases rather produce a vasogenic oedema, which usually did not contain many tumour cells (Stummer, 2007).

This difference regarding the oedema of these two tumour groups can also be examined with DWI and DKI. One study found that there are significant disparities in MD and MK values when comparing the peritumoral oedema of high-grade astrocytomas and solitary brain metastases (Tan et al., 2015). In this case, MK values demonstrated a better diagnostic performance. Other research supported these findings by discovering a significant difference in ADC values between the peritumoral area of high-grade gliomas and brain metastases (Liu et al., 2021; Pavlisa et al., 2009). The minimum ADC values of the peritumoral area were also proven to be helpful in differentiating between glioblastomas and metastases (Lee et al., 2011; Neska-Matuszewska et al., 2018).

Contrary to this, other investigations state that there are no significant disparities in ADC values regarding oedemas of gliomas and metastases (Guzman et al., 2008). The same previously mentioned study, which found significant discrepancies concerning the minimum ADC value of glioblastomas and metastases, did not observe the same for the mean ADC value (Neska-Matuszewska et al., 2018). Furthermore, studies compared the oedema of gliomas, meningiomas and metastases, and were also not able to find any significant ADC value differences (Oh et al., 2005; Server et al., 2009).

Another approach is the evaluation of the ADC value gradient regarding the peritumoral oedema. One work stated, that such a gradient existed especially in glioblastomas, in which case the ADC values were significantly higher in the outer region of the oedema than in the area lying right next to the tumour (Lemercier et al., 2014). They did not observe this gradient in metastases. Another study also used the ADC gradient in order to differentiate the oedema of glioblastomas and brain metastases (Tepe et al., 2021).

Moreover, some studies attempted to distinguish the oedema of various glioma and meningioma subtypes. One study stated, that ADC values were significantly different when comparing glioblastomas and LGG (Guzman et al., 2008). However, another investigation claimed that only MK values, and not MD values, could be useful for distinguishing low-grade from high-grade astrocytomas (Tan et al., 2016). Another study found significant disparities in MK values only

between grade 3 and 4 gliomas and none when comparing other glioma grades (Qiu et al., 2022). However, MD values were able to differentiate between grade 3 and 4 gliomas, as well as between grade 2 and 4 gliomas, according to this study. A further approach to this topic is the texture analysis of peritumoral oedema with ADC maps: Here, one of the three parameters was helpful in distinguishing LGG from HGG, which was not the case for the ADC value (Soliman et al., 2021).

Regarding meningiomas, ADC values of peritumoral oedema did not display any significant disparities when comparing typical to atypical tumours (Bano et al., 2013; Hakyemez et al., 2006).

Another question is the value of DWI in discriminating between tumour tissue and oedema. One study could not find any significant ADC discrepancy in this context when investigating gliomas (Pauleit et al., 2004). However, another study claimed that ADC values were significantly different between tumour and oedema in gliomas, meningiomas and metastases (Oh et al., 2005).

In conclusion, literature is discordant on the value of DWI and DKI in the differentiation of tumour subtypes by analysing the surrounding oedema. The here described histograms were not able to discriminate between different tumours by investigating the oedema or to distinguish between tumorous tissue and oedema in the case of gliomas. However, these diagrams could be helpful in separating oedema from meningiomas and metastases, as these kinds of tumours usually do not lie in the glioma/oedema histogram spike.

4.2 Limitations and outlook

A limitation of this study was that the analysis of the diffusion histograms was subjective. Especially the shape of the diagrams was investigated, in which case it was difficult to deduct any trends regarding the influence of the tumour subtype on the histogram. Here, it could be helpful to utilise image recognition software and machine learning in order to make our findings more objective. Furthermore, automatic tumour segmentation with the help of diffusion histograms could assist in proving our findings.

A further limitation was the comparatively low number of analysed patients with oligodendrogliomas, astrocytomas, meningiomas or metastases. In the group of gliomas, glioblastomas were most often investigated, because that was the tumour subcategory which underwent MR imaging most frequently at the institution where imaging was conducted. Thus, it would be advisable in the future to examine more oligodendrogliomas and astrocytomas to further analyse the diagnostic performance of the diffusion histograms in differentiating between the glioma subtypes. Moreover, a higher number of meningiomas and metastases would also help in gaining additional information on the representation of those tumour subcategories in the histograms. For example, reliable indications as to where the unknown primary tumour of the brain metastasis lies, could accelerate the diagnosis and could get the patient their suitable treatment faster.

Another possible way to expand the patient collective would also be to include inflammatory diseases of the brain. It would be interesting to see, how the histograms are affected by such pathologies and how those diagrams could potentially be useful in diagnosing inflammatory diseases.

When examining new patients, it would be ideal to conduct the MR imaging on one common scanner with the exact same parameters in order to generate a higher degree of comparability of the acquired images. Unfortunately, this was not possible for this study, as the DKI sequences were often measured after the previously scheduled normal MRI program for the respective patient at different MRI scanners.

In the future, one could also further investigate the representation of intratumoral necrosis in the histograms. In this work, it was shown that necrotic regions were located in very different histogram areas. It would be interesting to identify parameters, which influence the representation of necrosis in the diffusion diagrams. For example, the histogram area, to which the necrotic region correlates, could be connected to the prognosis of the patient.

Furthermore, another possible use of the diffusion histograms is gaining information about the extent of tumour cell proliferation. According to a study, MD inversely correlated with the proliferation marker Ki-67 in gliomas, while MK positively correlated with this marker (Zhao et al., 2019). Other works stated, that the Ki-67 value also correlated with one-dimensional histogram parameters of MD and MK (Chen et al., 2020) as well as with ADC values in meningiomas (Surov et al., 2016). In contrast to that, another investigation only observed a correlation between the Ki-67 value and MK, but not MD, in meningiomas (Xing et al., 2017). A meta-analysis merely detected a moderate inverse correlation of ADC with the Ki-67 value in this tumour group (Meyer et al., 2020). Concerning the peritumoral oedema of gliomas, DKI parameters did not display any connection to Ki-67 values (Qiu et al., 2022).

Moreover, the use of the diffusion histograms in estimating the prognosis and survival of brain tumour patients could be investigated. For example, low MK and high MD values represent beneficial prognostic parameters for overall and progression-free survival regarding gliomas with either no 1p/19q loss of heterozygosity or retained alpha-thalassemia/mental retardation syndrome X-linked (ATRX) gene expression (Hempel et al., 2019). Another study showed that ADC measurements of the whole brain also correlated with progression-free and overall survival in patients with glioblastomas (Rulseh & Vymazal, 2020). Regarding breast cancer brain metastases, some parameters of one-dimensional ADC histograms were indicators for a shorter period of progression-free survival if they were low (Ahn et al., 2018). Furthermore, a low ADC value was also shown to be a sign for progression or recurrence in meningiomas (Ko et al., 2018).

In addition, another useful application of the diffusion histograms could be the discrimination between pseudoprogression of gliomas and actual tumour recurrence. In this context, MK values demonstrated a superior diagnostic performance when compared to MD values (Wu et al., 2021). Furthermore, a study stated that the development of ADC values during therapy was able to predict the therapeutic effect of whole brain radiotherapy and the EGFR inhibitor gefitinib in patients with non-small-cell lung cancer (NSCLC) and resulting brain metastases (Ye et al., 2021).

4.3 Conclusions

In this work, it was possible to identify certain physiological brain regions like ventricles or subarachnoid space, which normally had the same representation in the diffusion histograms. Furthermore, it was shown that gliomas were mostly located in another part of the histogram when compared to meningiomas and metastases. Therefore, it was normally possible to differentiate these groups. The peritumoral oedema could usually also be found in that glioma histogram region, regardless of the tumour subcategory. In conclusion, this work succeeded in examining the physiological part of the diffusion histograms and describing the differences concerning the representation of various brain tumours in these diagrams.

5 Summary

Malignant brain tumours often possess an unfavourable prognosis and can severely diminish quality of life. Therefore, it is vital to improve the diagnostic process so that the differentiation between various tumour subgroups can be facilitated.

The objective of this work was to analyse two-dimensional histograms, which were generated with the help of diffusion kurtosis imaging (DKI). For this purpose, the DKI histograms of 10 subjects without a brain tumour and 39 patients with a brain tumour were analysed. The aim was to investigate, whether any possible differences could be recognised between these two groups and to compare the various tumour subcategories gliomas, meningiomas and brain metastases.

Regarding similarities between healthy subjects and patients, common histogram areas were identified that corresponded to specific regions like the ventricles or the subarachnoid space in the majority of subjects. Moreover, highlighting a specific histogram area marked corresponding layer-like regions in the brain. In tumour patients, these layers usually did not extend into the pathological tissue, rendering it distinguishable from physiological brain tissue.

With respect to the analysed brain tumours, gliomas and their peritumoral oedema were found to correspond to a specific spike-like extension of the histogram, which was not observed when analysing a healthy brain. This spike also represented the oedema from meningiomas and metastases and can therefore be referred to as the glioma/oedema spike. When comparing oligodendrogliomas and astrocytomas with glioblastomas, it was possible to recognize a slightly different shape and orientation of the glioma/oedema histogram extension.

In addition, the data suggest that various tumour subgroups of meningiomas and metastases may be distinguished. Moreover, it was mostly possible to differentiate between these two tumour categories and gliomas. In the future, these observations about the different behaviour of the tumour groups could improve the diagnostic process, for example with the help of artificial intelligence. Besides, the DKI histograms could be used for automatic tumour segmentation.

6 Zusammenfassung (German Summary)

Maligne Hirntumore besitzen oft eine ungünstige Prognose und können die Lebensqualität deutlich verringern. Daher ist es wichtig den diagnostischen Prozess zu verbessern, sodass die Unterscheidung zwischen verschiedenen Tumortypen vereinfacht werden kann.

Das Ziel dieser Arbeit war es, zwei-dimensionale Histogramme von Probanden mit und ohne Hirntumor zu analysieren, welche mit der Hilfe von Diffusion Kurtosis Imaging (DKI) generiert wurden. Hierzu wurden die DKI-Histogramme von 10 Probanden ohne Hirntumor und 39 Patienten mit Hirntumor untersucht. Es sollte geprüft werden, ob mögliche Unterschiede zwischen diesen zwei Gruppen erkannt und die verschiedenen Tumorsubgruppen Gliome, Meningeome und Metastasen verglichen werden können.

Hinsichtlich Gemeinsamkeiten von gesunden Probanden und Patienten wurden Histogrammareale identifiziert, welche bei der Mehrheit der Probanden den gleichen spezifischen Regionen wie zum Beispiel den Ventrikeln oder dem Subarachnoidalraum entsprachen. Außerdem wurden schichtartige Markierungen im Gehirn beobachtet, welche mit einer spezifischen Histogrammregion korrespondierten. In Hirntumorpatienten drangen diese Schichten nicht in das pathologische Gewebe ein, wodurch sich ein Unterschied zum Gewebe in gesunden Probanden ergab.

In der Gruppe der analysierten Hirntumoren konnte man beobachten, dass Gliome und deren peritumorales Ödem in einem spezifischen Ausläufer des Histogrammes repräsentiert wurden, welcher bei Patienten ohne Tumor nicht zu sehen war. Diese Diagrammzacke stellte auch das Ödem von Meningeomen und Metastasen dar und kann daher als Gliom/Ödemzacke beschrieben werden. Wenn man Oligodendrogliome und Astrozytome mit Glioblastomen vergleicht, konnte man eine etwas andere Form und Orientierung dieses Ausläufers beobachten.

Außerdem wiesen die Daten darauf hin, dass möglicherweise verschiedene Tumoruntergruppen von Meningeomen und Metastasen voneinander unterschieden werden können. Des Weiteren war es meist möglich, zwischen diesen zwei Tumorkategorien und Gliomen zu unterscheiden. In der Zukunft könnten diese Beobachtungen hinsichtlich des verschiedenen Verhaltens der Tumorgruppen den diagnostischen Prozess verbessern, zum Beispiel mit der Hilfe künstlicher Intelligenz. Außerdem könnten die DKI-Histogramme für automatische Tumorsegmentierung genutzt werden.

7 Reference List

Abdalla G, Dixon L, Sanverdi E, Machado PM, Kwong JSW, Panovska-Griffiths J, Rojas-Garcia A, Yoneoka D, Veraart J, Van Cauter S, Abdel-Khalek AM, Settein M, Yousry T and Bisdas S (2020) The diagnostic role of diffusional kurtosis imaging in glioma grading and differentiation of gliomas from other intra-axial brain tumours: a systematic review with critical appraisal and meta-analysis. Neuroradiology 62 (7): 791-802.

Ahn SJ, Park M, Bang S, Cho E, Ahn SG, Suh SH and Lee JM (2018) Apparent diffusion coefficient histogram in breast cancer brain metastases may predict their biological subtype and progression. Sci Rep 8 (1): 9947.

Alexander AL, Lee JE, Lazar M and Field AS (2007) Diffusion tensor imaging of the brain. Neurotherapeutics 4 (3): 316-329.

Bai Y, Lin Y, Tian J, Shi D, Cheng J, Haacke EM, Hong X, Ma B, Zhou J and Wang M (2016) Grading of Gliomas by Using Monoexponential, Biexponential, and Stretched Exponential Diffusion-weighted MR Imaging and Diffusion Kurtosis MR Imaging. Radiology 278 (2): 496-504.

Bammer R (2003) Basic principles of diffusion-weighted imaging. Eur J Radiol 45 (3): 169-184.

Bano S, Waraich MM, Khan MA, Buzdar SA and Manzur S (2013) Diagnostic value of apparent diffusion coefficient for the accurate assessment and differentiation of intracranial meningiomas. Acta Radiol Short Rep 2 (7): 2047981613512484.

Beaulieu C (2002) The basis of anisotropic water diffusion in the nervous system - a technical review. NMR Biomed 15 (7-8): 435-455.

Boire A, Brastianos PK, Garzia L and Valiente M (2020) Brain metastasis. Nat Rev Cancer 20 (1): 4-11.

Bozdağ M, Er A and Çinkooğlu A (2021) Histogram Analysis of ADC Maps for Differentiating Brain Metastases From Different Histological Types of Lung Cancers. Can Assoc Radiol J 72 (2): 271-278.

Buerki RA, Horbinski CM, Kruser T, Horowitz PM, James CD and Lukas RV (2018) An overview of meningiomas. Future Oncol 14 (21): 2161-2177.

Cagney DN, Martin AM, Catalano PJ, Redig AJ, Lin NU, Lee EQ, Wen PY, Dunn IF, Bi WL, Weiss SE, Haas-Kogan DA, Alexander BM and Aizer AA (2017) Incidence and prognosis of patients with brain metastases at diagnosis of systemic malignancy: a population-based study. Neuro Oncol 19 (11): 1511-1521.

Cha S (2006) Update on brain tumor imaging: from anatomy to physiology. AJNR Am J Neuroradiol 27 (3): 475-487.

Chen X, Lin L, Wu J, Yang G, Zhong T, Du X, Chen Z, Xu G, Song Y, Xue Y and Duan Q (2020) Histogram analysis in predicting the grade and histological subtype of meningiomas based on diffusion kurtosis imaging. Acta Radiol 61 (9): 1228-1239.

Chen Y, Zhao X, Ni H, Feng J, Ding H, Qi H, Wan B and Ming D (2012) Parametric mapping of brain tissues from diffusion kurtosis tensor. Comput Math Methods Med 2012: 820847.

Erira A, Velandia F, Penagos J, Zubieta C and Arboleda G (2021) Differential Regulation of the EGFR/PI3K/AKT/PTEN Pathway between Low- and High-Grade Gliomas. Brain Sci 11 (12).
Falk Delgado A, Nilsson M, van Westen D and Falk Delgado A (2018) Glioma Grade Discrimination with MR Diffusion Kurtosis Imaging: A Meta-Analysis of Diagnostic Accuracy. Radiology 287 (1): 119-127.
Gao E, Gao A, Kit Kung W, Shi L, Bai J, Zhao G and Cheng J (2022) Histogram analysis based on diffusion kurtosis imaging: Differentiating glioblastoma multiforme from single brain metastasis and comparing the diagnostic performance of two region of interest placements. Eur J Radiol 147: 110104.
Guzman R, Altrichter S, El-Koussy M, Gralla J, Weis J, Barth A, Seiler RW, Schroth G and Lövblad KO (2008) Contribution of the apparent diffusion coefficient in perilesional edema for the assessment of brain tumors. J Neuroradiol 35 (4): 224-229.
Hagmann P, Jonasson L, Maeder P, Thiran JP, Wedeen VJ and Meuli R (2006) Understanding diffusion MR imaging techniques: From scalar diffusion-weighted imaging to diffusion tensor imaging and beyond. Radiographics 26 Suppl 1: S205-223.
Hakyemez B, Yildirim N, Gokalp G, Erdogan C and Parlak M (2006) The contribution of diffusion-weighted MR imaging to distinguishing typical from atypical meningiomas. Neuroradiology 48 (8): 513-520.
Hempel JM, Bisdas S, Schittenhelm J, Brendle C, Bender B, Wassmann H, Skardelly M, Tabatabai G, Vega SC, Ernemann U and Klose U (2017) In vivo molecular profiling of human glioma using diffusion kurtosis imaging. J Neurooncol 131 (1): 93-101.
Hempel JM, Brendle C, Adib SD, Behling F, Tabatabai G, Castaneda Vega S, Schittenhelm J, Ernemann U and Klose U (2021) Glioma-Specific Diffusion Signature in Diffusion Kurtosis Imaging. J Clin Med 10 (11).
Hempel JM, Brendle C, Bender B, Bier G, Kraus MS, Skardelly M, Richter H, Eckert F, Schittenhelm J, Ernemann U and Klose U (2019) Diffusion kurtosis imaging histogram parameter metrics predicting survival in integrated molecular subtypes of diffuse glioma: An observational cohort study. Eur J Radiol 112: 144-152.
Hempel JM, Schittenhelm J, Bisdas S, Brendle C, Bender B, Bier G, Skardelly M, Tabatabai G, Castaneda Vega S, Ernemann U and Klose U (2018) In vivo assessment of tumor heterogeneity in WHO 2016 glioma grades using diffusion kurtosis imaging: Diagnostic performance and improvement of feasibility in routine clinical practice. J Neuroradiol 45 (1): 32-40.
Hu LS, Hawkins-Daarud A, Wang L, Li J and Swanson KR (2020) Imaging of intratumoral heterogeneity in high-grade glioma. Cancer Lett 477: 97-106.
Huisman TAGM (2003) Diffusion-weighted imaging: basic concepts and application in cerebral stroke and head trauma. Eur Radiol 13 (10): 2283-2297.
Jensen JH and Helpern JA (2010) MRI quantification of non-Gaussian water diffusion by kurtosis analysis. NMR Biomed 23 (7): 698-710.

Jensen JH, Helpern JA, Ramani A, Lu H and Kaczynski K (2005) Diffusional kurtosis imaging: the quantification of non-gaussian water diffusion by means of magnetic resonance imaging. Magn Reson Med 53 (6): 1432-1440.
Jung WS, Park CH, Hong CK, Suh SH and Ahn SJ (2018) Diffusion-Weighted Imaging of Brain Metastasis from Lung Cancer: Correlation of MRI Parameters with the Histologic Type and Gene Mutation Status. AJNR Am J Neuroradiol 39 (2): 273-279.
Kang Y, Choi SH, Kim YJ, Kim KG, Sohn CH, Kim JH, Yun TJ and Chang KH (2011) Gliomas: Histogram analysis of apparent diffusion coefficient maps with standard- or high-b-value diffusion-weighted MR imaging--correlation with tumor grade. Radiology 261 (3): 882-890.
Ko CC, Lim SW, Chen TY, Chen JH, Li CF and Shiue YL (2018) Prediction of progression in skull base meningiomas: additional benefits of apparent diffusion coefficient value. J Neurooncol 138 (1): 63-71.
Koh DM and Collins DJ (2007) Diffusion-weighted MRI in the body: applications and challenges in oncology. AJR Am J Roentgenol 188 (6): 1622-1635.
Lee EJ, terBrugge K, Mikulis D, Choi DS, Bae JM, Lee SK and Moon SY (2011) Diagnostic value of peritumoral minimum apparent diffusion coefficient for differentiation of glioblastoma multiforme from solitary metastatic lesions. AJR Am J Roentgenol 196 (1): 71-76.
Lemercier P, Paz Maya S, Patrie JT, Flors L and Leiva-Salinas C (2014) Gradient of apparent diffusion coefficient values in peritumoral edema helps in differentiation of glioblastoma from solitary metastatic lesions. AJR Am J Roentgenol 203 (1): 163-169.
Lin L, Bhawana R, Xue Y, Duan Q, Jiang R, Chen H, Chen X, Sun B and Lin H (2018) Comparative Analysis of Diffusional Kurtosis Imaging, Diffusion Tensor Imaging, and Diffusion-Weighted Imaging in Grading and Assessing Cellular Proliferation of Meningiomas. AJNR Am J Neuroradiol 39 (6): 1032-1038.
Lin L, Xue Y, Duan Q, Chen X, Chen H, Jiang R, Zhong T, Xu G, Geng D and Zhang J (2019) Grading meningiomas using mono-exponential, bi-exponential and stretched exponential model-based diffusion-weighted MR imaging. Clin Radiol 74 (8): 651.e615-651.e623.
Liu J, Han H, Xu Y, Jin Y, Ma F, Mu J and Wang Y (2021) A comparison of the multimodal magnetic resonance imaging features of brain metastases vs. high-grade gliomas. Am J Transl Res 13 (4): 3543-3548.
Louis DN, Perry A, Burger P, Ellison DW, Reifenberger G, von Deimling A, Aldape K, Brat D, Collins VP, Eberhart C, Figarella-Branger D, Fuller GN, Giangaspero F, Giannini C, Hawkins C, Kleihues P, Korshunov A, Kros JM, Beatriz Lopes M, Ng HK, Ohgaki H, Paulus W, Pietsch T, Rosenblum M, Rushing E, Soylemezoglu F, Wiestler O and Wesseling P (2014) International Society Of Neuropathology-Haarlem consensus guidelines for nervous system tumor classification and grading. Brain Pathol 24 (5): 429-435.
Louis DN, Perry A, Wesseling P, Brat DJ, Cree IA, Figarella-Branger D, Hawkins C, Ng HK, Pfister SM, Reifenberger G, Soffietti R, von Deimling

A and Ellison DW (2021) The 2021 WHO Classification of Tumors of the Central Nervous System: a summary. Neuro Oncol 23 (8): 1231-1251.
Lu H, Jensen JH, Ramani A and Helpern JA (2006) Three-dimensional characterization of non-gaussian water diffusion in humans using diffusion kurtosis imaging. NMR Biomed 19 (2): 236-247.
Maier SE, Sun Y and Mulkern RV (2010) Diffusion imaging of brain tumors. NMR Biomed 23 (7): 849-864.
Maiter A, Riemer F, Allinson K, Zaccagna F, Crispin-Ortuzar M, Gehrung M, McLean MA, Priest AN, Grist J, Matys T, Graves MJ and Gallagher FA (2021) Investigating the relationship between diffusion kurtosis tensor imaging (DKTI) and histology within the normal human brain. Sci Rep 11 (1): 8857.
Mao J, Zeng W, Zhang Q, Yang Z, Yan X, Zhang H, Wang M, Yang G, Zhou M and Shen J (2020) Differentiation between high-grade gliomas and solitary brain metastases: a comparison of five diffusion-weighted MRI models. BMC Med Imaging 20 (1): 124.
Marrale M, Collura G, Brai M, Toschi N, Midiri F, La Tona G, Lo Casto A and Gagliardo C (2016) Physics, Techniques and Review of Neuroradiological Applications of Diffusion Kurtosis Imaging (DKI). Clin Neuroradiol 26 (4): 391-403.
Maximov II, Tonoyan AS and Pronin IN (2017) Differentiation of glioma malignancy grade using diffusion MRI. Phys Med 40: 24-32.
Meyer HJ, Fiedler E, Kornhuber M, Spielmann RP and Surov A (2015) Comparison of diffusion-weighted imaging findings in brain metastases of different origin. Clin Imaging 39 (6): 965-969.
Meyer HJ, Wienke A and Surov A (2020) ADC values of benign and high grade meningiomas and associations with tumor cellularity and proliferation - A systematic review and meta-analysis. J Neurol Sci 415: 116975.
Mulkern RV, Gudbjartsson H, Westin CF, Zengingonul HP, Gartner W, Guttmann CR, Robertson RL, Kyriakos W, Schwartz R, Holtzman D, Jolesz FA and Maier SE (1999) Multi-component apparent diffusion coefficients in human brain. NMR Biomed 12 (1): 51-62.
Müller SJ, Khadhraoui E, Neef NE, Riedel CH and Ernst M (2021) Differentiation of brain metastases from small and non-small lung cancers using apparent diffusion coefficient (ADC) maps. BMC Med Imaging 21 (1): 70.
Neska-Matuszewska M, Bladowska J, Sąsiadek M and Zimny A (2018) Differentiation of glioblastoma multiforme, metastases and primary central nervous system lymphomas using multiparametric perfusion and diffusion MR imaging of a tumor core and a peritumoral zone-Searching for a practical approach. PLoS One 13 (1): e0191341.
Nuessle NC, Behling F, Tabatabai G, Castaneda Vega S, Schittenhelm J, Ernemann U, Klose U and Hempel JM (2021) ADC-Based Stratification of Molecular Glioma Subtypes Using High b-Value Diffusion-Weighted Imaging. J Clin Med 10 (16).
Ogasawara C, Philbrick BD and Adamson DC (2021) Meningioma: A Review of Epidemiology, Pathology, Diagnosis, Treatment, and Future Directions. Biomedicines 9 (3).

Oh J, Cha S, Aiken AH, Han ET, Crane JC, Stainsby JA, Wright GA, Dillon WP and Nelson SJ (2005) Quantitative apparent diffusion coefficients and T2 relaxation times in characterizing contrast enhancing brain tumors and regions of peritumoral edema. J Magn Reson Imaging 21 (6): 701-708.
Omuro A and DeAngelis LM (2013) Glioblastoma and other malignant gliomas: a clinical review. Jama 310 (17): 1842-1850.
Ostrom QT, Bauchet L, Davis FG, Deltour I, Fisher JL, Langer CE, Pekmezci M, Schwartzbaum JA, Turner MC, Walsh KM, Wrensch MR and Barnholtz-Sloan JS (2014) The epidemiology of glioma in adults: a "state of the science" review. Neuro Oncol 16 (7): 896-913.
Ostrom QT, Gittleman H, Xu J, Kromer C, Wolinsky Y, Kruchko C and Barnholtz-Sloan JS (2016) CBTRUS Statistical Report: Primary Brain and Other Central Nervous System Tumors Diagnosed in the United States in 2009-2013. Neuro Oncol 18 (suppl_5): v1-v75.
Patel AP, Tirosh I, Trombetta JJ, Shalek AK, Gillespie SM, Wakimoto H, Cahill DP, Nahed BV, Curry WT, Martuza RL, Louis DN, Rozenblatt-Rosen O, Suvà ML, Regev A and Bernstein BE (2014) Single-cell RNA-seq highlights intratumoral heterogeneity in primary glioblastoma. Science 344 (6190): 1396-1401.
Pauleit D, Langen KJ, Floeth F, Hautzel H, Riemenschneider MJ, Reifenberger G, Shah NJ and Müller HW (2004) Can the apparent diffusion coefficient be used as a noninvasive parameter to distinguish tumor tissue from peritumoral tissue in cerebral gliomas? J Magn Reson Imaging 20 (5): 758-764.
Pavlisa G, Rados M, Pavlisa G, Pavic L, Potocki K and Mayer D (2009) The differences of water diffusion between brain tissue infiltrated by tumor and peritumoral vasogenic edema. Clin Imaging 33 (2): 96-101.
Qi XX, Shi DF, Ren SX, Zhang SY, Li L, Li QC and Guan LM (2018) Histogram analysis of diffusion kurtosis imaging derived maps may distinguish between low and high grade gliomas before surgery. Eur Radiol 28 (4): 1748-1755.
Qiu J, Deng K, Wang P, Chen C, Luo Y, Yuan S and Wen J (2022) Application of diffusion kurtosis imaging to the study of edema in solid and peritumoral areas of glioma. Magn Reson Imaging 86: 10-16.
Raab P, Hattingen E, Franz K, Zanella FE and Lanfermann H (2010) Cerebral gliomas: diffusional kurtosis imaging analysis of microstructural differences. Radiology 254 (3): 876-881.
Roberts TP and Rowley HA (2003) Diffusion weighted magnetic resonance imaging in stroke. Eur J Radiol 45 (3): 185-194.
Rosenkrantz AB, Padhani AR, Chenevert TL, Koh DM, De Keyzer F, Taouli B and Le Bihan D (2015) Body diffusion kurtosis imaging: Basic principles, applications, and considerations for clinical practice. J Magn Reson Imaging 42 (5): 1190-1202.
Rulseh AM and Vymazal J (2020) Whole brain apparent diffusion coefficient measurements correlate with survival in glioblastoma patients. J Neurooncol 146 (1): 157-162.
Sacco S, Ballati F, Gaetani C, Lomoro P, Farina LM, Bacila A, Imparato S, Paganelli C, Buizza G, Iannalfi A, Baroni G, Valvo F, Bastianello S and

Preda L (2020) Multi-parametric qualitative and quantitative MRI assessment as predictor of histological grading in previously treated meningiomas. Neuroradiology 62 (11): 1441-1449.
Sacks P and Rahman M (2020) Epidemiology of Brain Metastases. Neurosurg Clin N Am 31 (4): 481-488.
Santelli L, Ramondo G, Della Puppa A, Ermani M, Scienza R, d'Avella D and Manara R (2010) Diffusion-weighted imaging does not predict histological grading in meningiomas. Acta Neurochir (Wien) 152 (8): 1315-1319; discussion 1319.
Seo HS, Chang KH, Na DG, Kwon BJ and Lee DH (2008) High b-value diffusion (b = 3000 s/mm2) MR imaging in cerebral gliomas at 3T: visual and quantitative comparisons with b = 1000 s/mm2. AJNR Am J Neuroradiol 29 (3): 458-463.
Server A, Kulle B, Maehlen J, Josefsen R, Schellhorn T, Kumar T, Langberg CW and Nakstad PH (2009) Quantitative apparent diffusion coefficients in the characterization of brain tumors and associated peritumoral edema. Acta Radiol 50 (6): 682-689.
Siempis T, Tsakiris C, Alexiou GA, Xydis VG, Voulgaris S and Argyropoulou MI (2020) Diagnostic performance of diffusion and perfusion MRI in differentiating high from low-grade meningiomas: A systematic review and meta-analysis. Clin Neurol Neurosurg 190: 105643.
Soffietti R, Ahluwalia M, Lin N and Rudà R (2020) Management of brain metastases according to molecular subtypes. Nat Rev Neurol 16 (10): 557-574.
Soffietti R, Cornu P, Delattre JY, Grant R, Graus F, Grisold W, Heimans J, Hildebrand J, Hoskin P, Kalljo M, Krauseneck P, Marosi C, Siegal T and Vecht C (2006) EFNS Guidelines on diagnosis and treatment of brain metastases: report of an EFNS Task Force. Eur J Neurol 13 (7): 674-681.
Soliman RK, Essa AA, Elhakeem AAS, Gamal SA and Zaitoun MMA (2021) Texture analysis of apparent diffusion coefficient (ADC) map for glioma grading: Analysis of whole tumoral and peri-tumoral tissue. Diagn Interv Imaging 102 (5): 287-295.
Stummer W (2007) Mechanisms of tumor-related brain edema. Neurosurg Focus 22 (5): E8.
Stupp R, Mason WP, van den Bent MJ, Weller M, Fisher B, Taphoorn MJ, Belanger K, Brandes AA, Marosi C, Bogdahn U, Curschmann J, Janzer RC, Ludwin SK, Gorlia T, Allgeier A, Lacombe D, Cairncross JG, Eisenhauer E and Mirimanoff RO (2005) Radiotherapy plus concomitant and adjuvant temozolomide for glioblastoma. N Engl J Med 352 (10): 987-996.
Surov A, Ginat DT, Sanverdi E, Lim CCT, Hakyemez B, Yogi A, Cabada T and Wienke A (2016) Use of Diffusion Weighted Imaging in Differentiating Between Maligant and Benign Meningiomas. A Multicenter Analysis. World Neurosurg 88: 598-602.
Tan Y, Wang XC, Zhang H, Wang J, Qin JB, Wu XF, Zhang L and Wang L (2015) Differentiation of high-grade-astrocytomas from solitary-brain-

metastases: Comparing diffusion kurtosis imaging and diffusion tensor imaging. Eur J Radiol 84 (12): 2618-2624.
Tan Y, Zhang H, Wang X, Qin J, Wang L, Yang G and Yan H (2019) Comparing the value of DKI and DTI in detecting isocitrate dehydrogenase genotype of astrocytomas. Clin Radiol 74 (4): 314-320.
Tan Y, Zhang H, Zhao RF, Wang XC, Qin JB and Wu XF (2016) Comparison of the values of MRI diffusion kurtosis imaging and diffusion tensor imaging in cerebral astrocytoma grading and their association with aquaporin-4. Neurol India 64 (2): 265-272.
Tepe M, Saylisoy S, Toprak U and Inan I (2021) The Potential Role of Peritumoral Apparent Diffusion Coefficient Evaluation in Differentiating Glioblastoma and Solitary Metastatic Lesions of the Brain. Curr Med Imaging 17 (10): 1200-1208.
Thammaroj J, Wongwichit N and Boonrod A (2020) Evaluation of Perienhancing Area in Differentiation between Glioblastoma and Solitary Brain Metastasis. Asian Pac J Cancer Prev 21 (9): 2525-2530.
Tobin WO, Meyer FB and Keegan BM (2015) Diagnostic Yield and Safety of Cerebellar and Brainstem Parenchymal Biopsy. World Neurosurg 84 (6): 1973-1976.
Watanabe M, Tanaka R and Takeda N (1992) Magnetic resonance imaging and histopathology of cerebral gliomas. Neuroradiology 34 (6): 463-469.
Wesseling P and Capper D (2018) WHO 2016 Classification of gliomas. Neuropathol Appl Neurobiol 44 (2): 139-150.
Wu XF, Liang X, Wang XC, Qin JB, Zhang L, Tan Y and Zhang H (2021) Differentiating high-grade glioma recurrence from pseudoprogression: Comparing diffusion kurtosis imaging and diffusion tensor imaging. Eur J Radiol 135: 109445.
Xing F, Tu N, Koh TS and Wu G (2017) MR diffusion kurtosis imaging predicts malignant potential and the histological type of meningioma. Eur J Radiol 95: 286-292.
Yamasaki F, Kurisu K, Aoki T, Yamanaka M, Kajiwara Y, Watanabe Y, Takayasu T, Akiyama Y and Sugiyama K (2012) Advantages of high b-value diffusion-weighted imaging to diagnose pseudo-responses in patients with recurrent glioma after bevacizumab treatment. Eur J Radiol 81 (10): 2805-2810.
Ye C, Lin Q, Jin Z, Zheng C and Ma S (2021) Predictive effect of DCE-MRI and DWI in brain metastases from NSCLC. Open Med (Wars) 16 (1): 1265-1275.
Zhang G, Chen X, Zhang S, Ruan X, Gao C, Liu Z and Wei X (2019) Discrimination Between Solitary Brain Metastasis and Glioblastoma Multiforme by Using ADC-Based Texture Analysis: A Comparison of Two Different ROI Placements. Acad Radiol 26 (11): 1466-1472.
Zhang P and Liu B (2020) Differentiation among Glioblastomas, Primary Cerebral Lymphomas, and Solitary Brain Metastases Using Diffusion-Weighted Imaging and Diffusion Tensor Imaging: A PRISMA-Compliant Meta-analysis. ACS Chem Neurosci 11 (3): 477-483.
Zhao J, Wang YL, Li XB, Hu MS, Li ZH, Song YK, Wang JY, Tian YS, Liu DW, Yan X, Jiang L, Yang ZY and Chu JP (2019) Comparative analysis of the

diffusion kurtosis imaging and diffusion tensor imaging in grading gliomas, predicting tumour cell proliferation and IDH-1 gene mutation status. J Neurooncol 141 (1): 195-203.

8 Declaration of contributions

This work was generated in the department for diagnostic and interventional neuroradiology of the University Hospital Tübingen under the supervision of Prof. Dr. rer. nat. Uwe Klose.

The MRI measurements were conducted by medical technical assistants and Dr. med. Nils Nüssle. The planning of these measurements was carried out by Dr. med. Nils Nüssle, PD Dr. med. Johann-Martin Hempel and me.

The analysis of the data was conducted by me with support of Prof. Dr. rer. nat. Uwe Klose.

This manuscript was corrected by Prof. Dr. rer. nat. Uwe Klose.

I wrote this manuscript independently and used no other sources than those I mentioned.

Clara Heilker

9 Acknowledgments

I would like to thank everyone that helped me with the development of this dissertation. Especially, I would like to thank Prof. Dr. Uwe Klose for the possibility to work on this topic and for the continuous and excellent supervision.

Furthermore, I would like to thank PD Dr. Johann-Martin Hempel and Dr. Nils Nüssle for the support in acquiring patients for this dissertation.

I would also like to express my gratitude to Prof. Dr. Thomas Nägele, PD Dr. Benjamin Bender and Dr. Till-Karsten Hauser for their advice.

My thanks also go to the medical technical assistants for conducting the measurements.

Moreover, I would like to thank the patients and control subjects for providing the necessary data for this dissertation.

Finally, I would like to thank my parents for their unwavering support. Thank you for motivating me not only during this project but also for your lifelong assistance in every situation.